SPIRE
Sustainable Process Industry through Resource and Energy Efficiency

DISIRE

Grant Agreement no.	**636834**
Project Acronym	**DISIRE**
Project full title	**Integrated Process Control Based on Distributed In-Situ Sensors into Raw Materials and Energy**
Dissemination level	PU (after the embargo date)
Embargo date	5 May 2017
Date of delivery	5/6/2016
Deliverable number	D5.1
Deliverable name	On the modelling and control of belt conveyor network
AL / Task related	T5.1, T5.2, T5.3
Authors	R. Zimroz [WUT], R. Król [WUT], W. Kawalec [WUT], L. Jurdziak [WUT], D. Kaszuba [WUT], L. Gładysiewicz [WUT], M. Bajda [WUT], A. Wyłomańska [WUT], P. Kruczek [CUP], M. Polak [CUP], J. Sokołowski [CUP], P. Stefaniak [CUP], J. Obuchowski [CUP], J. Wodecki [CUP], A. Rożek [KGHM], A. Godek [KGHM], M. Jach [KGHM], R. Pilut [KGHM], G. Georgoulas [LTU]
Contributors	CUP, KGHM, WUT, LTU
Keywords	Data quality assessment, Data acquisition systems, Copper ore stream modelling, Belt conveyor system monitoring, Fault detection
Abstract	This report concerns the belt conveyor network in KGHM. The general principles of the transportation system are given, including the rules and constraints. The network data is provided and sensor data is described. Stochastic models of ore mass flow are fitted and validated. In this report also an analysis of Cu content in ore streams for IPC and modeling of ore lithology are included. The problem of energy efficiency in belt conveyor network is investigated, including analysis of belt conveyor resistance to motion. Finally, sensor data relations are modelled for continuous-time fault detection system.

Acronym	*Meaning*
AIC	Akaike Information Criterion
AIPS	Averaged Instantaneous Power Spectrum
ANOVA	Analysis Of Variance
ARMA	Autoregressive Moving Average
BC	Belt Conveyor
BSS	Blind Source Separation
CBJ	Centrum Badania Jakosci (Centre of Quality Research)
CMS	Cyclic Modulation Spectrum
DFT	Discrete Fourier Transform
FFT	Fast Fourier Transform
HPP	Homogeneous Poisson Process
ICA	Intependent Component Analysis
ICAM	Integrated Computer Aided Manufacturing
IDEF0	Icam DEFinition for Function Modeling
LSD	Least Significant Difference
MA	Moving Average
MLE	Maximum Likelihood Estimation
OED	Ore Enrichment Division
PAT	Process Analyser Technology
PDF	Probablity Density Function
QA/QC	Quality Assurance/Quality Control
QQ-plot	Quantile-Quantile plot
SCADA	Supervisory Control And Data Acquisition
SDFT	Sliding Discrete Fourier Transform

Contents

Chapter 1

Introduction

1.1 Summary (abstract)

In this report the belt conveyor network in KGHM is described. The transportation system is complex, thus some basic issues such as ore characteristics and excavation technology used in KGHM were described. The general principles of the transportation system are described, including the rules and constraints of conveyor belt network operation. The data of the network is provided and sensor data acquired in KGHM is described. Appropriate stochastic models of ore mass flow are fitted, verified and validated. In this report also a computer model of the ore flow is presented which includes analysis of Cu content in ore streams for IPC, modeling of ore lithology. The problem of energy efficiency in belt conveyor network is investigated, including analysis of belt conveyor resistance to motion. Finally, sensor data relations are modelled which enables to use the change detection algorithms for continuous-time fault detection system.

1.2 Purpose of document

The purpose of this document is to represent the belt conveyor network as a set of rules, data, measurements and actions performed to transport the copper ore. Such simplified representation allows to analyze behavior of the network, to study the influence of several factors on performance of the network, to make predictions about behaviour of the system, and, finally, to improve general performance of the mine by making appropriate decisions based on it.

1.3 Partners involved

Partner	*Contribution*
CUP	CUP is the WP5 leader and manage the work flow in this WP. CUP participated in meetings of D5.1 contributors where, together with WUT, described the need of consistent and up-to-date data from KGHM, and asked for hypothesis about the modelled processes. CUP derived and verified models of ore mass flow (Section 3) and modeled relationships in data provided by KGHM (Section 6). CUP compiled the input of D5.1 contributors in LaTeX.
WUT	WUT is a key partner of WP5. WUT hosted several meetings related to this deliverable. WUT, together with CUP, defined the specification of data required from KGHM, and posed relevant questions about the modelled process of ore transportation. WUT delivered comprehensive description of ore transportation in KGHM (Section 2), computer model of ore flow (Section 4) and analysis of belt conveyor energy efficiency (Section 5).
KGHM	KGHM hosted several meetings of the partners. KGHM provided expert knowledge about the transportation of copper ore, including thoroughly description of the data acquired in KGHM, principles of ore transportation, and answers to the on-going questions from partners. KGHM provided the partners with up-to-date and good quality data, including information about the belt conveyor network. During the work on D5.1 KGHM responded to missing data requests that arose after preliminary analysis.
LTU	LTU provided proofreading and finally checked the entire report.

Table 1.1: Contributions of DISIRE partners to this report.

Chapter 2

Copper ore transportation in KGHM

2.1 Ore characteristics

The copper ore deposit in the area of the Fore-Sudetic monocline was discovered in 1957, when copper mineralization was identified in the borehole formerly marked as Sieroszowice IG-1 (at present borehole S-1). The minerals found in the rock samples collected from the drill core were dominated by copper sulphide - chalcocite. The first geological documentation of the Lubin-Sieroszowice deposit (the furthest south-western part of the current deposit area of KGHM), in category C2, submitted on 4 April 1959 by a team from the Polish Geological Institute led by Jan Wyżykowski, was prepared based on the results from 24 boreholes, with 18 of them used to calculate the resources. Based on Polish geological standards, the so-called balance ore resources were estimated at 700 million tonnes, containing 16.5 million tonnes of metal, over an area of 175 km^2. (KGHM Polska Miedź S.A., 2012)

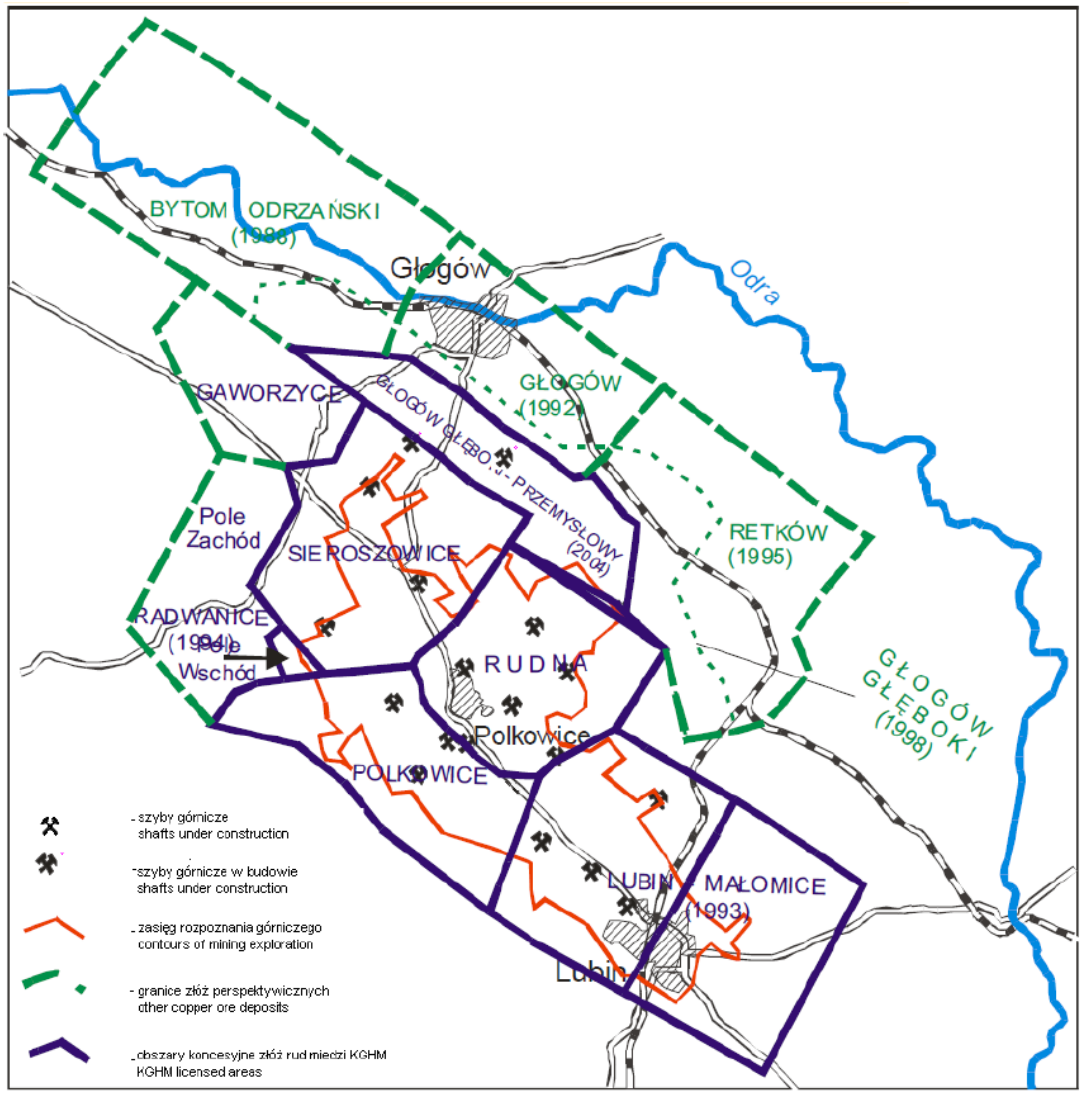

Figure 2.1 Location of documented copper deposits in the Legnica-Głogów Copper Belt (LGCB) (KGHM Polska Miedź S.A., 2012)

The copper ore deposits mined by KGHM are located in Lower Silesia between Lubin and Głogów (Figure 2.1). The documented area of the deposit occupies an area of 40 km by 20 km along the dip, at the depth ranging from approx. 370 to 1380 m. The deposit series is associated with the formations of Upper Permian (Zechstein) dipping along the monocline to the north. (KGHM Polska Miedź S.A., 2012)

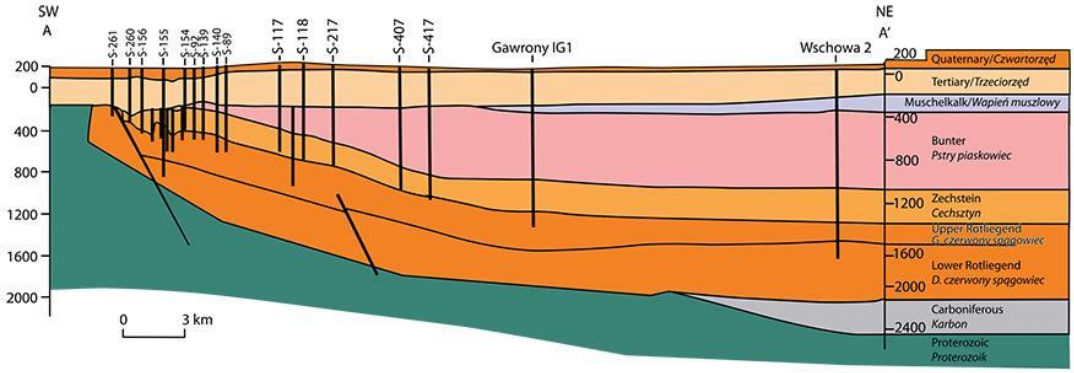

Figure 2.2. Geological cross section of copper ore deposit in Fore-Sudetic Monocline (KGHM Polska Miedź S.A., 2016a)

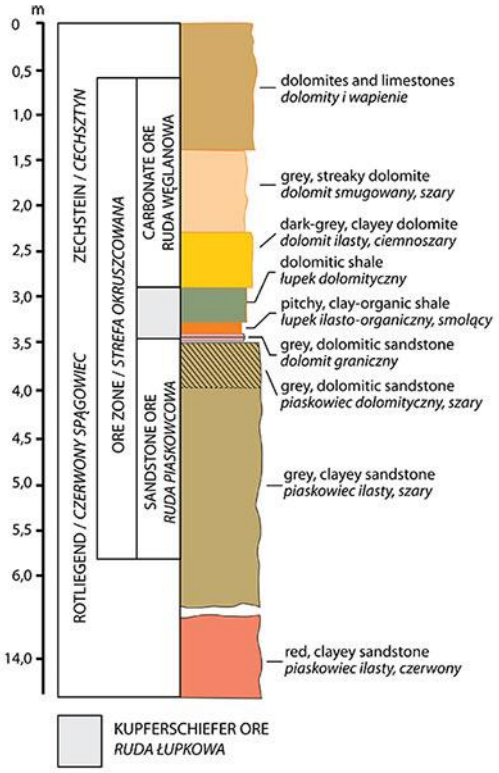

Figure 2.3 Geological profile of copper ore deposit in Fore-Sudetic Monocline. (KGHM Polska Miedź S.A., 2016a)

The deposit is located in the border zone of the Fore-Sudetic monocline. The substrate of the the Fore-Sudetic monocline is formed of a complex of poorly explored crystal and sedimentary rocks of the Palaeozoic and Proterozoic eras. The monocline, in the area where the copper ore is found, is formed of sedimentary rocks belonging to the Permian and Triassic eras, dipping at the angle of a few degrees, sporadically several tens or so degrees, in a NE direction (Figure 2.2). The Permian-Triassic formations of the monocline are discordantly covered by Tertiary and Quaternary sediments. The copper ore deposit of the Fore-Sudetic monocline dipping to the NE, similarly to the layers creating the monocline, is classified as of the stratified type in the sedimentary rocks (sediment-hosted copper ore deposit). The deposit is formed of accumulations of copper sulphides, occuring in the white and grey-white sandstones of Red Footwall Sandstone (Rotliegendes) and Upper Permian (Zechstein), and in the cupriferous shales and carbonate rocks (mainly dolomites) of the Upper

Permian (Zechstein) (Figure 2.3.). The deposit is divided into smaller areas where mining and development is currently underway: “Lubin-Małomice”, “Polkowice”, “Sieroszowice”, “Rudna”, “Radwanice-Wschód” and “Głogów Głęboki-Przemysłowy”. The areas showing the domination of sandstone ore (“Lubin-Małomice”, “Rudna”) are located in the northern and eastern parts of the deposit. The “Radwanice-Wschód” deposit, with no sandstone ore at all, and the “Polkowice” deposit mainly contain carbonate ores. The ”Sieroszowice” deposit is divided into two lithological zones: the south-western part with no sandstone ore and the north-eastern side with the inclusion of sandstone ore (KGHM Polska Miedź S.A., 2012). The copper ore deposit operated by KGHM in Fore-Sudetic Monocline is one of the largest copper ore deposits in the World. Geological resources according to state on 31.12.2015 in particular deposits are, as follows: (KGHM Polska Miedź S.A., 2016a)

Table 2.1 Geological resources summary of deposits in Fore-Sudetic Monocline (according to state from 31.12.2015) (KGHM Polska Miedź S.A., 2016a)

		Deposits						
	Resources	**Lubin-Małomice**	**Polkowice**	**Rudna**	**Sieroszowice**	**Radwanice - Gaworzyce**	**Głogów Głęboki - Przemysłowy**	**KGHM**
Geological resources	Ore [k tonnes]	380 670	105 148	358 681	256 921	344 300	289 510	1 735 230
	Cu [%]	1,32	2,35	1,65	2,67	1,37	2,39	1,84
	Cu [k tonnes]	5 018	2 474	5 920	6 864	4 730	6 920	31 926
	Ag [g/tonne]	55,3	46,8	47,3	63,1	26,4	79	52,5
	Ag [tonnes]	21 043	4 919	16 961	16 219	9 078	22 869	91 088

Geological resources of copper ore according to state on 31.12.2015 are above 1,7 billion Mg, of average grade of Cu 1,84% and Ag around 52,5 g/Mg. The amount of metals in geological resources is over 31 million Mg Cu and over 90 thousand Mg of Ag. (KGHM Polska Miedź S.A., 2016a). Contribution of particular deposits in geological resources are shown in Figure 2.4 and Table 2.1 Geological resources summary of deposits in Fore-Sudetic Monocline (according to state from 31.12.2015) (KGHM Polska Miedź S.A., 2016a).

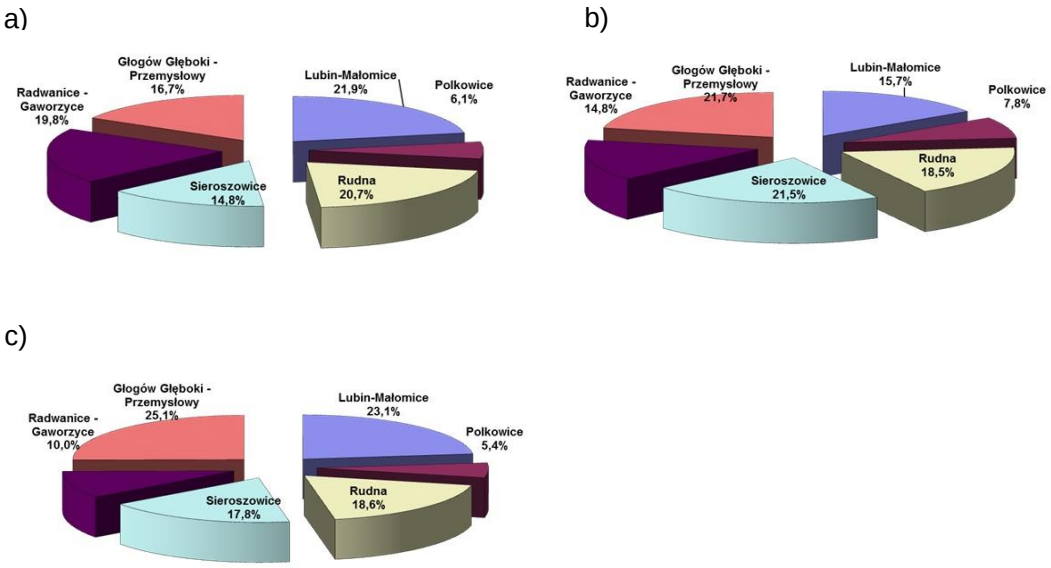

Figure 2.4 Contribution of particular Fore-Sudetic Monocline deposits in geological resources of: a) copper ore., b) copper, c) silver.(KGHM Polska Miedź S.A., 2016a)

The average thickness of the documented industrial deposit is highest in the "Rudna" deposit - 4.28 m, and lowest in the “Radwanice-Wschód” deposit – 1.56 m. Compared to the level of the reserves in recent years, the share of the reserves with a thickness of 3.01-7.00 m continues to decrease. All of the sulphide-type mineral ores contain silver, lead, zinc, cobalt, molybdenum and vanadium. They may occur as their own separate minerals or in the form of isomorphic additions in the copper aggregate minerals. Their documented concentrations do not meet the economic conditions to be classified as suitable for mining, due to the thinness of the zones mineralized with precious metals, the discontinuity of mineralization and its high irregularity. Nonetheless, a substantial part of the precious metals contained in the copper ore deposit goes into the concentrate and is recovered at the smelter during the processing of anode slime. (KGHM Polska Miedź S.A., 2012)

2.2 Room and pillar technology

KGHM employs the room-and-pillar mining method at all of its mines, although the detailed application of the method varies from place to place, depending on ore thickness and the geotechnical parameters of the orebody and surrounding rocks. KGHM’s mines were initially developed using longwall mining methods, but the room-and pillar method is now used exclusively. Under the current system of ore development, primary access to production areas is provided by main development headings driven from the shafts. Each production area is divided into mining panels and each panel is prepared for mining by driving tunnels on all four sides to verify geological continuity and ore grade. Mining panels are located primarily beyond the limits of the major pillars required to protect shafts, permanent underground installations and surface facilities. To gain access to the ore in a mining panel, a network of headings are driven from the shaft, with support provided by roof bolts. Then, a series of parallel rooms and cross-cuts are driven, essentially at right angles. The result is that a series of rectangular pillars

are left in place between the rooms and the cross-cuts. This phase of mining is referred to as primary extraction. A subsequent phase of secondary extraction involves removing ore from all sides of the pillar, thereby reducing its size (Barlett S. et al., 2013). The scheme of room-and-pillar is shown in Figure 2.5. Figure 2.6 shows typical visualisation of a digital 3-D model of underground room-and-pillar developments.

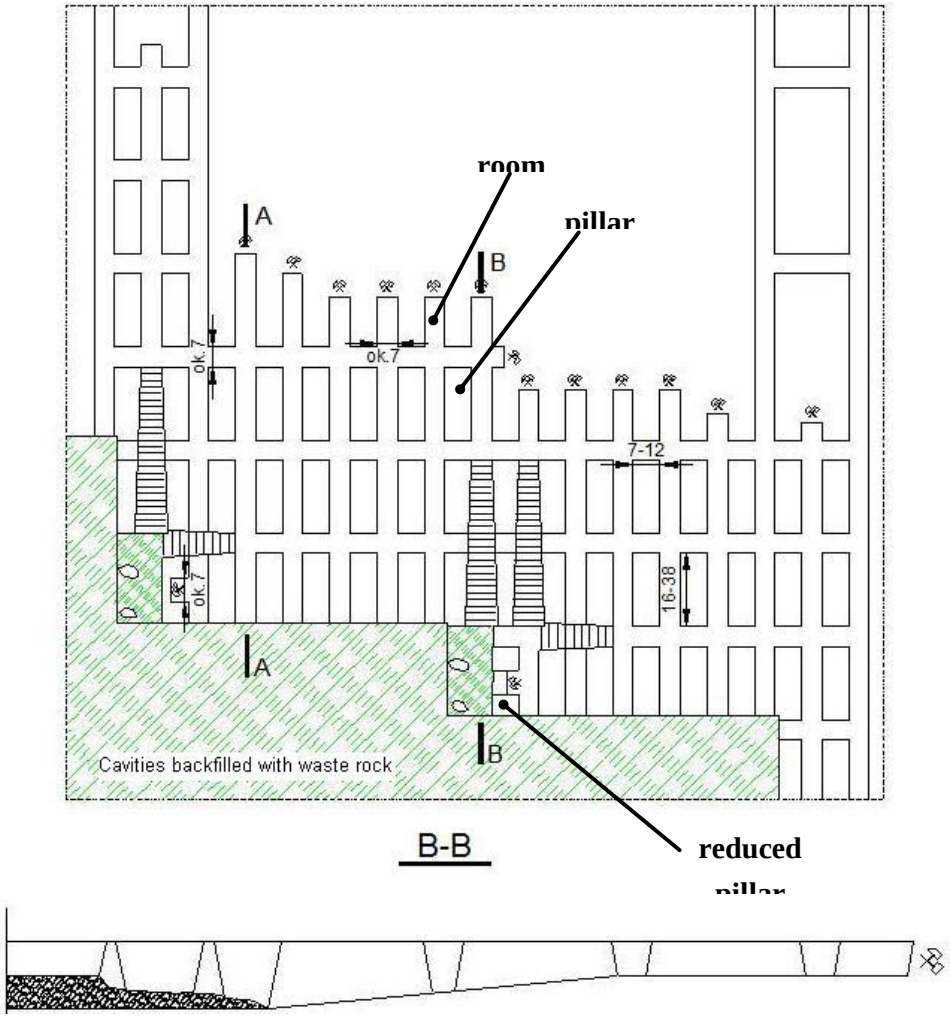

Figure 2.5 Scheme of exploitation with the room and pillar method with roof displacement and placement of waste rock in cavities. Backfilling in the exploitation field, by copper ore deposit extraction of thickness over 7 m. (OLKGHM PSKA MIEDŹ SA, RUDNA MINE DIVISION, 2016)

At KGHM's mines, mining areas are sealed following secondary extraction, in order to prevent further access, and are then allowed to cave naturally. It is understood that the current system of primary and secondary mining is capable of extracting 75% to over 90% of the in-situ ore. KGHM utilizes many variations of the basic room-and-pillar system. The basic technical parameters which determine which of the variations will be used under given conditions include:

method of support :

- natural caving of the hanging wall,
- hydraulic sandfill or backfilling with waste rock,

thickness of ore :

- up to 2.5 metres,
- 2.5 to 5 metres,
- 5 to 7 metres,
- 7 to 15 metres,

dip of ore :

- up to 8 degrees,
- 8 to 16 degrees,
- greater than 16 degrees.

For each of the variations, there is a defined range of permitted pillar dimensions. Actual pillar dimensions from within the specified range are determined after consideration of additional criteria, such as depth, degree of folding or faulting, proximity to other working areas, stress conditions and the potential for rock burst hazards.

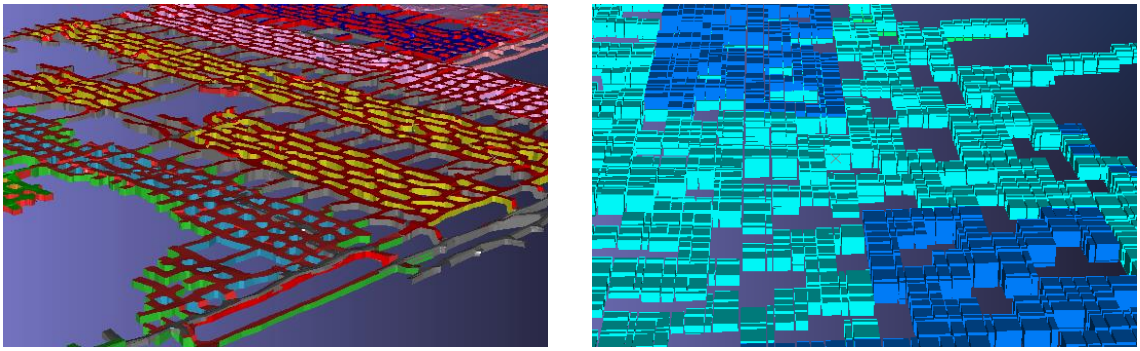

Figure 2.6 Typical visualisation of a digital 3-D model of underground room-and-pillar developments: left panel: solid wireframes, right panel: block model cells coloured by mining fields numbering (Kawalec et al. 2016)

Typically, where the ore is less than about 7 m thick, large open stopes are created, with pillar dimensions varying from 6 m to 12 m in width by 8 m to 38 m in length. Production pillars are designed with their long axes parallel to the working front. In the thicker ore zones at Rudna the ore may be extracted in two horizontal slices, starting at the top, directly under the roof, and benching down in steps. The resulting void is filled with hydraulically-placed sand. KGHM's underground mining operations are fully mechanized and, generally, employ sufficient units of equipment of appropriate size. Surface facilities at all shafts visited were extensive and entirely adequate. Housekeeping, both on surface and underground, is of a uniformly high standard. (Barlett S. et al., 2013)

2.3 Underground transportation basics

The transport systems used in the KGHM copper mines were chosen and designed for the room and pillar mining system. Taken into consideration were factors such as the methods of mining and loading, the properties of mined material, the ore flow characteristics, and the required capacity and length of transport routes. (Hardygóra & Gładysiewicz, 2003). The mining

of copper ore and its delivery to the ore enrichment plant is associated with the following technological operations (KGHM Polska Miedź S.A., 2016b):

- drilling of blasting holes,
- placement of explosives in the holes,
- construction of roof bolting,
- execution of ripping in the mine faces and access headings,
- transport of the production to the unit discharge places onto the belt conveyors,
- crushing of large rocks (excessive dimensions) on the unit discharge crate,
- transport of ore by belt conveyors (or by rail transport) to the crushing chambers by the shaft retention reservoirs,
- transport of the ore to the surface with using the skips of extraction shafts,
- transport of the ore by belt conveyor to OEP (ore enrichment plant).

The scheme of operations mentioned above is shown in Figure 2.7.

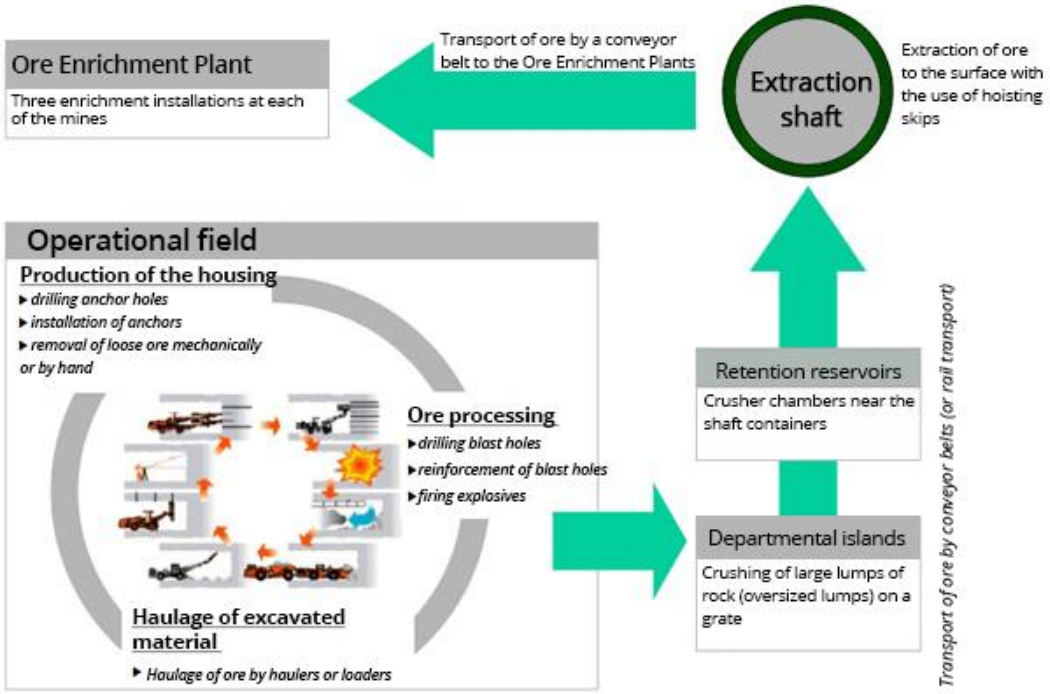

Figure 2.7 Scheme of mining of copper ore and its delivery to the ore enrichment plant (KGHM Polska Miedź S.A., 2016b)

A transport system in a broad sense embraces a set of machines and devices for conveying ore from mine faces to ore dressing plants. The system includes also containers and appurtenances, ore crushers and devices for transfer of ore from one transport system onto another. The characteristic feature of the horizontal transport in the three KGHM mines is the use, at the various stages and on a different scale, of both cyclic transport (LHDs, trucks and rail transport) and the high-capacity continuous transport (belt conveyors). The transport function

within mining panels in all the copper ore mines is carried out by LHDs feeding the ore onto tracks. The tracks transport the ore to mining panel reloading points where it is dumped directly onto a screen functioning as a classifier (Figure 2.8a,b). Oversize lumps left on the screen are crushed mechanically by hydraulic hammers controlled by an operator who monitors the dumping proceeds. The screen is situated immediately over a chute that feeds the belt conveyor via a vibrating feeder (Figure 2.8c). The feeder discharge panel is positioned 60 cm above the belt so the impact of material falling on the belt is minimal. Up to several loading points with either fixed or vibrating screens can be set up along the route of a single conveyor. (Hardygóra & Gładysiewicz, 2003).

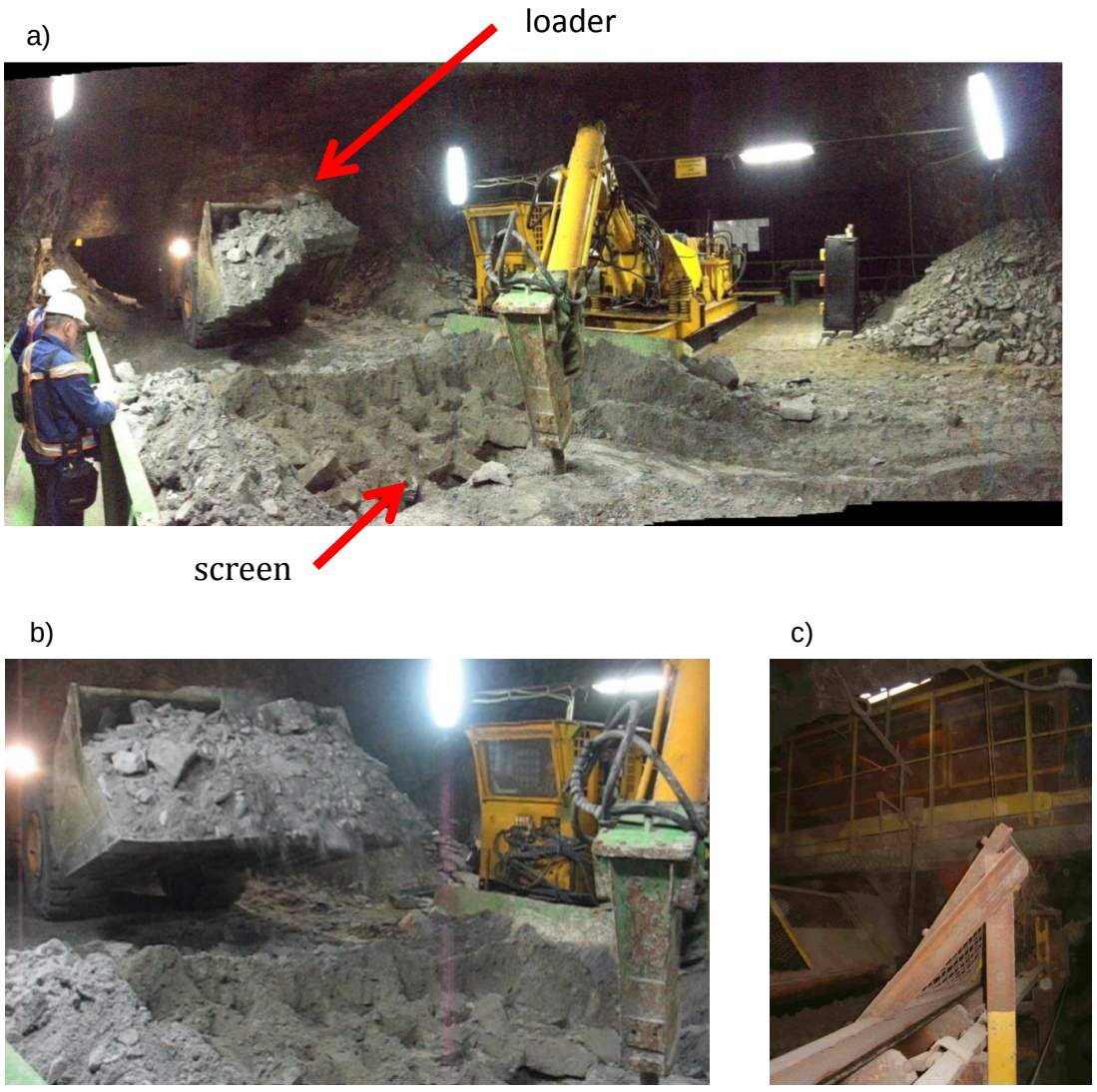

Figure 2.8 View of the reloading point: a,b) screen, c) chute

Ore leaving mine panels is usually stored in panel storage bunkers that have a form of blind shafts from which it is transported to the surface by skip hoisting shafts (Figure 2.9). The panels can have either one storage bunker, as is the case of Lubin mine, or one bunker may be

servicing two or more panels (Rudna mine). In the two oldest mines, Lubin and Polkowice, the primary transport from the panel bunker to ore loading pockets that adjoin the shafts is by rail. Rail car loading stations are used for conveyors to load the trains and car dumps are used to unload trains in the shaft area. The latter are either of tipple type (Lubin and Polkowice mines) or bottom dump cars are used (Sieroszowice mine). Rudna mine uses only belt conveyor transport and the experience with it has been very positive. The newest Sieroszowice mine has a mixed primary transport system where it is possible to transport ore from panels to shaft both by rail or a series of belt conveyors. The mine also has a system of belt conveyors that allows to transport ore to adjacent Polkowice-Sieroszowice mine. Surge stockpiles, whose purpose is to provide an efficient interface between the continuous and cyclical transport system play a major role in transportation systems. There is a need to store output in stockpile to average the erratic flow of the ore coming from mine panels and to match the transportation capacities of various links in the transportation system, many of which operate at different output levels and at different times.

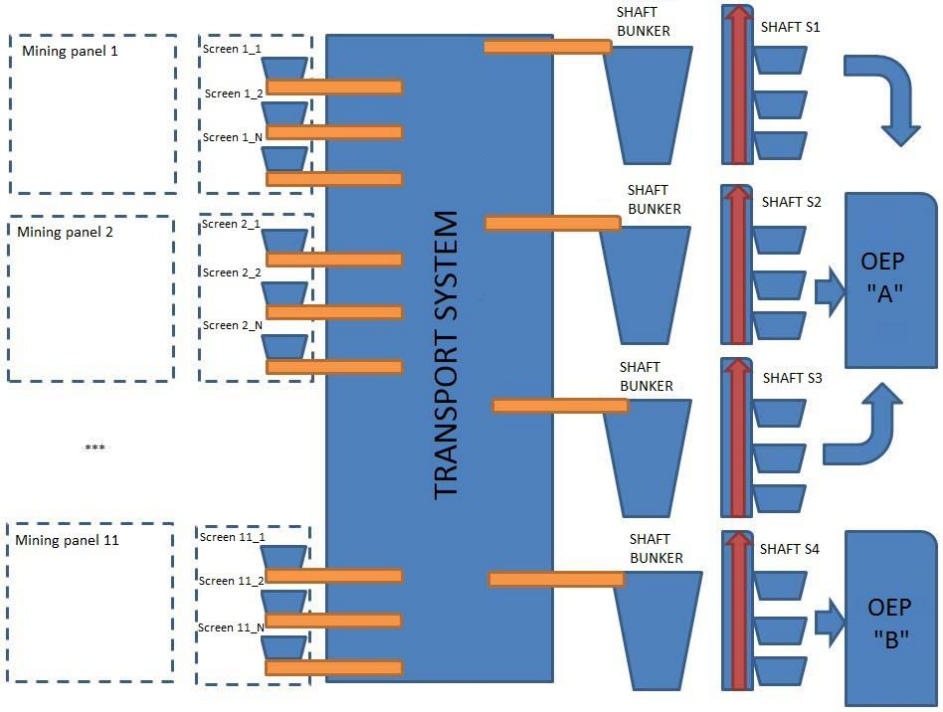

Figure 2.9 Block structure of production (mining and transport, both horizontal and vertical)

Stockpiling material in panels and by the shaft loading stations makes the panel operation independent of that of shaft, and both of these independent of the main transport system. As a result, it is easier to organize the work of all the links in the ore transport system and to utilize the equipment to its full capacity. Short breakdowns of individual links of the transportation system do not interfere with operation of other links and do not restrict system capacity. Construction of bunkers and stockpiles, although costly and time-consuming, is justified by benefits it brings to organization of work and to utilization of workforce and equipment. As a result it improves the overall economics of mining operations. (Hardygóra & Gładysiewicz, 2003)

Transport systems in all three KGHM's mines are similar to each other. Experiments with use of PAT (Process Analyser Technology) will be held at Lubin Mine. The whole analysed underground BC system of the Lubin mine is presented on the Figure 2.10.

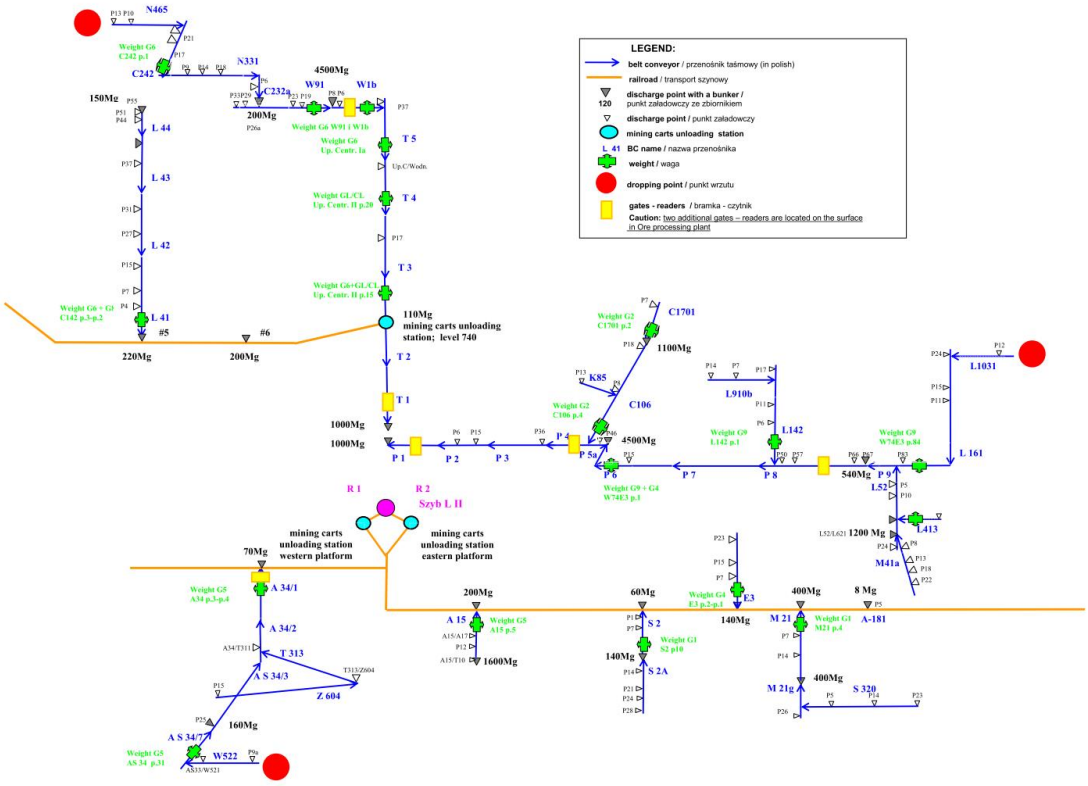

Figure 2.10 Schematic overview of the Lubin mine with planned RFID drop positions as red circles and planned RFID identification antennas as yellow rectangles

The presented transportation system consists of 3 main branches:

- ***Left branch*** (conveyors: N465 – T1, L44 – L41 and the railroad leading to the T2 conveyor). The T1 conveyor supplies the ore to the one 1000 t shaft bunker that feeds the skip. Notes: At the moment only the conveyor line N465 – T1 operates. The second transportation line consisting of belt conveyors line L44 – L41 and the railroad has not operated for the last 6 months. This means that the ore is supplied to the shaft R1 only by conveyors.
- ***Right branch*** (conveyors: L1031 – P1 and its subbranches: C1701 – C106, L910b – L142, M41a – L52). The P1 conveyor supplies the ore to the second 1000 t shaft bunker that feeds the skip. There are no switches between the shaft bunkers nor the possibility of enlarging their capacity. The key data of the belt conveyors of the right branch of the Lubin mine BC system are shown in Table 2.2.
- ***Bottom branch*** (conveyors AS34/7 – A34/1, A15, S2A – S2, S310, S320 – M21, E3 and the railroad to the shafts).

Table 2.2 Key data of the belt conveyors of the right branch of the Lubin mine BC system

Number of a belt conveyor	Con-veyor length, m	belt speed, m/s	Distance from a head pulley* to a drive station, m	Distance from weight to a head pulley*, m	Distance from loading points to a head pulley*, m	Distance from a bunker to a head pulley*, m
P-1	300	2.5	39,5 m	X	X	X
P-2	820	2.5	25 m	X	X	X
P-3	990	2.5	11,5 m	X	P-36a - 948.5	X
P-4	700	2.5	13 m	X	X	b 1 - 682.5 b 2 - 691
P5a	350	2.5	250 m	X	X	X
P6	1020	2.5	225m	175	970	X
P7	1250	2.5	50 m	X	X	X
P8	1350	2.5	15 m	X	I # 465 II # 770 III # 1225	1340
L142	980	1.94	150 m	30	I # 400 II # 675 III # 980	X
L910b	750	2	165 m	X	I # 400 II # 750	X
P9	1350	2.5	150 m	800	755	X
L52	1300	2.5	170 m	X	I # 340 II # 590 II #1300	b I - 870 b II - 1160
M41a	1150	2.5	225 m	X	I # 375 II # 675 III # 875 IV # 1150	X
L413	830	2	175 m	275	830	X
A183	710	2.5	100 m	55	710	X
L161	1250	1.94	50 m	X	I # 650 II # 850 III # 1250	X
L1031	800	2	75 m	X	I # 410 II # 800	X

* head pulley is the end point of a conveyor – the belt runs from a tail pulley to a head pulley (where usually the conveyor is discharged)

The work of the BC system is managed with regard to the following constraints and rules:

- There is a serial connection between an ore bunker and belt conveyors – a BC supplies a bunker which then supplies the consecutive BC, there is no bypass of this connection.
- An ore bunker can be either opened to supply the next BC or closed; no partial opening is feasible.
- The shaft ore bunkers are controlled by shaft operators, the bunkers inside the BC system are controlled by a foreman on the spot.
- A division ore bunker is usually open (not filled up) to maintain the continuous flow of ore and closed only in case of stoppage the conveyors succeeding the bunker. This allows mining divisions not to stop supplying the ore onto the loading points of preceding BCs.
- The above rule does not apply to the large „East" bunker (4500t) that supplies the P4 BC. This bunker is used for systematic storing the ore since Monday till Friday which is then released during the „non-mining" shifts in a weekend (when mining divisions do not mine the ore from mining panels).
- The actual level of ore in a bunker is controlled by a gauge which automatically stops the preceding BCs when the ore reaches the top crest of the bunker. Practically (including the „dead" margins in the bottom and the conical shape on the top formed due to the angle of repose) some 80% of the theoretical bunker capacity can be used.
- The division BCs usually operate since the first loader or truck discharges ore onto a screen in the loading point up to the end of the shift. There were undertaken tests of temporary switching off the BCs but the savings were considered to be smaller than the decrease of ore supply involved. Moreover any stoppage of not fully emptied BC means that it has to be then started when loaded which raises the start-up, dynamic belt tensions and can cause premature fatigue of belt splices. Therefore the staff responsible on BC maintenance was reluctant to implementing the strategy of switching off and on partially loaded conveyors.
- BCs are switched on and of in cascades. A cascade consists of all BCs between ore bunkers. All BCs in one cascade have to be switched off. The preceding cascade can operate until the bunker between them is fully filled.
- The start-up procedure of a BC takes approximately 30 seconds.
- Conveyors that are supplied by a bunker and another BC (like P4) can be supplied simultaneously by both sources. In case of the risk of overloading, the priority is given to the preceding conveyor over the preceding bunker.
- The shaft bunkers are considered to be too small and provide the limited storing capacity.

The rules and constraints listed above have been developed over the years of use the BC transportation systems in the KGHM S.A. underground mines. They are used for any control of the BCs and any modelling of the work of BCs should assume them as the obligatory ones.

2.4 Underground transportation modeling basics

The BC transportation systems in the the KGHM S.A. underground mines are vast and complex. The BC routes have to link the mining panels to the existing main transportation lines and it has to be understood that the scheme of the BC transportation is dictated by the needs of mine advancing which is driven by the metal grade recovery and safety precautions rather than optimization of transport.

In the following chapters various aspects of modeling the BC transportation systems in the underground KGHM S.A. mines are presented. The need of analysis of the transportation system is not new and it has been investigated over the years. Some basic notes can be done upon the paper published in the domestic technical journal Transport Przemyslowy (Kulinowski 2005).

In order to perform any investigations of the BC transportation network it has to be analysed and divided into sectors of BC lines that has to work simultaneously (Figure 2.11).

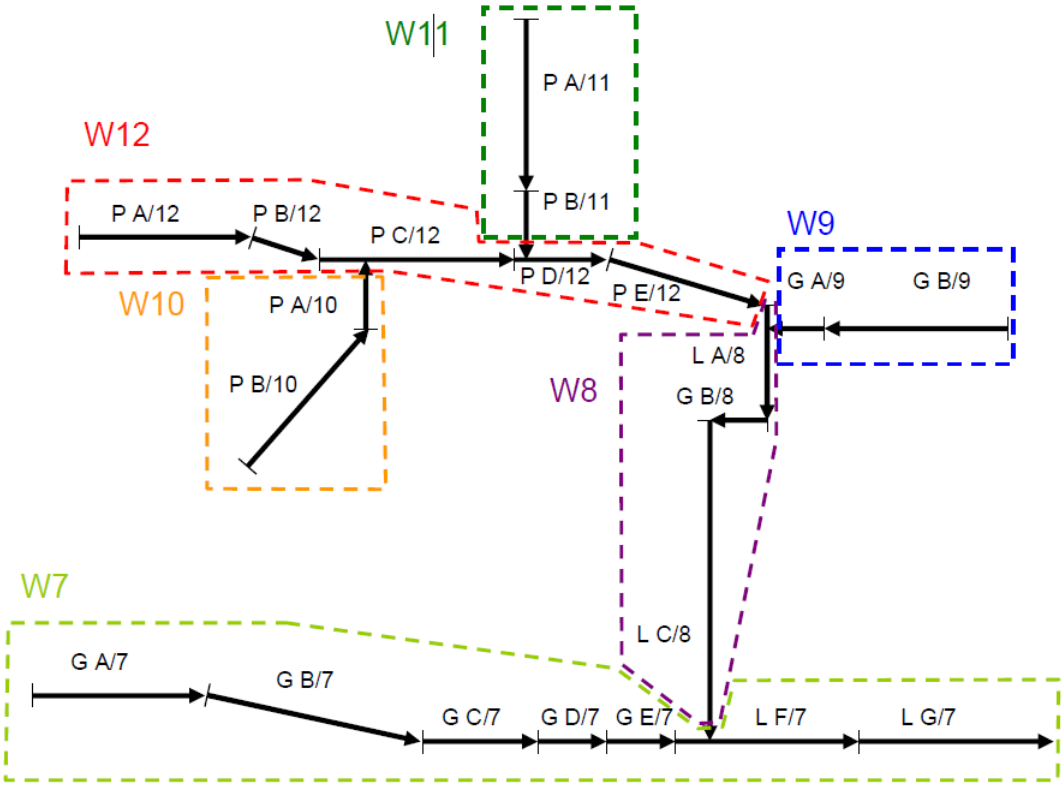

Figure 2.11 Typical scheme of a BC transportation system (Kulinowski 2005)

The whole scheme is usually too big and complex to present all necessary information. However after decomposition on the sub-systems, their objects can be described with some details (Figure 2.12).

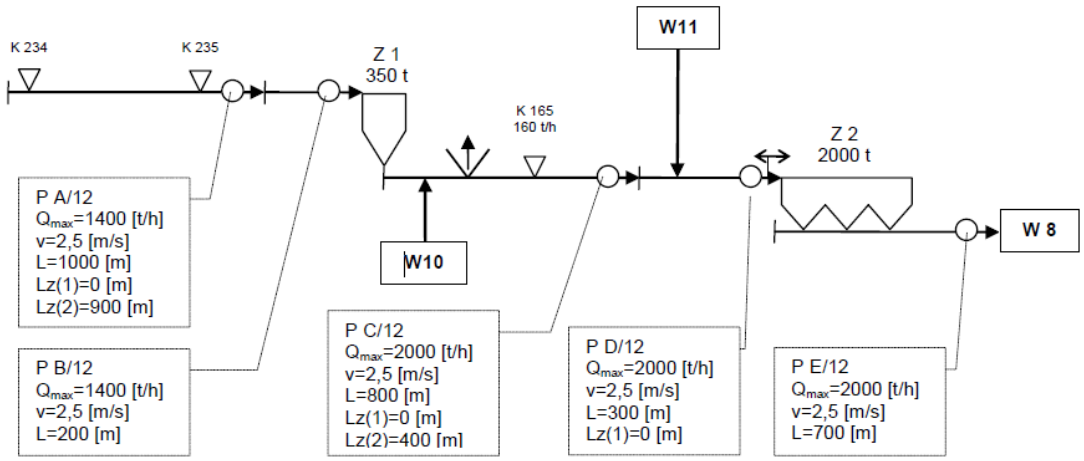

Figure 2.12 Description of the BC sub-system W12 (Kulinowski 2005)

Depending on the available information systems there is a possibility of recording the actual loading of the transportation objects. The ore is supplied onto the loading points on BCs by trucks and LHD. The typical distribution of ore loaded onto several loading points throughout the working shift hours (annotated on Figure 2.12) is presented on the below Figure 2.13.

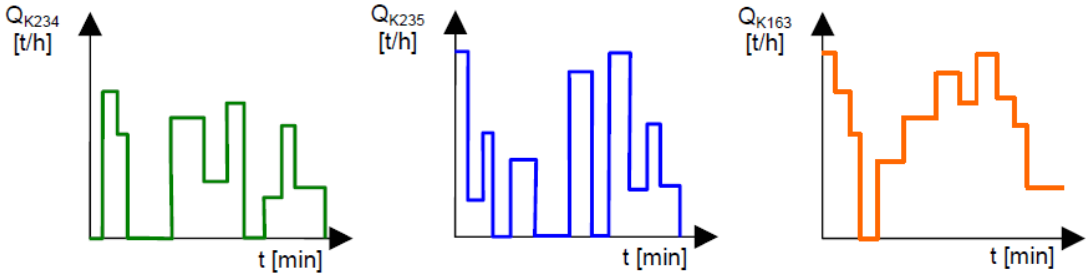

Figure 2.13 Ore supply onto the loading points (Kulinowski 2005)

By adding the given ore flow from the loading points and applying rules of control of the work of BCs and ore bunkers (see 2.3) one can get the simple simulations of the ore flow over the chosen objects (Figure 2.14 Actual output of a chosen BC feeding the ore bunker (Kulinowski 2005)and Figure 2.15 Actual ore tonnage in the ore bunker (Kulinowski 2005)).

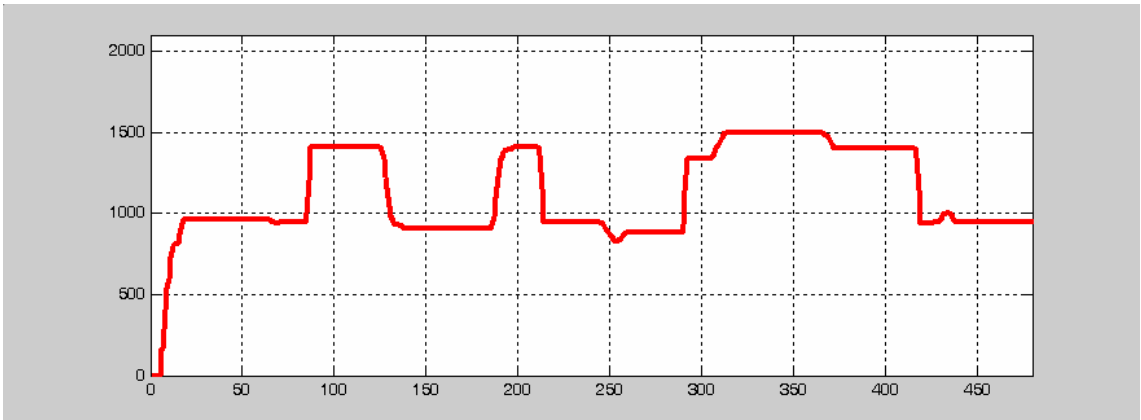

Figure 2.14 Actual output of a chosen BC feeding the ore bunker (Kulinowski 2005)

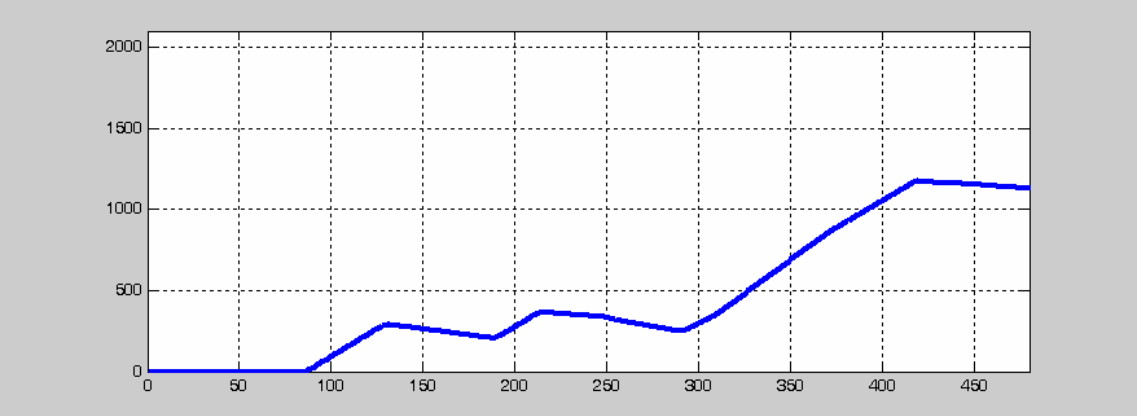

Figure 2.15 Actual ore tonnage in the ore bunker (Kulinowski 2005)

The presented results are only examples of a simply, single simulation. The analysis necessary for the DISIRE Project have to take into consideration the random nature of investigated processes. These are described in the following chapters.

References

[1] Barlett S., Burgess P., Damjanović B., Gowans R., Lattanzi Ch., TECHNICAL REPORT ON THE COPPER-SILVER PRODUCTION OPERATIONS OF KGHM POLSKA MIEDŹ S.A. IN THE LEGNICA-GLOGÓW COPPER BELT AREA OF SOUTHWESTERN POLAND, 2013

[2] Hardygóra M., Gładysiewicz L., ANALYSIS OF TRANSPORTATION SYSTEMS IN POLISH MINING INDUSTRY, Proceedings of 12th International Symposium on MPES 2003,Kalgoorlie, Western Australia, 2003

[3] Kawalec W., Król R, Zimroz R., Jurdziak L., Jach M., Pilut R., Project DISIRE (H2020) – an idea of annotating of ore with sensors in the KGHM PM S.A. underground

copper ore mines, E3S Web of Conferences, Mineral Engineering Conference (MEC2016), Swieradow-Zdroj, Poland, 2016

[4] KGHM Polska Miedź S.A.: Report on the Mining Assets of KGHM Polska Miedź S.A. located within the Legnica-Głogów Copper Belt Area, 2012

[5] KGHM Polska Miedź S.A.: (29.06.2016), access online: http://kghm.com/en/our-business/mining-and-enrichment, 2016a

[6] KGHM Polska Miedź S.A.: (29.06.2016), access online: http://kghm.com/en/our-business/processes/ore-mining, 2016b

[7] KGHM Polska Miedź S.A. RUDNA MINE DIVISION: (29.06.2016), access online: http://www.min-novation.eu/uploads/COMPENDIUM/MINIMALIZATION/BASE_INDUS TRIL/KGHM%20POLSKA%20MIED%C5%B9%20SA,%20RUDNA%20MINE%20DIVISION,%20POLAND.pdf, 2016

[8] Król R. Methods of testing and selection of the belt conveyor equipment with regard to random loading of a transported bulk material (in Polish: Metody badań i doboru elementów przenośnika taśmowego z uwzględnieniem losowo zmiennej strugi urobku), Oficyna Wydawnicza Politechniki Wrocławskiej, Poland, 2013.

[9] Kulinowski P., 2005, Simulation model of a belt transportation system, Transport Przemyslowy 3(21), 2005 (in Polish)

Chapter 3

Modelling of ore mass flow through the conveyor network

In this chapter we present advanced models of the ore mass flow. These models cover two main cases of ore charging that might be noticed in the KGHM Lubin mine, Lubin, Poland. The first one addresses the case when the copper ore is charged to the conveyor cyclically. This is caused by cyclic transport used in the mine. Ore is blasted by using explosives, then it is loaded by the loader and transported to the screen by loader itself or by a hauling truck. The cycle in not constant in time, since the loading time and transportation time might vary. The expected ore flow model is a cyclic train of weight increments. The aggregated ore mass of a single increment depends on the hauling truck (or loader) capacity. Another kind of ore charging is linked to the retention bunker. When the conveyor is supplied by the ore from bunker only, then periods of constant ore mass flow mixed with periods of no ore flow might be expected, since there is no possibility to open the bunker in part. Deviations from the average flow might be caused by uncertainty of the conveyor scale, deviations of ore granulation etc.

Some exemplary results and the theoretical background of ore mass flow modelling is contained also in DISIRE deliverable D2.1. In this deliverable we provide comprehensive analysis of data from KGHM Lubin mine, including methods of pre-processing, theoretical background of the fitted models (redundant with D2.1) - methods for models fitting and verification and results (model parameters and p-values of statistical tests) for the entire data set covering period from November 2015 to March 2016, and simulations of the fitted processes, including final verification. In order to not demand from the Reader to switch between D5.1 and D2.1 and to preserve consistency among deliverables we decided to recall some content from D2.1 here. This is consistent with the objective of this deliverable, since WP5-8 are more related to application of developments from WP2-4 in specific industries.

3.1 Cyclic charging - grid

3.1.1 Introduction

In analyzed data the ore is supplied to the grid cyclically. It is related to the time which the loader spent on an ore transportation from the mining face to the dumping point. One conveyor belt can be supported by several loaders, which transport the ore from different mining faces. In view of that, it is important to model the process of loaders' arrivals to the dumping point and how many tons of the ore they supplied on the conveyor belt.

The application of compound Poisson process to the ore flow on the grid and the conveyor belt seems to be relevant in this problem. The compound Poisson process is defined as:

$$X_t = \sum_{i=1}^{N_t} Y_i, \tag{3.1}$$

where $\{N_t\}_{t\geq 0}$ is homogeneous Poisson process with the intensity parameter λ and Y_i are independent and identically distributed (i.i.d.) the random variables. The process N_t can be considered as the moments of loaders' arrivals to the dumping point. To estimate parameters of the N_t process we use times between consecutive discharges, which will be called *waiting times*. The amount of ore discharged by the loader will be treated as the random variable Y described

by a distribution function and called *increments*. In that approach two tasks are essential:

- estimation of intensity λ of the homogeneous Poisson process $\{N_t\}_{t\geq 0}$ based on real data,
- fitting the distribution of compound Poisson process increments Y_i and estimation of its parameters.

Generally, the continuous-time stochastic process $\{N_t\}_{t\geq 0}$ is homogeneous Poisson process (HPP) with the intensity parameter $\lambda > 0$ if (Cizek, Härdle, and Weron 2005):

- $\{N_t\}$ is the counting process,
- the waiting times are independent and identically exponentially distributed.

To solve above problems it is needed to analyze the real data of the weight of ore supplied on the conveyor belt. The data acquired from the weight measurement system installed on the conveyor belt of ID $L413$ will be taken to show the results of the proposed methodology. This conveyor is not supplied by any other conveyor or any bunker, moreover it is supplied by only one grid. Its length is equal to 830 and the nominal speed is 2m/s. The available data include the measurements of weight from November 2015 to March 2016. To use collected data it is necessary to clean acquired signals from outliers observations and measurement errors. All pre-processing procedures will be described in the next section.

3.1.2 Real data pre-processing

The pre-processing procedures will be showed on the example of weight data from March 2016. The raw data are presented in Fig. 3.1. The measurement system acquires cumulative weight of ore mass transported through the conveyor scale. As one can see the outliers values are present in the plot of weight, thus it is needed to eliminate them before further analysis. For this purpose the raw data was differentiated (Fig. 3.2a). Moreover values bigger than 1 are also set to zero. The data after pre-processing is presented in Fig. 3.3. First conclusion from the visual analysis of cleaned data is that the ore is not constantly supplied on the conveyor belt. One can notice the breaks in work at Sundays ($6th$, $13th$, $20th$, $27th$ of March), moreover the regular stoppage of conveyor belt are related to blasting (about 6 a.m. and 6 p.m.). In the zoomed plot of the differentiated data (Fig. 3.2b) one can see the ,,1 ton" value, which are related to cyclic discharging ore from the loader. To clean data from the measurement errors, all negative values of differentiated weight data were set to zero.

Next step of the pre-processing will be an extraction of the times between consecutive arrivals of the loaders to the dumping point. It is strictly associated with the ore appearance on the conveyor belt. Let us consider exemplary data from one shift. In Fig. 3.4b it is showed data acquired during second shift at $10th$ of March 2016. The difference between consecutive discharges was at least 50 seconds. That approach allows to determine the moments of discharging starts which are marked in Fig. 3.4b. The sum of differentiated weight between two consecutive discharges are treated as weight of ore mass supplied on the conveyor belt by one loader.

The obtained data of waiting times and weights are presented in Fig. 3.5. For further analysis there were taken only with waiting times less than 1500 seconds (25 min.) and weights higher than 1 ton and less than 40 tons. In view of reality in the mine, the other observations were determined incorrectly by the algorithm. Namely, the waiting times longer then 25 min. correspond

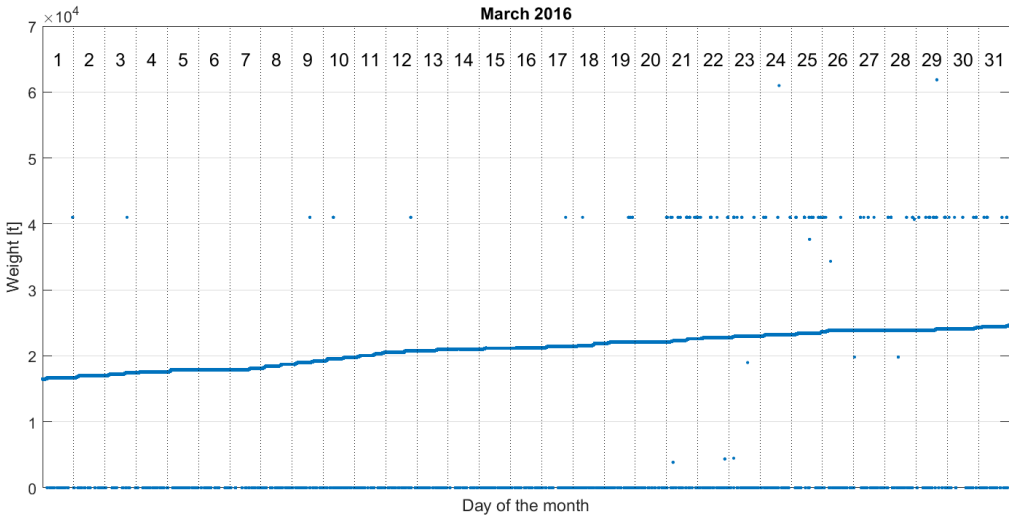

Figure 3.1: Raw weight data from $L413$ conveyor belt (March 2016)

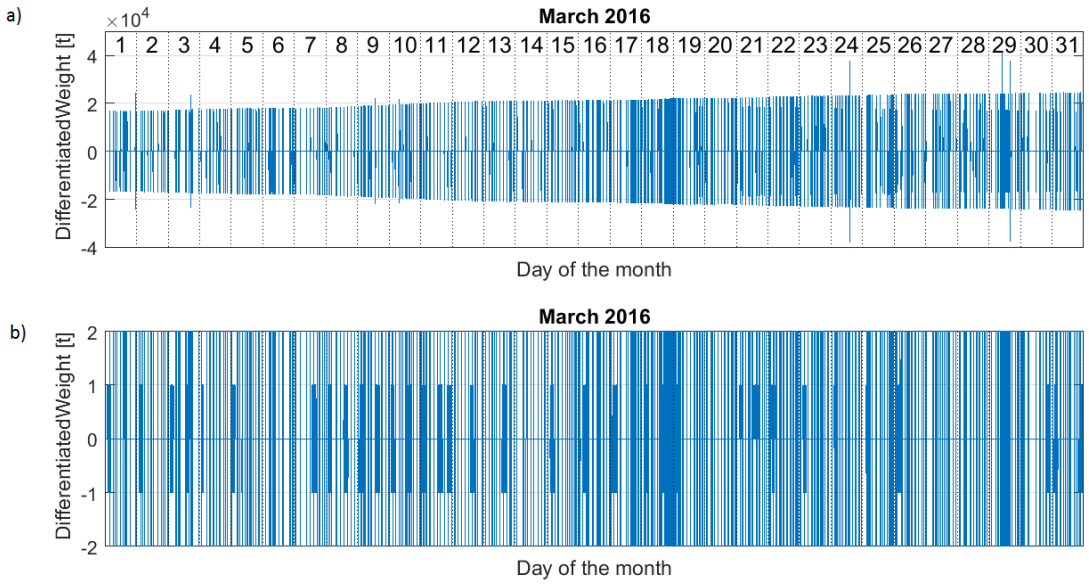

Figure 3.2: Differentiated weight data from $L413$ conveyor belt (March 2016): a) normal view, b) zoomed view.

to the blasting or the shift change, then clearly the ore can not be transported. Long breaks are deterministic or are related to break downs. Moreover, typically loader transport at least 3 tons of the ore and significantly less than 40 tons. The data obtained this way is a starting point to solve the problem of estimation intensity of Poisson process $\{N_t\}_{t\geq 0}$ and fit the distribution of compound Poisson process increments Y_i.

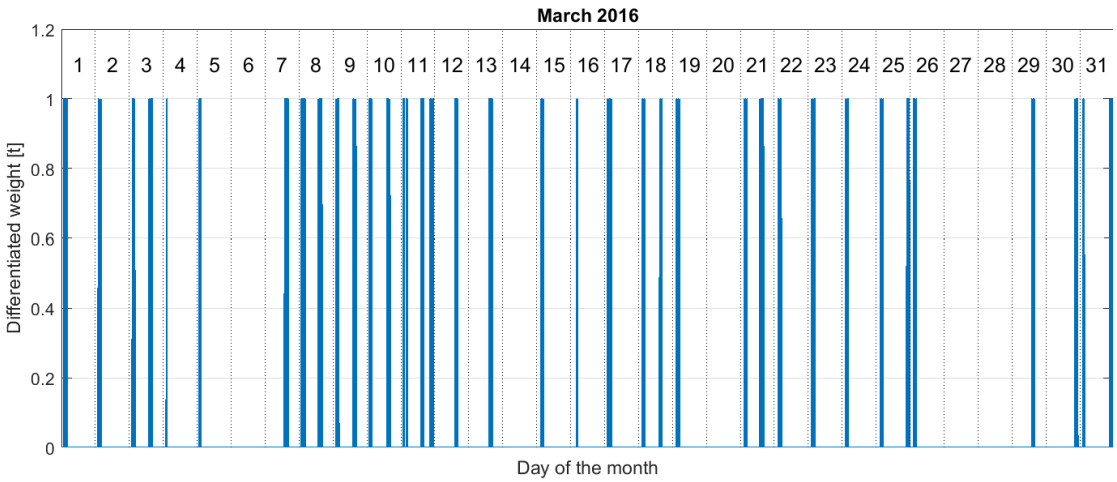

Figure 3.3: Cleaned differentiated weight data from $L413$ conveyor belt (March 2016).

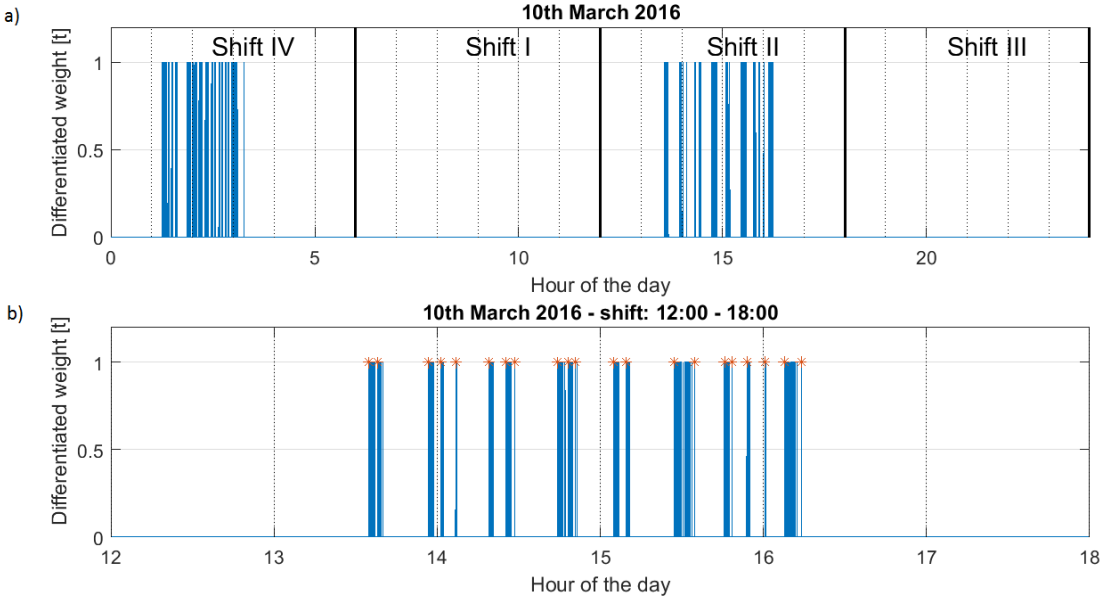

Figure 3.4: Differentiated weight data from $L413$ conveyor belt: a) data acquired from $10th$ March 2016, b) data acquired from II shift at $10th$ of March 2016. The moments of beginnings of discharging are marked by red stars.

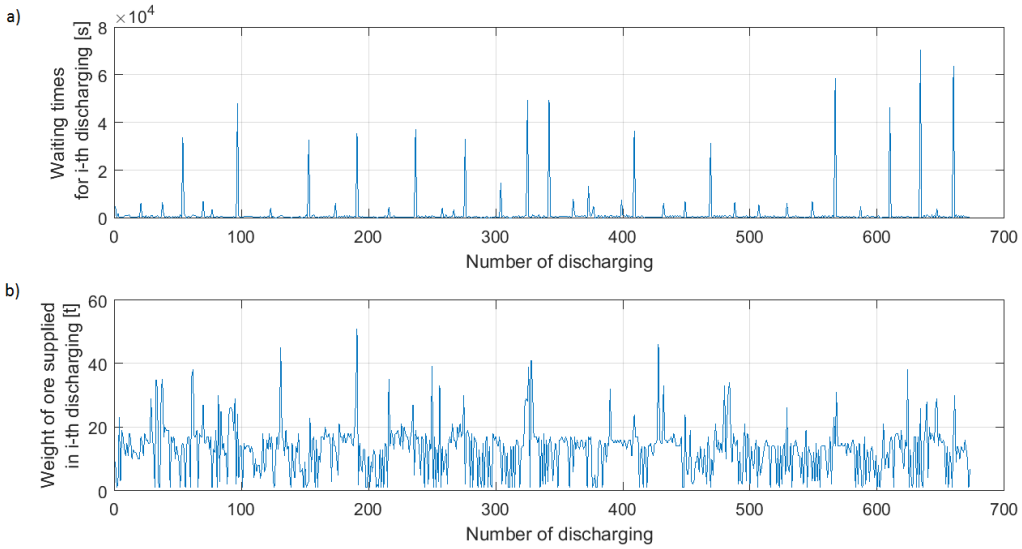

Figure 3.5: a) Waiting times for *i*-th discharges, b) weight of ore mass supplied on the conveyor in *i*-th discharge.

3.1.3 Estimation of intensity of the Poisson process $\{N_t\}_{t\geq 0}$

The estimation of the intensity λ of the Poisson process $\{N_t\}_{t\geq 0}$ starts with by fitting a kernel density estimator to waiting times data from each month from the period between November 2015 and March 2016. As one can see in Fig. 3.6a the shape of the kernel density estimator is similar for different months. It may suggest that variables describing behaviour of waiting times have the same distribution. The differences between particular months are reflected only in the parameters of this distribution.

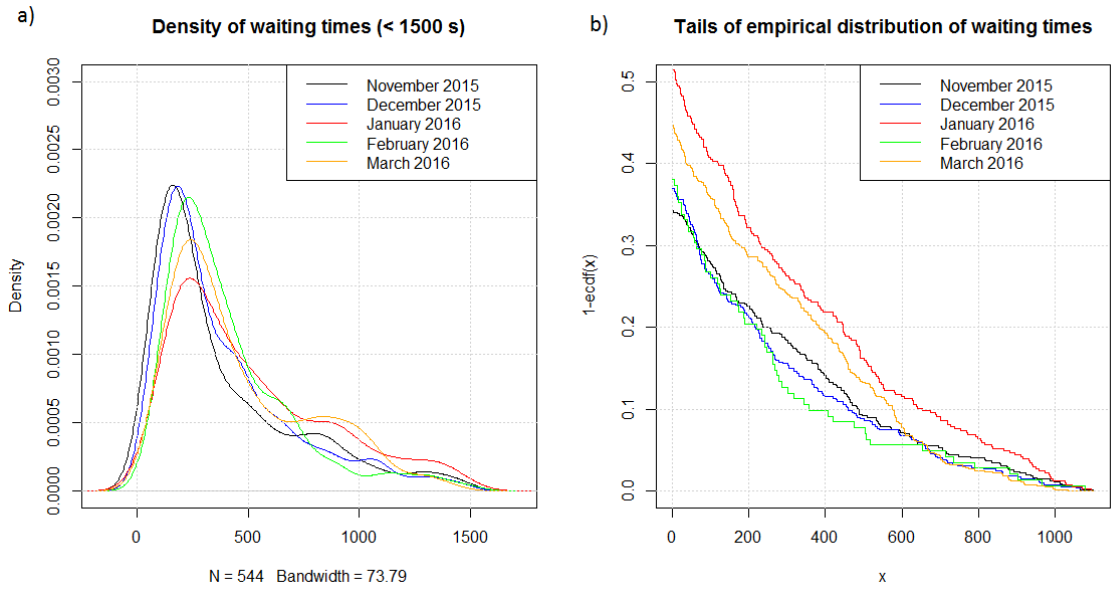

Figure 3.6: For waiting times of each month between November 2015 and March 2016 there are presented: a) fitted kernel density estimator and b) tails of empirical distribution function

The variable describing distances between two consecutive points of a homogeneous Poisson process are exponentially distributed with the intensity parameter $\lambda > 0$. The cumulative distribution function in that case is defined as (Cizek, Härdle, and Weron 2005):

$$F(t) = 1 - e^{-\lambda t}, \quad t > 0. \tag{3.2}$$

Remind that in our case the described variable is related to the waiting times. One of the solutions for estimation the intensity parameter λ is fitting the exponential function $f(x) = ae^{-bx}$ to the tail of the empirical distribution function, which is defined as follows (Cizek, Härdle, and Weron 2005):

$$\hat{F}_n(t) = \frac{1}{n}\sum_{i=1}^{n} 1_{\{x_i \leq t\}}, \tag{3.3}$$

where x_i is the i-th observation. Now it is easy to define the tail of the empirical distribution function as $1 - \hat{F}_n(t)$.

The tails of the empirical distribution function from real data are showed in Fig. 3.6b. The non-linear least squares method (Bates and Watts 1988) was used to fit exponential function to the tail of empirical distribution function. The results of the analysis are presented in Fig.

3.7. The estimated b parameters of exponential function for different months are the same and equal 0.003. The values of a parameter are close to 1, so the assumption about exponential distribution of tails is fulfilled. Therefore the intensity estimator $\hat{\lambda}$ of the homogeneous Poisson process is equal to the estimated parameter b equals 0.003.

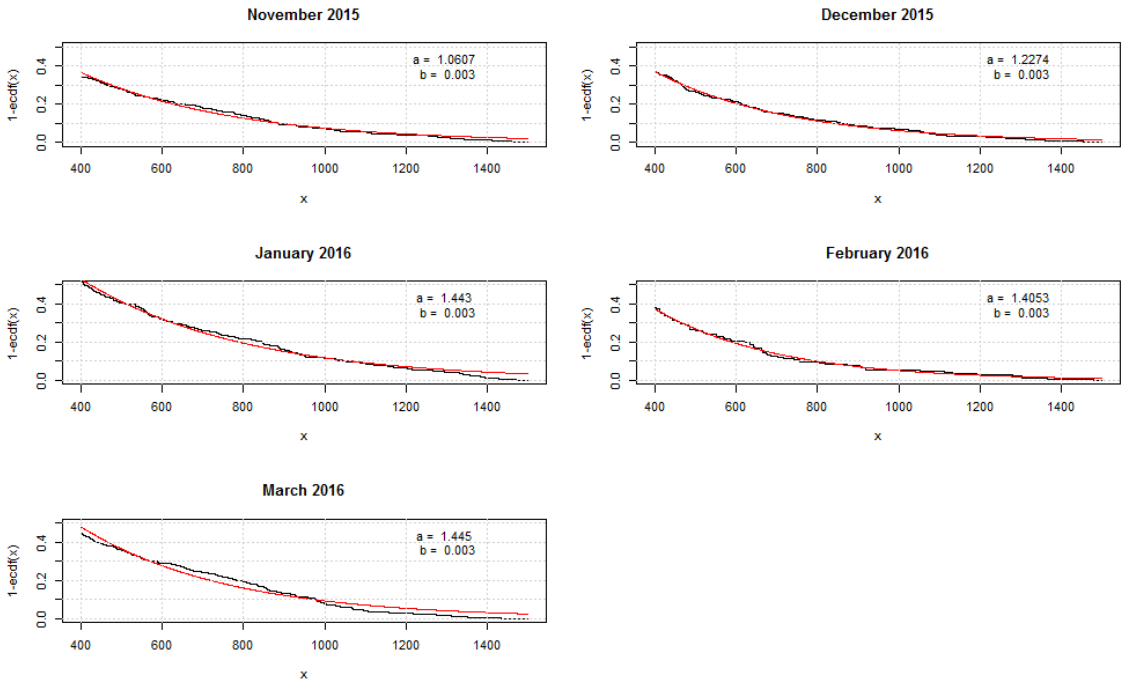

Figure 3.7: Fitted exponential function $f(x) = ae^{-bx}$ (red line) to the tails of empirical distribution function (black line) related to data from each month between November 2015 and March 2016. Estimators of a and b parameters are showed on the plots.

3.1.4 Estimation of the compound Poisson process increments

Assuming that analysed signal follows compound Poisson process the increments Y_i are i.i.d. random variables. Clearly, the proper distribution has to be fitted to the data. Analysed data sample consists of ore mass, which flow through the grid. Obviously, the mass cannot be smaller than zero, hence only non-negative distribution can be fitted. In modelling process we tried to fit some positive distributions. Let us firstly recall some of the well-known distributions that can be useful in this case.

Let Z be a Gaussian random variable with mean equals to μ and variance σ^2. Then the random variable $X = \exp(Z)$ is log-normal. Its probability density function (pdf) $f_X(x)$ and cumulative distribution function (cdf) $F_X(x)$ are given by following equations:

$$f_X(x) = \frac{1}{x\sigma\sqrt{2\pi}} \exp\left(-\frac{(\ln(x)-\mu)^2}{2\sigma^2}\right),$$

$$F_X(x) = \frac{1}{2} erfc\left(-\frac{\ln(x)-\mu}{\sigma\sqrt{2}}\right),$$

where $x > 0$, $\mu \in \mathbb{R}$, $\sigma > 0$ and $erfc(x) = \frac{2}{\sqrt{\pi}} \int_x^\infty e^{-t^2} dt$ is the complementary error function. When the parameter σ is small the log-normal distribution can be similar to normal one. On the other hand, for large σ the tails are semi-heavy (Cizek, Härdle, and Weron 2005).

The second analysed distribution was the Gamma one. It is described by two parameters shape $k > 0$ and scale $\theta > 0$, then the probability density function and cumulative distribution function are following:

$$f_X(x) = \frac{1}{\Gamma(k)\theta^k} x^{k-1} \exp\left(-\frac{x}{\theta}\right),$$

$$F_X(x) = \frac{1}{\Gamma(k)} \gamma\left(k, \frac{x}{\theta}\right),$$

where $x > 0$, $\Gamma(\cdot)$ is a gamma function and $\gamma\left(k, \frac{x}{\theta}\right) = \int_0^{\frac{x}{\theta}} t^{k-1} e^{-t} dt$ is a lower incomplete gamma function. It is worth mentioning that the sum of k i.i.d. exponentially distributed random variables $\sum_{i=1}^k X_i$ follows Gamma distribution with shape parameter k and scale λ^{-1}, where λ is an intensity of the X_i.

Another non-negative distribution, which we tried to fit, is the Weibull distribution. It also depends on two positive parameters: λ - scale and k - shape. For $x \geq 0$ the probability density function and the cumulative distribution function are given by the formulas:

$$f_X(x) = \frac{k}{\lambda}\left(\frac{x}{\lambda}\right)^{k-1} \exp\left(-\left(\frac{x}{\lambda}\right)^k\right),$$

$$F_X(x) = 1 - \exp\left(-\left(\frac{x}{\lambda}\right)^k\right).$$

In case of $k = 0$ the Weibull distribution reduces to the exponential one.

Finally, let us present the three parameters family of positive Burr distribution. Its probability

density function and cumulative distribution function are:

$$f_X(x) = \frac{\frac{kc}{\alpha}\left(\frac{x}{\alpha}\right)^{c-1}}{\left(1+\left(\frac{x}{\alpha}\right)^{c}\right)^{k+1}},$$

$$F_X(x) = 1 - \frac{1}{\left(1+\left(\frac{x}{\alpha}\right)^{c}\right)^{k}},$$

where $x > 0$, $\alpha > 0$ is the scale parameter, $c > 0$ and $k > 0$ are the shape parameters. This distribution is very flexible and can express many types of real data. The limit distribution when $k \to \infty$ is the Weibull one (Tadikamalla 1980).

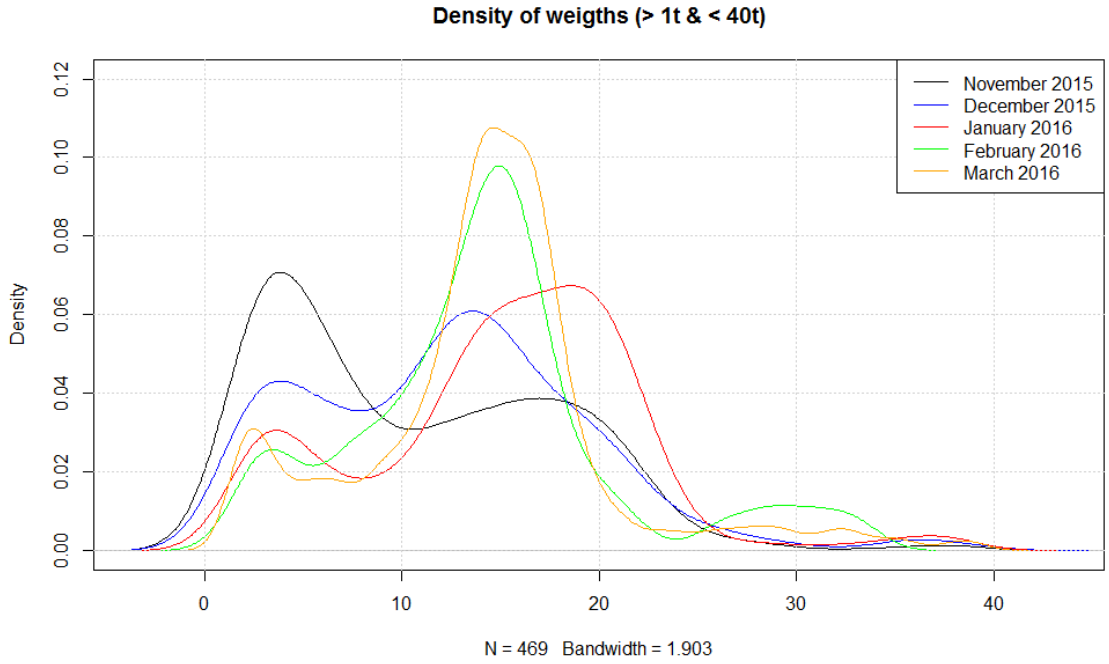

Figure 3.8: The fitted kernel density estimator for the weights in tons distribution for each month between November 2015 and March 2016. The weights smaller than 1 ton and bigger than 40 tons are ignored.

In Fig. 3.8 there are presented the kernel density estimators for the weights distribution. One can observe that the densities significantly differ for each month. Furthermore, they are bimodal, hence none of the previously introduced distribution can be fitted directly. In order to overcome this problem we would like to analyze the mixture of the distributions. Namely, let us assume that X is a random variable which probability distribution function $f_X(x)$ is following:

$$f_X(x) = pg_1(x) + (1-p)g_2(x), \tag{3.4}$$

where $p \in [0,1]$ is a mixing parameter, $g_1(x)$ and $g_2(x)$ are the probability distribution functions. One can observe that it is a linear combination of two other probability distribution functions.

Clearly the similar relation can be observed in the cdf:

$$F_X(x) = pF_1(x) + (1-p)F_2(x), \tag{3.5}$$

where $F_1(x)$ and $F_2(x)$ are the cumulative distribution functions related to g_1 and g_2 respectively. Using such mixing techniques we are able to create a wide class of the distributions. Each distribution with the explicit form of pdf can be applied. Moreover, as one can expect it is possible to create bimodal density functions.

The parameter estimation for such mixture of distributions can be performed with Maximum Likelihood Estimation (MLE) method. For the vector of independent observation $x = (x_1, \ldots, x_n)$ and the set of the distribution parameters θ the estimation is done by maximizing the log-likelihood function:

$$\max_{\theta} \{L(\theta)\} = \max_{\theta} \left\{ \sum_{i=1}^{n} \tilde{f}(x_i; \theta) \right\}.$$

The method can be easily applied for the distribution with known pdf. In Fig. 3.9 there is

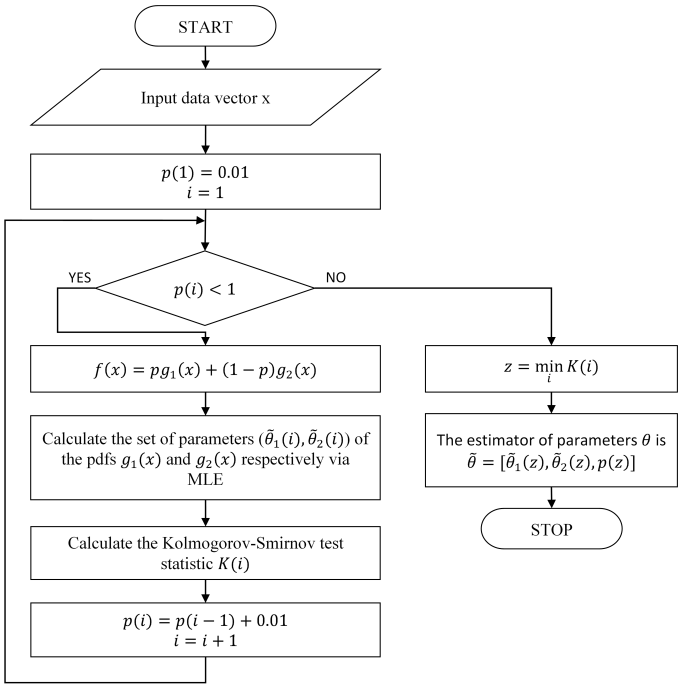

Figure 3.9: Flowchart of the estimation method for the mixture of the densities parameters

presented a flowchart of the estimation method. One can observe that MLE method is used to estimate the set of parameters for densities $g_1(x)$ and $g_2(x)$ with a priori given value of the mixing parameter p. In order to find the best p the Kolmogorov-Smirnov test is performed. The test statistics is defined as:

$$K(\theta, p) = \max_{x} \{|F_E(x) - F_T(x)|\},$$

where $F_E(x)$ is the empirical cumulative distribution function and $F_T(x)$ is the fitted theoretical

cdf. The statistic measures the maximum distance between the theoretical and empirical cdf. Hence, minimizing the value of the $K(\theta, p)$ we are able to chose the best value for the mixing parameter. This procedure allows us to fit the bimodal distribution to the data.

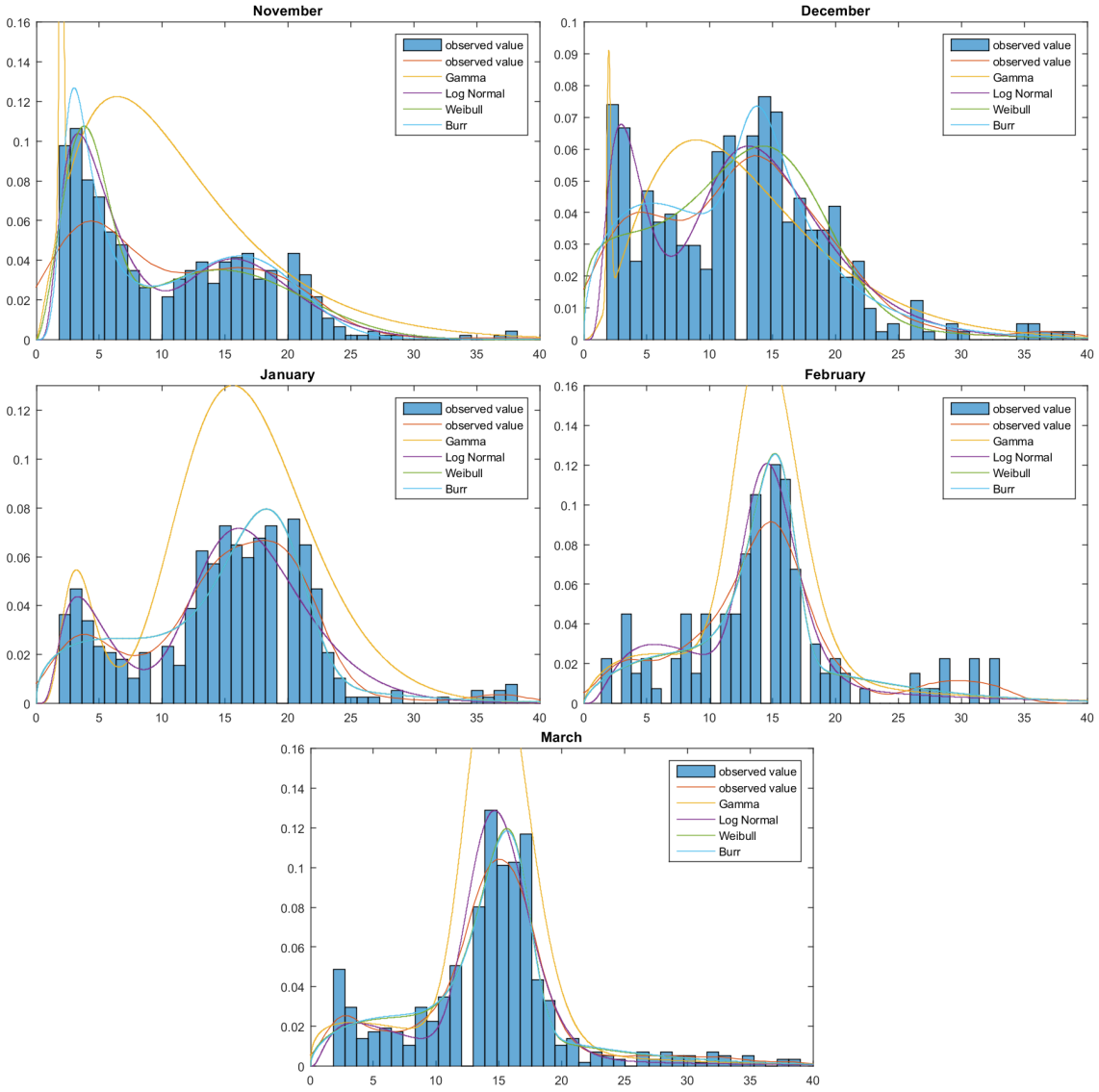

Figure 3.10: Comparison of histograms for real data, kernel density estimators and several mixtures of fitted distributions.

In Fig. 3.10 the fitted densities are presented and compared with the normalized histogram and the kernel density estimator. Some of the distributions explain the data really good. Indeed, especially mixture of log-normal and Weibull distributions fit to the observation. They are able to detect both modes in the data. Interestingly, in March 2016 the result for Weibull and Burr cases are almost similar. One can observe that only mixture of Gamma distributions significantly differs from the real data.

In order to ensure the correctness of the fitting, the statistical tests can be performed. Obviously, the Kolmogorov-Smirnov test can be applied. Let us also recall three other tests based on the empirical distribution function: Kuiper test, Cramer-von Mises test and Anderson-Darling

test. Let us assume that $F(x)$ is a true cdf of the random variable X and $z_i = F(x_i)$, where Z is uniformly distributed on $(0, 1)$ and z_i is a realization of Z. Then the distance between empirical cdf of z_i and uniform distribution are the same as for empirical cdf of x_i and its true cdf (Cizek, Härdle, and Weron 2005) for any $i = 1, \ldots, n$. This fact can be used in computation of the test statistics. Let us assume that $z_{(1)} < \cdots < z_{(n)}$ are the order statistics of z then the test statistics (V- Kuiper, W^2-Cramer-von Mises, A^2-Anderson-Darling) are following:

$$V = \max_{1 \le i \le n} \left\{ \frac{i}{n} - z_{(i)} \right\} + \max_{1 \le i \le n} \left\{ z_{(i)} - \frac{i-1}{n} \right\},$$

$$W^2 = \sum_{i=1}^{n} \left(z_{(i)} - \frac{2i-1}{2n} \right)^2 + \frac{1}{12n},$$

$$A^2 = -n - \frac{1}{n} \sum_{i=1}^{n} \left[(2i-1) \log z_{(i)} + (2n+1-2i) \log(1 - z_{(i)}) \right].$$

Having four statistical tests we are able to compare the results for different distributions. In order to calculate test p-value, the Monte Carlo method can be applied. Namely, the n-long random vector from assumed distribution with estimated values of parameters is generated 10000 times. Then for each random vector the test statistics are computed and compared to the test statistics for real data. The p-value is given by equation:

$$p - value = \frac{\#(TS_i > TR)}{10000},$$

where TS_i is a test statistics for $i-$th random vector and TR is a test statistics for real data. The output of the test for each month is presented in Tab.3.1. For November, January, Febryary and March the best results are obtained for mixture of Weibull distributions. Only in December 2015 the mixture of log-normal fits the data significantly better. It is worth mentioning that expect November 2015 the p-values are high and there is no evidence to reject the hypothesis that our data sample is following the mixture of Weibull distributions (or log-normal in December 2015). The test results ensure us that the fit of mixture of two positive distributions can by beneficial in case of modelling the ore weight.

Table 3.1: Test statistics and the p-value for different mixing distributions and estimation performed by algorithm presented in Fig.3.9.

Mix distribution	K	p-val	V	p-val	W^2	p-val	A^2	p-val
November 2015								
Gamma	2.13	0.00	4.05	0.00	1.09	0.00	7.19	0.00
log-normal	1.48	0.01	2.46	0.00	0.35	0.13	2.28	0.03
Weibull	1.42	0.03	2.82	0.00	0.38	0.06	2.99	0.02
Burr	1.30	0.04	2.58	0.00	0.20	0.21	2.05	0.05
December 2015								
Gamma	2.07	0.00	4.00	0.00	0.95	0.00	8.73	0.00
log-normal	1.02	0.20	2.02	0.00	0.15	0.40	1.38	0.26
Weibull	1.28	0.03	2.35	0.00	0.28	0.06	2.25	0.01
Burr	1.13	0.09	2.11	0.00	0.18	0.23	1.59	0.08
January 2016								
Gamma	1.45	0.00	2.94	0.00	0.45	0.01	3.04	0.00
log-normal	1.26	0.03	2.51	0.00	0.25	0.09	1.99	0.03
Weibull	1.02	0.30	2.01	0.01	0.17	0.37	1.26	0.24
Burr	1.02	0.40	2.01	0.00	0.17	0.54	1.26	0.44
February 2016								
Gamma	1.08	0.49	1.73	0.10	0.12	0.83	0.69	0.86
log-normal	0.93	0.46	1.45	0.37	0.09	0.76	0.72	0.68
Weibull	0.72	0.62	1.43	0.21	0.08	0.64	0.56	0.70
Burr	0.72	0.51	1.43	0.12	0.08	0.49	0.54	0.45
March 2016								
Gamma	2.11	0.00	3.41	0.00	0.48	0.05	2.71	0.05
log-normal	1.78	0.00	3.55	0.00	0.54	0.00	3.88	0.00
Weibull	1.55	0.06	3.11	0.00	0.42	0.34	2.43	0.40
Burr	1.59	0.00	3.11	0.00	0.44	0.03	2.57	0.02

3.1.5 Simulation of compound Poisson process

As it was mentioned in section 3.1.1 the aim of the analysis is to model the process of ore flow on the grid using compound Poisson process defined by:

$$X_t = \sum_{i=1}^{N_t} Y_i.$$

In section 3.1.3 the process $\{N_t\}_{t>0}$ was identified as homogeneous Poisson process with the intensity $\lambda = 0.003$. Moreover, in section 3.1.4 the assumption about bimodal probability distribution function of variable Y_i was confirmed. In the simulation two scenarios were analysed, where the weight data were modeled by:

- mixture of log-normal distributions (I scenario),
- mixture of two distributions the best fitted to the data basing on results of statistical tests presented in Tab. 3.1 (II scenario).

To validate proposed mixed model the simulations were carried out. For simulation of the compound Poisson process on the interval $[0, T]$ the following algorithm can be used (Tankov 2003):

1. Initialize $k = 0$.
2. Repeat while $\sum_{i=1}^{k} T_i < T$
   (a) Set: $k = k + 1$.
   (b) Simulate $T_k \sim exp(\lambda)$.
   (c) Simulate Y_k from the distribution F_Y (in our case: mixture of distributions)

The trajectory of the simulated compound Poisson process is given by:

$$X_t = \sum_{i=1}^{N_t} Y_i, \;\; where \;\; N_t = sup\{k : \sum_{i=1}^{k} T_i \leq t\}.$$

The simulation of increments random variable Y can be performed by composition method. Namely, when the pdf of Y is

$$f_Y(x) = pg_1(x) + (1-p)g_2(x),$$

where p is a parameter and $g_1(x)$ and $g_2(x)$ are the pdfs. Moreover, we know how to simulate the random variable X_1 which pdf is $g_1(x)$ and X_2 which pdf is $g_2(x)$. The algorithm for simulation of Y is following:

1. Generate a discrete random variable $I \in \{1, 2\}$.
2. $P(I = 1) = p$ and $P(I = 2) = 1 - p$.
3. Generate X_I with pdf g_I.
4. Return $Y = X_I$.

The simulation results will be conducted for one shift time interval, namely 6 hours between 12 a.m. and 6 p.m. It should be mentioned specific behaviour of data during the shift. At the beginning and the end of the shift in most cases the ore is not discharging on the conveyor belt. That observation based on real data could be connected with the change of the crew for the next shift. Due to that the compound Poisson process was simulated between 1:30 p.m. and

4:30 p.m. We assumed that during first and last one and half of hour of the shift there is no supplies on the conveyor belt.

I scenario

In the first scenario we assumed that the variable Y_i is modeled by bimodal probability distribution function composed of two log-normal distributions mixed by parameter p. The best distribution parameters were determined using MLE. The results of the analysis are showed in Tab. 3.2. Using the estimated parameters, for each month there were simulated 50 trajectories. Moreover, basing on the simulated data the quantile lines of order 0.05 and 0.95 were determined. The results of the simulation are presented in Fig. 3.11. Moreover, on the plot are added three exemplary trajectories from real weight data related to work of the conveyor belt during the second shift (respectively for each month). Such plot can be a visual validation of the proposed model.

Table 3.2: Estimated parameters of bimodal probability density function for different months for mixture of two log-normal distributions.

Month	p	μ_1	σ_1	μ_2	σ_2
November 2015	0.61	1.55	0.59	2.84	0.25
December 2015	0.29	1.24	0.51	2.69	0.34
January 2016	0.24	1.51	0.57	2.85	0.26
February 2016	0.45	2.35	0.79	2.70	0.14
March 2016	0.27	2.11	0.92	2.71	0.16

According to Fig. 3.11 one can observe that not all of the real trajectories are between the quantile lines. This drawback can be caused by the fact that the real trajectories start in different time points and we always assume that it is equal to 1:30 p.m. The drawing the moment of starting work from the fitted distribution may improve the results. Moreover, according to Tab. 3.1 the mixture of log-normal distributions is the best only for December 2015. For that reason we showed below the results of simulation for the best mixture of distributions selected by using statistical tests (II scenario).

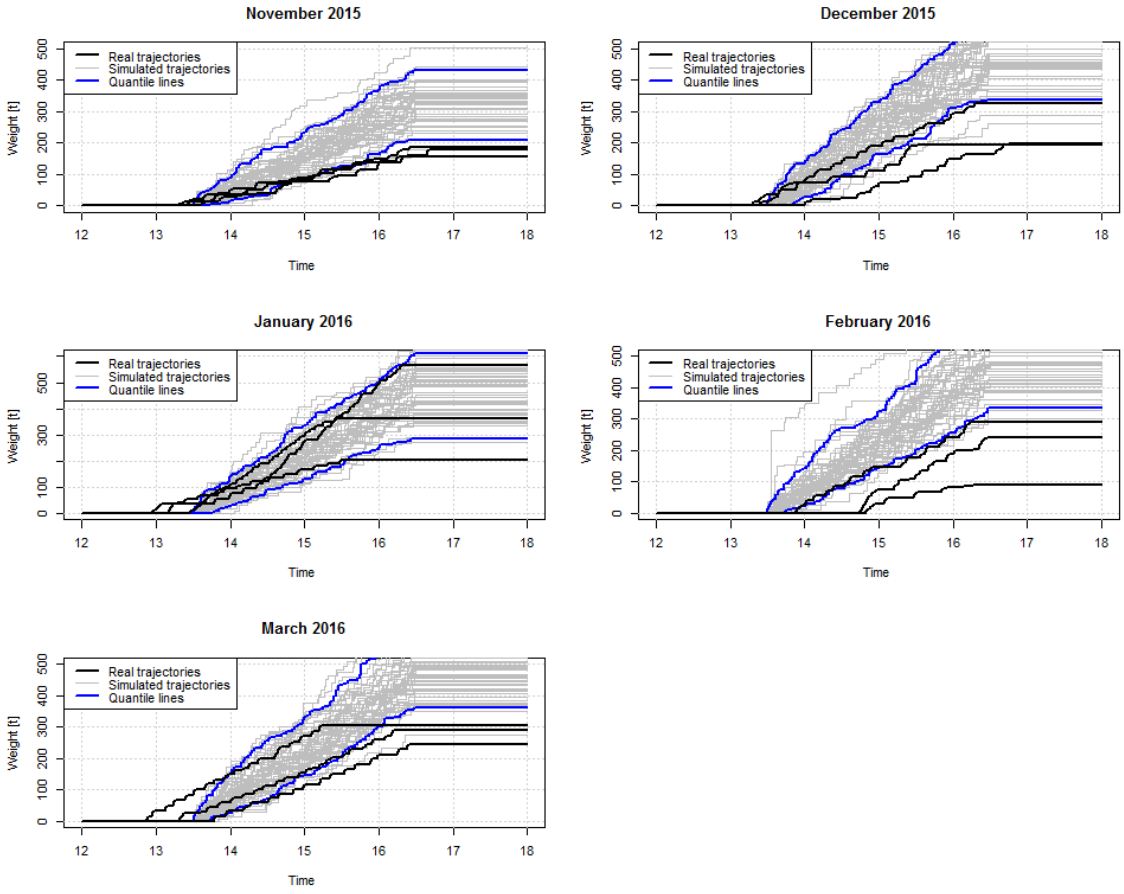

Figure 3.11: Simulated trajectories for mixture of log-normal distributions determined in Tab. 3.2 for each month between November 2015 and March 2016 (gray lines), quantile lines of order 0.05 and 0.95 (blue lines) and real data trajectories (black lines).

II scenario

In the II scenario we also assumed that the variable Y_i has bimodal probability distribution function, but as was mentioned in that case the best mixture of distributions were selected basing on results of statistical tests (Tab. 3.1 in section 3.1.4). For each month and the best selected mixture of distributions there were estimated parameters using MLE. The summary of the analysis is presented in Tab. 3.3. Similarly to the first scenario, basing on the estimated parameters of mixture of distributions, the 50 trajectories were simulated. The results are showed in Fig. 3.12 together with the quantile lines of order 0.05 and 0.95 and three exemplary trajectories from real weight data related to work of the conveyor belt during the second shift (respectively for each month).

Table 3.3: Estimated parameters of bimodal probability density function. For each month the best distribution was chosen according to statistical tests.

Month	**Mixing distribution**	**Parameters**				
November 2015	Weibull	p 0.45	λ_1 4.52	k_1 2.53	λ_2 17.17	k_2 2.77
December 2015	log-normal	p 0.29	μ_1 1.34	σ_1 0.51	μ_2 2.69	σ_2 0.34
January 2016	Weibull	p 0.47	λ_1 13.19	k_1 1.42	λ_2 19.92	k_2 6.50
February 2016	Weibull	p 0.53	λ_1 15.96	k_1 1.63	λ_2 15.40	k_2 9.29
March 2016	Weibull	p 0.48	λ_1 14.76	k_1 1.47	λ_2 15.90	k_2 8.50

Similarly to I scenario, in case of using the best mixture of distributions some of the trajectories are not between the quantile lines (Fig. 3.12). However, the results are slightly better, although there is still a problem with the indication of work starting point. In order to improve the results it should not be fixed. Further analysis of that problem may be related to fitting the distribution of the time points of the start and the end of conveyor belt's work during the shift based on real data. If we have had the distribution, we could have extended the model of ore flow by drawing the time of the beginning of discharging the ore on the conveyor belt and the drawing the moment when that process ends.

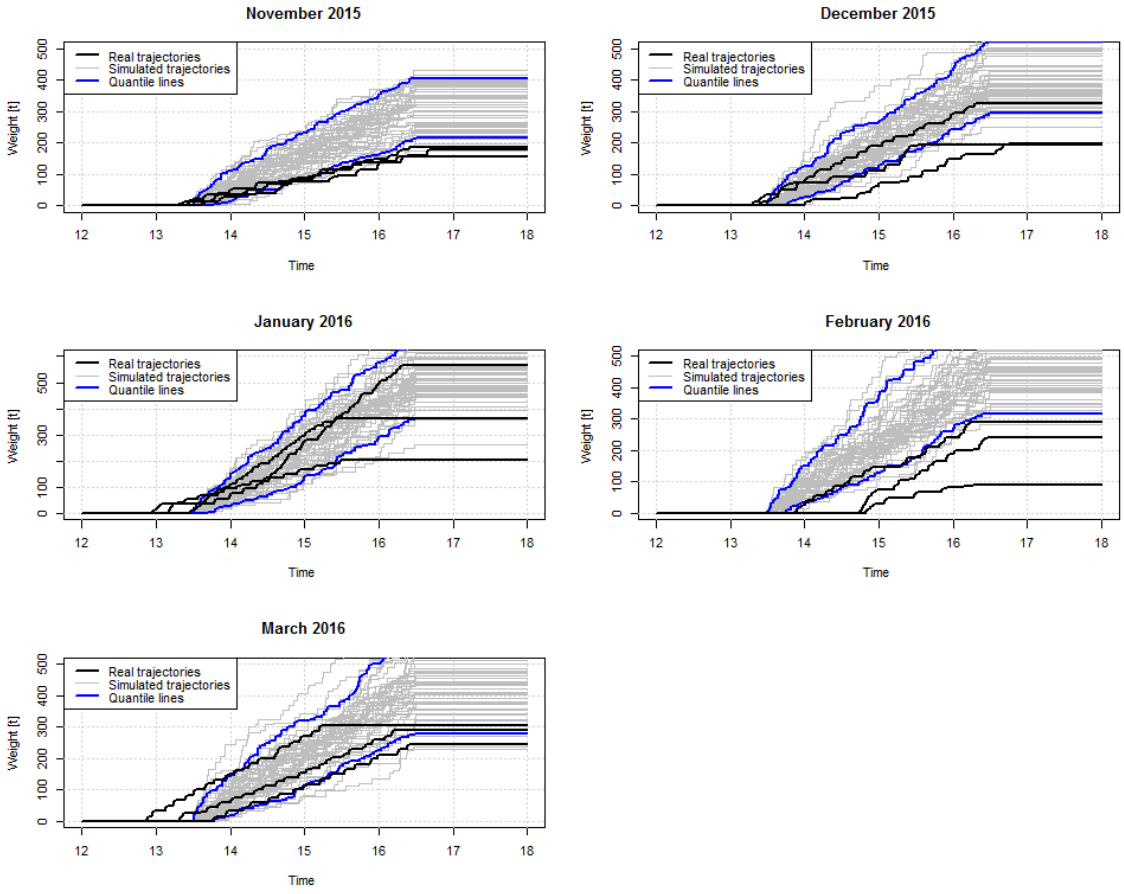

Figure 3.12: Simulated trajectories for mixture of distributions determined in Tab. 3.3 for each month between November 2015 and March 2016 (gray lines), quantile lines of order 0.05 and 0.95 (blue lines) and real data trajectories (black lines).

3.1.6 Conclusions

In this report there was considered the problem of modeling the process of loaders' arrivals to the dumping point and the mass of the ore supplied on the conveyor belt. The compound Poisson process was considered as a mathematical tool to describing that stochastic process. Firstly, we pre-processed weight data from the conveyor belt to obtain information about waiting times between two consecutive loaders' arrivals and the discharged ore mass. Then the homogeneous Poisson process was identified as a process modeled of the waiting times. Based on the fitted exponential function to the tail of the empirical distribution function, the intensity parameter was estimated. The next step was to identify the distribution of the variable described supplied ore mass. Since the kernel density estimator fitted to the real weight data revealed the bimodal probability distribution function, we considered the mixture of the different distributions with the mixing parameter p. The best mixture of distributions were selected by statistical test and their parameters were estimated using MLE. To validate proposed model of compound Poisson process the simulated trajectories were compared with exemplary real data trajectories. The analysis were carried out for available data from the $L413$ conveyor belt related to the five month period of time between November 2015 and March 2016.

3.2 Continuous charging - retention bunker

3.2.1 Introduction

The observed ore mass which occurs on belt conveyor can be contained in separable heaps or in relatively constant ore mass flow. First issue primarily characterise the case when the ore comes directly from dumping point, and the second one characterise the event when the ore comes from the retention bunker. The retention bunker task is to fulfil one of following purposes:

- equalise the level of ore mass flow,
- provide the constant character of ore mass flow,
- store the mined ore in place where the haulage changes from district to main.

In this report the problem of modelling a behaviour of mined rock which comes from retention bunker is undertaken. It will be shown that in general, the process describing how the flow of ore mass falls from retention bunker can be modelled with comparatively low order ARMA process . The base for this report analysis are recordings from belt conveyor L212 from Polkowice - Sieroszowice copper ore mine which transports ore mass from retention bunker. The belt conveyor is equipped with a weight which collects the data describing temporary mass. The data consist of periods that have stationary or changing character and in this report only the stationary ones will be considered (as with high probability they describe ore from retention bunker). To validate the results couple exemplary segments with relatively constant temporary mass will be analysed.

3.2.2 Methodology

In this section all essential definitions and algorithms which were the part of the analysis are included.

Definition 1. (Brockwell and Davis 2006)
Time series $\{X_t\}$ is **weakly stationary** if

1. $\mu_X(t)$ is independent of t,
2. $\forall h$, $\gamma_X(t+h,t)$ is independent of t,

where $\mu_X(\cdot)$ and $\gamma_X(\cdot,\cdot)$ are mean and covariance function respectively.

In the following part of this report, whenever the term 'stationary' is used in time series context it means that the time series is weakly stationary.

Definition 2. (Brockwell and Davis 2006)
The time series $\{X_t\}$ is an **ARMA(p,q) process** if it is stationary and $\forall t$ it satisfies

$$X_t - \phi X_{t-1} - ... - \phi_p X_p = Z_t + \theta_1 Z_{t-1} + ... + \theta_q Z_{t-q},$$

where $\{Z_t\} \sim \text{WN}(0,\sigma^2)$ and polynomials $1-\sum_{i=1}^{p}\phi_i z^i$ and $1+\sum_{i=1}^{q}\theta_i z^i$ do not posses common factors.
Classical ARMA version assumes that $\{Z_t\} \sim \mathcal{N}(0,\sigma^2)$

Theorem 1. (Brockwell and Davis 2006)
Stationary solution of $X_t - \phi X_{t-1} - ... - \phi_p X_p = Z_t + \theta_1 Z_{t-1} + ... + \theta_q Z_{t-q}$ for $\{X_t\}$ exists (and is unique) if and only if

$$\phi(z) = 1 - \phi_1 z - ... - \phi_p z^p \neq 0, \forall |z| = 1.$$

Modelling time series $\{X_t\}$ with ARMA requires $\{X_t\}$ observations being made at fixed constant time intervals, namely $t \in t_0 + k\Delta t$, $k \in \mathbb{N}$, where Δt- time interval. When dealing with time series whose time intervals are varied one can interpolate the values in new time points (which are distributed equally) with e.g. linear interpolation.

Definition 3. (Billingsley 2008) A random variable X with distribution f has **characteristic function** defined as

$$\phi_X(t) = \int_{\mathbb{R}} e^{its} f(s) ds = \mathbb{E} e^{itX}$$

Definition 4. (Samoradnitsky and Taqqu 1994; Weron 2004) A random variable X is from α-stable distribution with parameters:

- α- index of stability ($\alpha \in (0, 2]$)
- β- skewness parameter ($\beta \in [-1, 1]$)
- σ- scale parameter ($\sigma > 0$)
- μ- location parameter ($\mu \in \mathbb{R}$)

if and only if it's characteristic function $\phi_X(t)$ appears as

$$\log \phi(t) = \begin{cases} -\sigma^\alpha |t|^\alpha \{1 - i\beta \text{sign}(t) \tan \frac{\pi\alpha}{2}\} + i\mu t, & \alpha \neq 1 \\ -\sigma |t| \{1 + i\beta \text{sign}(t) \frac{2}{\pi} \log |t|\} + i\mu t & \alpha = 1 \end{cases} \tag{3.6}$$

and it is denoted as $X \sim S_{\alpha,\sigma,\beta,\mu}$

In most cases the form of α-stable random variable's probability density function is unknown in terms of elementary functions (with exceptions: $\alpha = 1$- Cauchy distribution, $\alpha = 2, \beta = 0$- normal distribution, $\alpha = 0.5, \beta = 1$ Levy distribution, $\alpha = 0.5, \beta = -1$ Levy distribution reflection).

Definition 5. The time series $\{X_t\}$ is an **ARMA(p, q) process with α-stable residuals** if it is stationary and $\forall t$ it satisfies

$$X_t - \phi X_{t-1} - ... - \phi_p X_p = Z_t + \theta_1 Z_{t-1} + ... + \theta_q Z_{t-q},$$

where polynomials $1 - \sum_{i=1}^{p} \phi_i z^i$ and $1 + \sum_{i=1}^{q} \theta_i z^i$ do not posses common factors, and $\{Z_t\}$ is a time series of independent identically distributed (i.i.d.) random variables from α-stable distribution.

The problem of evaluating optimal model order is often solved with use of Akaike information criterion (AIC) (Parzen, Tanabe, and Kitagawa 2012). However when dealing with models that has residuals from α-stable distribution one has to use e.g. modified AIC (Kruczek et al. 2016) as the classical one requires to know the form of distribution function. The modified AIC uses approximation of probability distribution function.
The value of AIC is evaluated as follows:

$$AIC = -2 \sum_{i=1}^{N} \log p_{S_{\alpha,\sigma,\beta,\mu}}(Z_i) + 2p,$$

where $p_{S_{\alpha,\sigma,\beta,\mu}}$ is approximated density function, Z_i are residuals of the model, p- number of model parameters. The criterion suggests that the model is optimal when the AIC is minimized.

Definition 6. Let $\{X_t\}$ be a time series which is ARMA process. It's **periodogram** is defined as:

$$I_{n,X}(\lambda) = |\frac{1}{n^{1/\alpha}} \sum_{i=1}^{n} X_t e^{-i\lambda t}|^2,$$

where $-\pi < \lambda < \pi$

To estimate the parameters of ARMA model **Whittle estimator** $\overline{\beta_n}$ is used (Mikosch et al. 1995). The method is universal as it does not require any assumptions about residuals' distribution. The estimator is defined as a value which minimises following function:

$$\hat{\sigma}_n^2(\beta) = \frac{1}{n} \sum_j \frac{I_{n,X}(\lambda_j)}{g(\lambda_j,\beta)},$$

where $\lambda_j = \frac{2\pi j}{n} \in (-\pi, \pi]$, $\beta = (\phi_1, ..., \phi_p, \theta_1, ..., \theta_q)$- ARMA$(p,q)$ estimated parameters, $g(\lambda, \beta) = \frac{|1+\sum_{k=1}^{q} \theta_k e^{-i\lambda k}|^2}{|1-\sum_{k=1}^{p} \phi_k e^{-i\lambda k}|^2}$, $-\pi < \lambda < \pi$.

The parameters of residuals distribution is obtained from following characteristic function relation (Samoradnitsky and Taqqu 1994; Weron 2004):

$$\log(-\log|\phi_X(t)|^2) = \log(2\sigma^\alpha) + \alpha \log|t|,$$

where $\phi_X(t)$- characteristic function of $X \sim S_{\alpha,\sigma,\beta,\mu}$.
The equation above depends only on α and σ which suggests to estimate parameters by regressing $y = \log(-\log|\phi_n(t)|^2)$ on $w = \log|t|$ in the model:

$$y_k = m + \alpha w_k + \epsilon_k, k = 1, 2, ..., K,$$

where $m = \log(2\sigma^\alpha), t_k$ is an appropriate set of real numbers (e.g. $t_k = \frac{\pi k}{25}, k = 1, 2, ..., K$, and K from $\{9, ..., 134\}$ (Koutrouvelis 1980)). When $\hat{\alpha}, \hat{\sigma}$ are obtained, the α, σ are fixed at these values, and the estimates $\hat{\beta}, \hat{\mu}$ can be obtained from

$$\arctan(\frac{Im(\phi(t))}{Re(\phi(t))}) = \mu t + \beta\sigma^\alpha \tan(\frac{\pi\alpha}{2}) sign(t)|t|^\alpha.$$

Next the regressions are repeated with $\hat{\alpha}, \hat{\sigma}, \hat{\beta}, \hat{\mu}$ as initial parameters. The iterations continue until previously fixed convergence criterion is satisfied.

To test the differences between the empirical distribution $F_n(x)$ and the estimated one $F(x;\theta)$ of residuals (θ- estimated parameters' vector) 5 different tests are used (Kolmogorov–Smirnov, Kuiper, Cramer–von Mises, modified Cramer–von Mises, Anderson–Darling). These tests are based on following statistics:

1. $D = max(D^+, D^-) = max(max_{1\le i\le n}\{\frac{i}{n} - z_{(i)}\}, max_{1\le i\le n}\{z_{(i)} - \frac{i-1}{n}\})$,
2. $V = D^+ + D^-$,
3. $W^2 = \sum_{i=1}^{n}\{z_{(i)}, -\frac{2i-1}{2n}\}^2 + \frac{1}{12n}$
4. $U^2 = W^2 - n(\frac{1}{n}\sum_{i=1}^{n} z_{(i)} - \frac{1}{2})^2$
5. $A^2 = -n - \frac{1}{n}\sum_{i=1}^{n}\{\log z_{(i)} + \log(1 - z_{(n+1-i)})\}$,

where $z_{(i)}$ $i = 1, ..., n$ is sample i-th order statistics.

We test the null hiphotesis (Cizek, Härdle, and Weron 2005):

$$H_0 : F_n(x) = F(x; \theta),$$

against the:

$$H_1 : F_n(x) \neq F(x; \theta).$$

Small values of test statistics T (any of previously proposed), for sample from distribution $F(x; \theta)$ confirm H_0, and the large values give evidence to reject the null hipothesis and accept H_1. The decision is to made upon the tests' p-value quantity which is defined as:

$$p\text{-value} = P(T \geq t),$$

where t is statistic's value for sample which distribution is estimated. Common p-value which borders acceptance and rejection of H_0 is 0.05. The probability is estimated with Monte Carlo simulations.
The complete block diagram how the temporary mass data is modelled and simulated with ARMA model with residuals from α-stable distribution is included below.

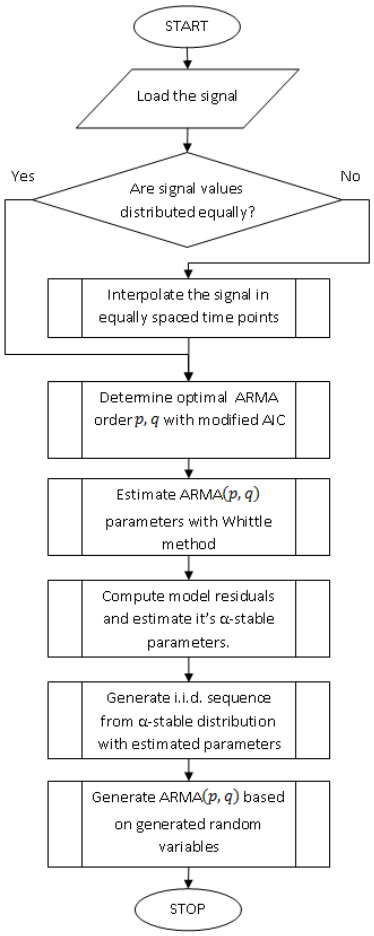

Figure 3.13: AMRA modeling of temporary mass flow data.

Table 3.4: Optimal ARMA order and estimated parameters

Segment	1.	2.	3.	4.	5.
AR part order	1	1	3	1	1
MA part order	2	2	2	3	4
ϕ_1	0.8456	0.8589	0.7300	0.9345	0.9623
ϕ_2			0.4117		
ϕ_3			-0.1916		
θ_1	-0.1081	-0.3374	-0.1658	-0.4141	-0.3423
θ_2	-0.1492	-0.1359	-0.6128	-0.2652	-0.3280
θ_3				-0.1223	-0.0649
θ_4					-0.0481

3.2.3 Application

In this report temporary mass signal of belt conveyor L212 is analyzed. The conveyor is located in Polkowice-Sieroszowice copper ore mine. The readings are dated from 15^{th} June to 30^{th} September.

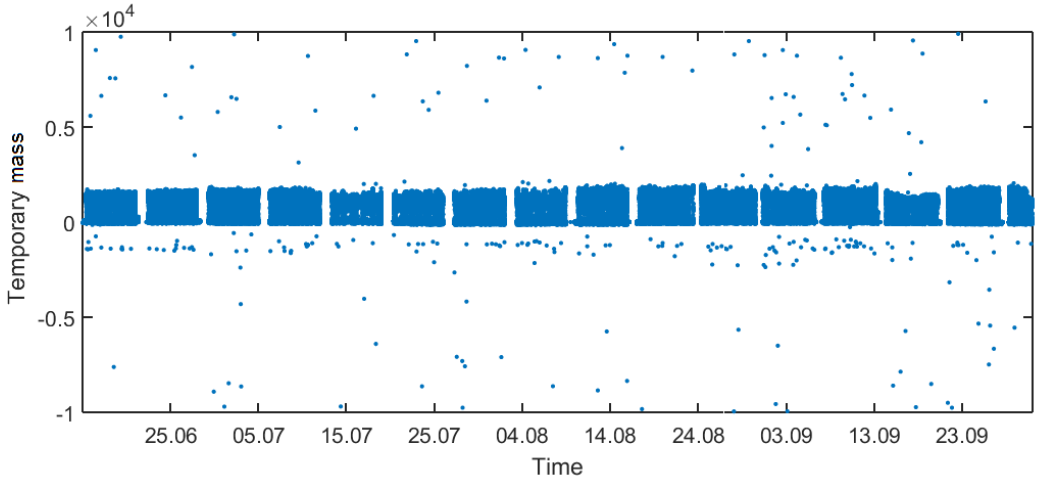

Figure 3.14: Temporary mass readings of belt conveyor L212

As it can be seen in Fig. 3.14 there are values that greatly differ from common ones. They were recognised as outliers and erased before the analysis. The data was not sampled with equal intervals thus it was subjected to linear interpolation with 10 seconds intervals (which is slightly more often than original dominant 11 seconds intervals).

Five signal's segments that were registered during the period with retention bunker opened were chosen (Fig. 3.15). The chosen segments differ in terms of dominant temporary mass (2 upper in Fig. 3.15 $\sim$1500, the rest $\sim$1100) and length (from $\sim$1 hour to $\sim$7 hours).

Each of signals was subjected to modified AIC method to obtain optimal ARMA order. The results can be seen in Tab. 3.4. The table also includes the parameters of optimal model. After the receiving of optimal ARMA orders and parameters, models' residuals were computed. Their autocorrelation functions are included in Fig. 3.16 and partial autocorrelation functions

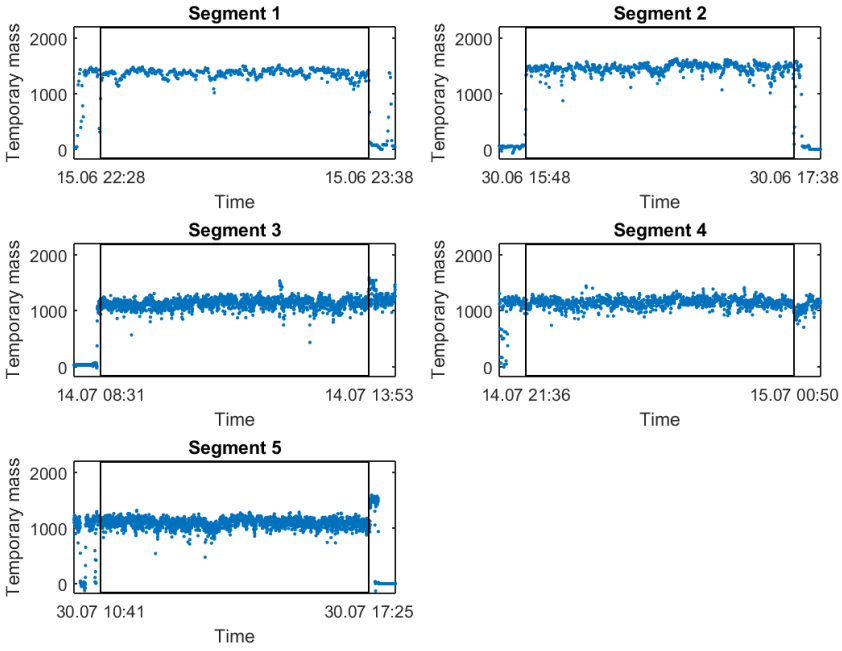

Figure 3.15: Chosen segments of temporary mass

Table 3.5: Tests' p-values

Segment	1.	2.	3.	4.	5.
p-value 1.	0.6880	0.1040	0.4940	0.6040	0.0580
p-value 2.	0.6060	0.4360	0.2220	0.4380	0.0960
p-value 3.	0.6700	0.1300	0.1580	0.5440	0.1860
p-value 4.	0.5440	0.3760	0.1260	0.4560	0.1720
p-value 5.	0.3980	0.2240	0.1820	0.1980	0.1500

in Fig. 3.17. The analysis of both Fig. 3.16 and Fig. 3.17 give a conclusion that for each segment residuals are sequence of independent random values. This suggest, that the ARMA parameters were computed properly.

The QQ-plots of residuals empirical distribution (vs standard normal distribution) can be seen in Fig. 3.18. Based on results presented in Fig. 3.18 one can observe, that the residuals distributions possess heavier tails than the standard normal distribution.

Thus it was determined to check whether the residuals belong to α-stable distribution which is characterized by heavy tails. In Tab. 3.5. the p-values of 5 different tests are included.

The p-values in Tab. 3.5 do not give reasons that the residuals do not belong to α-stable distribution as all values are greater than 0,05. Thus the α-stable distribution was fitted to residuals empirical distribution.

In Tab. 3.6 there are estimated α-stable parameters of residuals' distribution. The parameters are estimated by regression method.

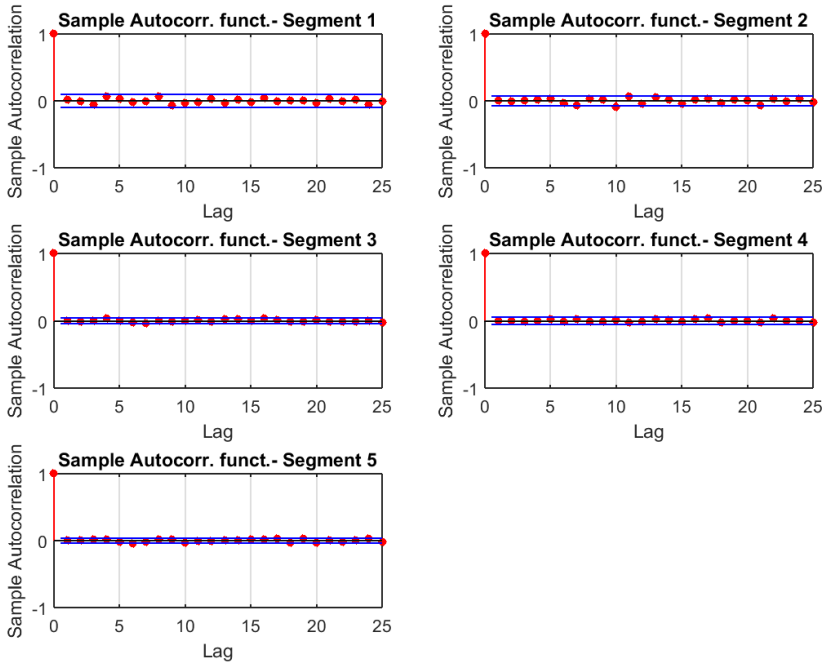

Figure 3.16: Sample autocorrelation functions of chosen segments' residuals

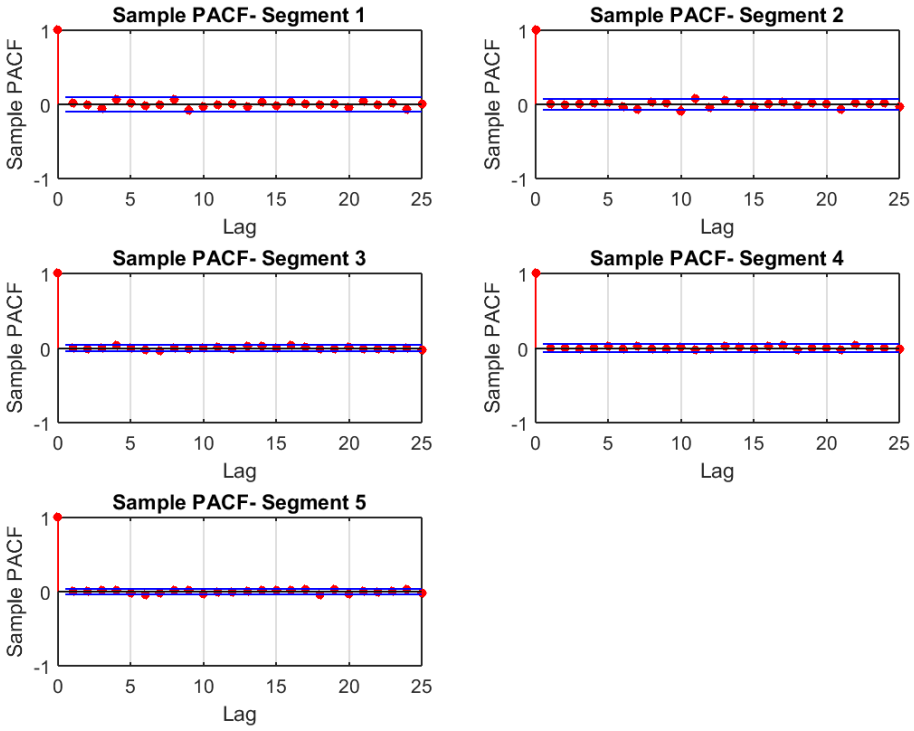

Figure 3.17: Sample partial autocorrelation functions of chosen segments' residuals

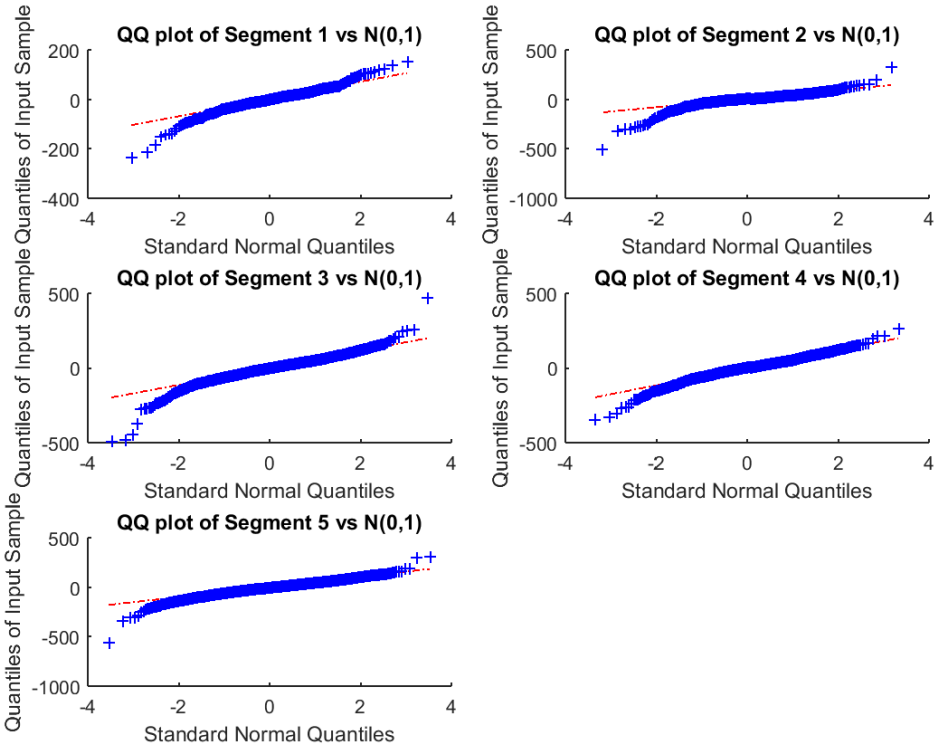

Figure 3.18: Residual quantiles vs quantiles of standard normal distribution

Table 3.6: Estimated α-stable parameters

Segment	1.	2.	3.	4.	5.
α	1.6548	1.5110	1.7956	1.8225	1.8368
σ	25.1136	30.0865	39.8250	41.8703	36.4238
β	-0.2498	-0.4230	-0.6062	-0.8025	-0.8562
μ	0.3557	0.2258	-1.2653	-2.1198	-2.0016

Based on results included in Tab. 3.6 one can observe that chosen segments' residuals are characterised by α parameter (index of stability) which is significantly lower than 2 which is indication of heavy tails. The scale parameter that is higher than 25. All distributions are left-skewed. Considering scale parameters, location parameters are near the 0.

To check whether the temporary mass can be successfully estimated by ARMA models with α-stable residuals it was decided to generate 1000 trajectories of estimated ARMA process with previously estimated parameters and check how the original signal would fit in quantile lines.

Fig. 3.19 includes chosen segments temporary mass with quantile lines of 1000 trajectories of fitted ARMA process with α-stable residuals. The quantiles are from 0.05 to 0.95, step 0.1. Fig. 3.19 shows that the temporary mass can be succesfully modelled with ARMA process with α-stable residuals.

3.2.4 Conclusions

In this report problem of modelling the retention bunker originated temporary mass with ARMA process with residues from α-stable distribution was undertaken. The report is based on tempo-

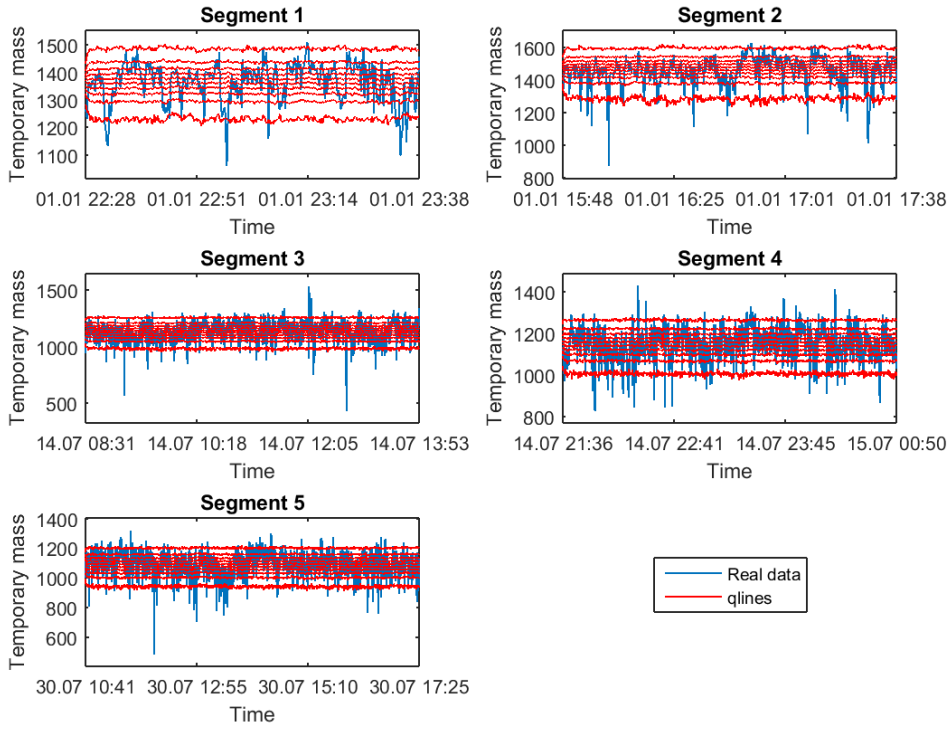

Figure 3.19: Segment's temporary mass and qlines of simulated temporary mass

rary mass signals from belt conveyor L212 that is placed in Polkowice-Sieroszowice copper ore mine. The signal was dated from 15^{th} June to 30^{th} September. Five different segments which were registered during the time when the retention bunker was opened and the temporary mass possessed relatively equal characteristic was chosen.

For each of these segments the optimal order of ARMA model was fitted. For received models residuals were computed and tested whether they are from α-stable distribution. The confirmation of these tests allowed to fit α-stable distribution to residuals. With fitted distribution it was possible to generate random variables from corresponding distribution. This allowed to simulate the process of temporary mass. Multiple iterations let the build of quantile lines which confirmed that the ARMA model with residuals from α-stable distribution precisely describe the temporary mass which originated from retention bunker. The fact that the result was repeated for each of the segments can be treated as an evidence that the retention bunker originated temporary mass can be modelled with ARMA process in general.

3.3 Multiple charging sources

The belt conveyor system in copper ore Lubin mine can be divided on few groups. First of them are the belt conveyors which are supplied only by ore from the one grid. In the previous section only that problem was considered. It should be mentioned that in belt conveyor system there are also belt conveyors which are supplied by many different sources. Namely, they have two, three or four grids or they are supplied by more than one bunker. Clearly, this situation is significantly different and in that case the other modelling methods should be introduced. One can imagine that the multiple source charging influence the electric current and the transported ore mass.

As one can see in Fig. 3.20, the signal related to weight of the ore mass is different than in considered previously the belt conveyor $L413$, which was supplied only by one source. The discharging are visually more frequent, so the waiting time between consecutive loader's arrivals are shorter. In that case the procedures of identification separated dischargings should be more complex and take into account the number and location of each grid.

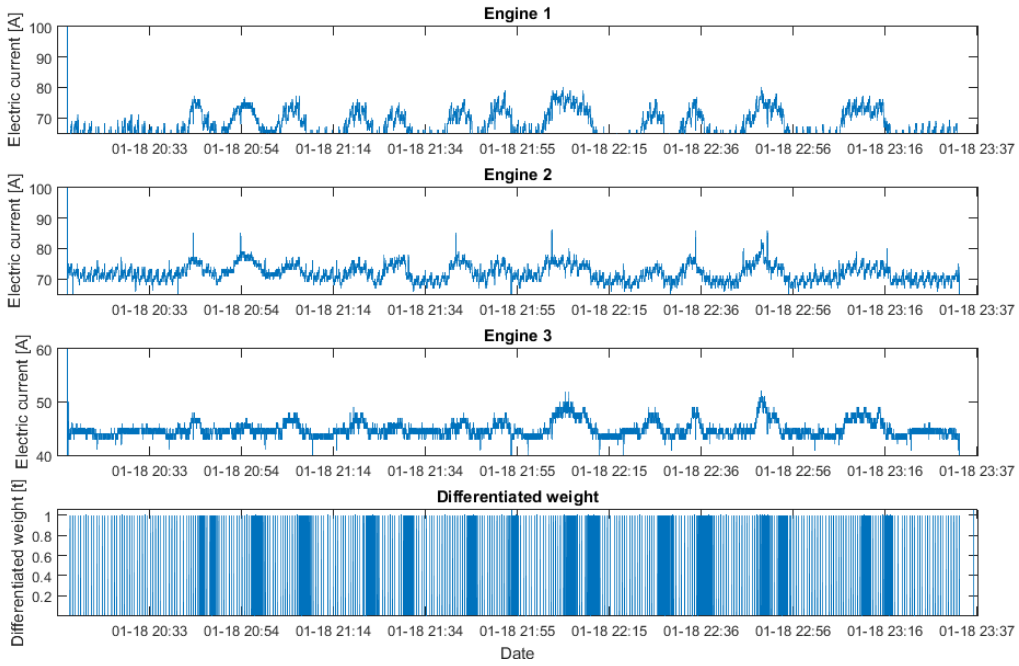

Figure 3.20: The electric current consumption and the differentiated weight for belt conveyor L142

Moreover, in case of more grids supplying particular belt conveyor we do not know exactly which discharging ore is derived from which loader. In situation that loaders are driving to the different face where the ore has different mineral structure, we should model ore flow from each grid separately. Due to that to model the process of coming the loaders to the grid should be extended for modelling the variable describing the process of choice the grid by the loader arrived from mining face. For that reason it is needed the deeper analysis of character of loader's work and rules related to transport roads in Lubin mine.

References

[1] Douglas M Bates and Donald G Watts. “Nonlinear regression: iterative estimation and linear approximations”. In: *Nonlinear Regression Analysis and Its Applications* (1988), pp. 32–66.

[2] Patrick Billingsley. *Probability and measure*. John Wiley & Sons, 2008.

[3] Peter J Brockwell and Richard A Davis. *Introduction to time series and forecasting*. Springer Science & Business Media, 2006.

[4] Pavel Cizek, Wolfgang Karl Härdle, and Rafał Weron. *Statistical tools for finance and insurance*. Springer Science & Business Media, 2005.

[5] Ioannis A Koutrouvelis. “Regression-type estimation of the parameters of stable laws”. In: *Journal of the American Statistical Association* 75.372 (1980), pp. 918–928.

[6] Piotr Kruczek et al. “The modified Yule-Walker method for alpha-stable time series models”. In: *submitted* (2016).

[7] Thomas Mikosch et al. “Parameter estimation for ARMA models with infinite variance innovations”. In: *The Annals of Statistics* (1995), pp. 305–326.

[8] Emanuel Parzen, Kunio Tanabe, and Genshiro Kitagawa. *Selected Papers of Hirotugu Akaike*. Springer Science & Business Media, 2012.

[9] Gennady Samoradnitsky and Murad S Taqqu. *Stable non-Gaussian random processes: stochastic models with infinite variance*. Vol. 1. CRC press, 1994.

[10] Pandu R Tadikamalla. “A look at the Burr and related distributions”. In: *International Statistical Review/Revue Internationale de Statistique* (1980), pp. 337–344.

[11] Peter Tankov. *Financial modelling with jump processes*. Vol. 2. CRC press, 2003.

[12] Rafał Weron. “Handbook of computational statistics: concepts and methods”. In: ed. by James E Gentle, Wolfgang Karl Härdle, and Yuichi Mori. Springer Science & Business Media, 2004. Chap. Computationally intensive Value at Risk calculations.

Chapter 4

Computer model of ore flow

The use of complex BC systems for underground transportation of mined ore meets the expectations of haulage millions of tonnes of ore (some 40 million tonnes per annum) but causes - difficult to be controlled and predicted - blending of ore on its way from numerous active mining panels to the shaft ore bunkers. Ore mined in different mining panels differs from one another in terms of pure metal content, lithological compound and granulation of blasted material. These differences are important for various reasons:

- Metal content is the key factor of the final production of the pure metal in smelters – it represents the main value of the whole value chain consisted of mining, transporting, concentrating and refining processes.
- Lithology of ore is important from the point of view of the specialists responsible on concentrating processes because the specific processes of grinding and floatation should be tuned with regard to the type of ore.
- Granulation of ore, its distribution along its transportation way have a great impact on the operational parameters of the BC system objects.

Therefore modeling of ore flow throughout the BC system should be investigated in various aspects. Some of them are discussed hereinafter.

4.1 Methods and possibilities to determine the variability of the Cu content in copper ore on a conveyor belt in one of the KGHM S.A. mines

The copper ore lode mined by the underground mines of KGHM S.A. comprises three different rock types: dolomite and sandstone separated by a main layer of copper-bearing black shale. The height of extracted seam (different in different mines) is established by channel sampling in the grid from 20x20 m up to 40x40 m. In each mining area both the copper content and the proportion of different rock types can substantially vary. Variability of ore excavated in different locations and transported in a complicated network of about 130 km of belt conveying systems with many mixing and switching points as well as stores causes ore quality control to become a significant problem (Tasdemir and Kowalczuk 2014).

For improving the enrichment process, the identification of both the copper content and the proportion of type of rocks supplied are important. In fact, despite the latter one is the most important, it is never controlled on conveyors. Cu content measurements from samples on a conveyor are done on a regular basis on one conveyor linking two mines. Samples are taken in order to make financial accounting between both mines after each shift.

One month measurements data were used to analyse the variability of Cu content in ore transported by one of KGHM PM SA mines (Drzymala and Kowalczuk 2010). Results can be compared with Cu content variability in feed of one of ore enrichment plants [3] as well as in ore supplied from mining face on divisional conveyor (Holodnik et al. 2015).

4.1.1 Methodology of ore sampling on a belt conveyor

A sampling station led by staff from the Centre of Quality Research (Centrum Badania Jakosci – abbreviated to CBJ) is placed on a transfer belt conveyor linking two KGHM mines. Ore is weighed on the conveyor by weightometer and is manually sampled by CBJ personnel for metal accounting purposes. These measurements and sampling/assay dictates the com-mercial payment between the mine which supplies ore through this conveyor and the mine which receives it and sends it together with its own ore to the ore processing plant.

The following description come from the QA/QC audit provided to KGHM PM SA by Wroclaw University of Technology and SRK Consulting from UK (Holodnik et al. 2015).

The ore from the supplying mine is loaded into four bins from which it is fed onto the gathering conveyor which thus transports ore from four sites of potentially different grade levels. The operations personnel advised that the finer fractions were generally higher grade. The loading of material onto the analysed gathering conveyor is controlled by supplying mine's operators while the sampling regime is selected independently by CBJ personnel based on an agreed protocol.

Ore in the supplying mine is fed after blasting onto sectional conveyors by loaders through a 400 x 400 mm grille limiting the maximum lump size fed forward onto the analysed gathering conveyor linking both mines. Cumulative sampling was carried out exactly on this conveyor on each shift. It consisted of a dozen of partial samples drawn from equal masses (or periods) according to special procedure described in the protocol.

The loading station comprises four 300 Mg ore bins fed by a single conveyor. The first three bins are filled via three moveable heavy duty ploughs on the conveyor. The local operator raises or lowers the ploughs to push ore off the conveyor to discharge into the bins in order to maintain ore levels in the bins. The final bin receives ore from the discharge of the conveyor and does not incorporate a plough. The height of the plough can be adjusted allowing partial removal of solids from the conveyor and consequently selective filling of different bins with finer or coarser material is possible. The ore in the bins exhibited some degree of size segre-gation. The bins incorporate level measurement instrumentation.

The bins discharge via feeders onto the transfer conveyor to feed ore to the receiving mine's conveying system via the CBJ weightometer and ore sampling point. The local operator, em-ployed by the supplying mine, selects the plough position and the bin discharge point. The procedure indicates that one feeder should be used at any time but that two feeders can be used if required. The first feeder is larger than the others. The operator records the tim-ing/us-age of the feeders but does not record the bin loading times.

Conveyors in the receiving mine are shut down one hour earlier than the supplying mine con-veyors and during this time the bins at the load out point are usually filled.

The conveyor tonnage is measured by two weightometers located upstream of the sample point. One weightometer is maintained by the supplying mine, which uses the results, and the other is used and maintained by the receiving mine.

The sample cut was 0.3 m wide marked on the conveyor structure. This represented a 30 kg sample. The sampling process – from stopping the conveyor, breaking larger lumps, removing the sample, screening, crushing of oversize, mixing, splitting through labelling – was satisfactory. The CBJ sampling operators seemed well drilled in the procedures.

The summarized protocol is as follows:

- Based on total planned tonnage to be transferred over the shift, the sampling proce-dure defines the number of samples to be taken, the sample interval in terms of ton-nage and the minimum tonnage between successive samples.
- The sample is 300 mm wide and is taken from the conveyor between two defined marks.
- The conveyor is stopped and samples are taken at tonnages selected by the CBJ op-erators within the parameters described below. This procedure introduces randomness to the sample timing in order to reduce any potential bias in the type of material fed onto the conveyor at any particular time and to prevent the sampling exercise from being predicted (by loading operators).
- Pieces of ore lying across the sampling width are manually broken.
- The sample is removed and screened at 10 mm. The oversize is removed and crushed to -10 mm. The undersize and crushed solids are mixed by hand on a steel plate. The mixed sample is collected and riffled to produce an approximately 4 kg sample. The sample is added to the mixer. All samples are combined and mixed and then riffled to produce the final sample.

The parameters for selecting sample intervals are given in Table 4.1.

Table 4.1 Sampling interval protocol

The planned supply of dredged material {Mg]/shift	Mass range (layer) [Mg]	Minimum interval by mass [Mg]	Number of incremental samples/shift
to 999	75	37.5	10-13
from 1000 to 1499	100	50	10-15
from 1500 to 1999	125	62.5	12-16
from 2000 to 2499	150	75	13-16
from 2500 to 2999	175	87.5	14-17
over 3000	200	100	15 and more

At the start of the shift the planned tonnage to be transferred from the supplying mine is used to define the sampling plan. The CBJ sampling team identifies the number of samples and the

sampling tonnage interval. The team then identifies the random tonnages at which the conveyor will be stopped. These figures are noted on a log sheet. During the shift the actual tonnage transferred as measured by the CBJ weightometer is noted. All samples are given a unique sample reference number which is noted on the sheet.

The sample size was reported to be approximately 30 kg per cut depending on the loading of the conveyor. The particle size varied from around 300 mm to zero. Larger particles were common.

The sample size taken from the belt appeared to be too small considering the maximum particle size on the conveyor. Observation indicated some particles in excess of 250x250x100 mm were possible, which would be 30% of mass contained in a typical 30 kg sample cut. Typically a sample of this size should not contain particles greater than about 40 mm. Increasing the sample width even to 1 m width would not improve this situation significantly and would probably result in a sample size unrealistic for manual processing.

The final sample is split into four separate samples: one for the supplying mine, one for the receiving mine, one for assay and one as a control sample.

Similar sampling procedures are used for sampling ore on other conveyors e.g. irregular control sampling for establishing Cu content in ore supplied from mining faces on divisional conveyors. The aim of control sampling is checking the level of dilution.

4.1.2 Analysis of the variation of ore tonnage and quality on a belt conveyor on the route from the section to the Ore Enrichment Division

Figure 4.1 and Figure 4.2 show the change of the quantity and quality of ore during 120 subsequent shifts. On Saturday and especially on Sunday the analysed conveyor belt was practically not used for ore transportation and therefore some studies exclude the "zero" shift from the analysis.

Ore quality variations are random, which is seen from the results of the process test run recorded above and below the median, as well as from the change of the increase and decrease directions (Table 4.3). Meanwhile, in case of ore quantity, a statistically important data clustering was observed with a 95% confidence level (Table 4.2).

Out of 120 shifts, ore was transported only during 77 shifts (the quantity of ore was greater than zero). The quantity range was between 560 and 3500 Mg. The median was 3000 Mg. The P value for values above and below the median is below 0.025 (0.00978) and therefore a statistically significant clustering exists of the sequence value, with statistical significance of 95%.

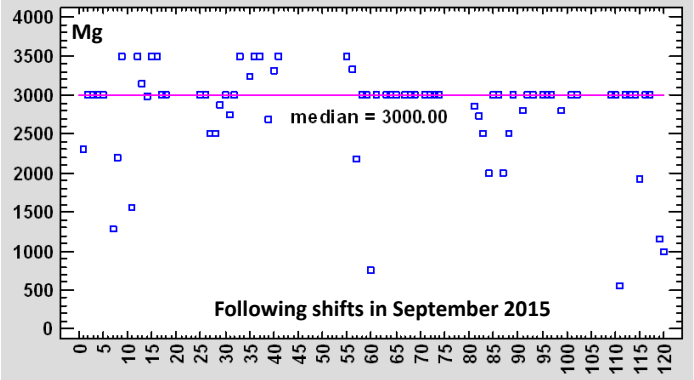

Figure 4.1 Variations of ore quantity on the conveyor analysed in 120 subsequent shifts in September 2015

Table 4.2 The results of Wald-Wolfowitz test of time sequence for the quantity of run-of-mine material

Test	*Observed*	*Expected*	*Longest*	*P(>=)*	*P(<=)*
Values above and below the median	11	17.8649	44	0.996549	0.00977954
Increase and decrease of the sequence value	32	29.6667	4	0.254099	0.846738

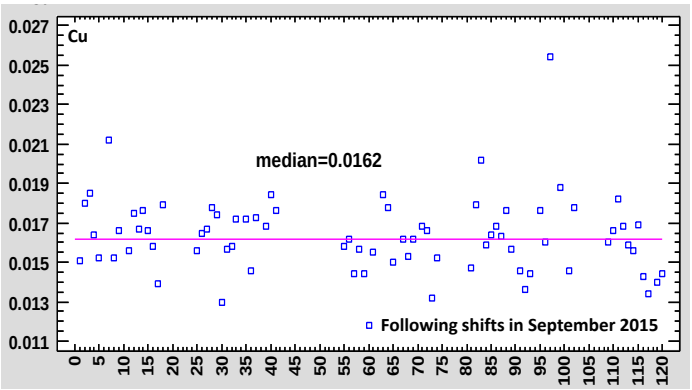

Figure 4.2 Variations of copper content in the ore transported on the analysed conveyor in September 2015

Table 4.3 The results of Wald-Wolfowitz test of time sequence for the copper content in the ore

Test	*Observed*	*Expected*	*Longest*	*P(>=)*	*P(<=)*
Values above and below the median	35	37.973	7	0.792076	0.281171
Increase and decrease of the sequence value	49	50.3333	3	0.693159	0.409252

Numerous instances of shift output at the level of 3000 Mg indicate that this is the target value and probably such tonnage is usually planned for transportation from one mine to the other using underground transport. Maintaining control of this value is possible, while maintaining control of quality may be difficult and quality variations may be random.

Ore grade was determined for 77 of 120 shifts, as the discussed conveyor was not used to transport ore during the rest of the shifts. The grade varied from 0.0118 to 0.0254 and the median was 0.0162. As none of the P values in the table was below 0.025, non-random patterns were not observed at the significance level of 95% (Table 4.3).

Further part of this work includes the description of the variations in copper quantity and content in the ore transported on the analysed conveyor, depending on the shift and the day of the week, supplemented by the analysis of their significance.

In September 2015, the quantity of the ore transported on the analysed conveyor varied depending on the day of the week (Figure 4.3), shift number and day of the week/shift number combined. The variation of the weight of the transported run-of-mine material is significantly smaller if idle shifts are excluded.

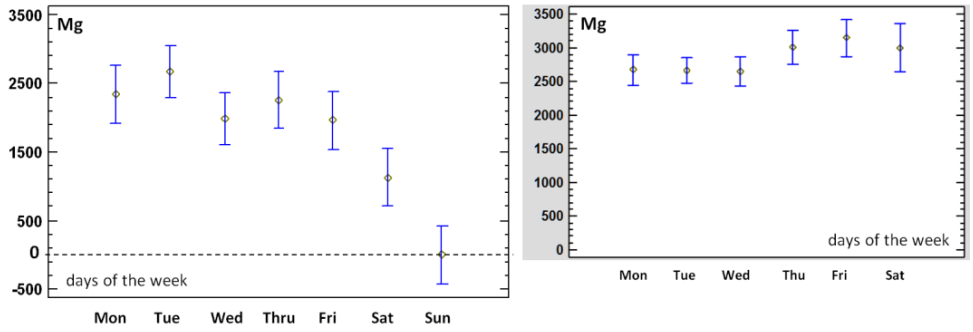

Figure 4.3 The variation of the average quantity of the transported ore with 95% confidence intervals depending on days of the week (including idle shift – on the left and excluding idle shift – on the right).

Such statistical differences – occasionally significant (especially if idle shifts with zero transportation are included) – were not reflected in grade variations, which showed to be more

stable in the discussed subgroups. As far as days of the week are concerned, two homogeneous but not disjoint groups were formed (Mon-Thu + Sat and Thu-Fri + Mon), with significant differences for the following pairs: Tue-Fri, Wed-Fri and Fri-Sat. Such differences may be difficult to explain, however, without the knowledge of the extent to which the production plans were followed.

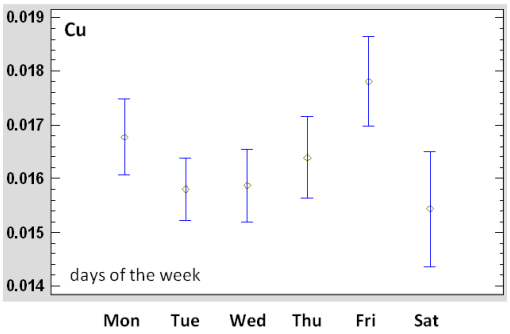

Figure 4.4 The variation of the average copper content in the ore transported on the analysed conveyor with 95% confidence intervals depending on days of the week

Although some variations of copper content may be observed depending on the shift number, they do not seem statistically significant. This is confirmed in the quartile graph (box and whiskers type – Figure 4.5, left side). Similar statistically insignificant variation of average grade values may be observed, if they are grouped depending on days of the week (Figure 4.5, right side). Although average grade variations seem to be considerable, especially on Saturday, when represented in the quartile graph, they prove to have a similar variation range for all days of the week. Two non-homogenous but joint groups may be identified (Mon-Thu + Sat and Thu-Fri + Mon). Significant differences can be observed for the following pairs: Tue-Fri, Wed-Fri and Fri-Sat.

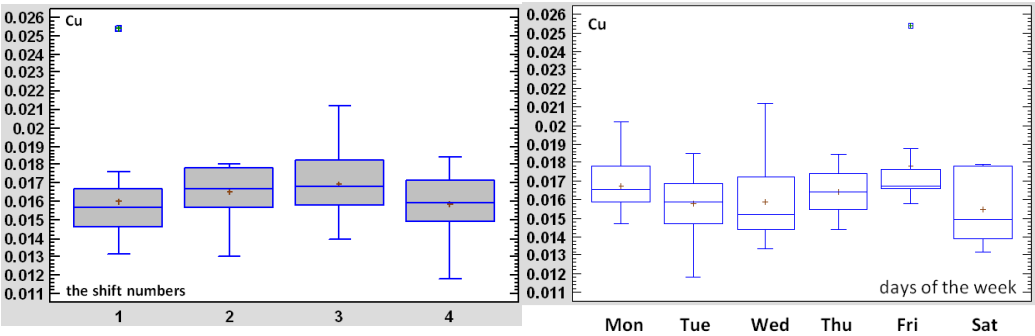

Figure 4.5 The variation of the average copper content in the transported ore shown as a quartile graphs depending on the shift number (left side) and on days of the week (right side).

Another comparison may be made depending on days of the week and shift number (Figure 4.6). Statgraphics Centurion XVII computer software, which was used in the calculations, identified as many as 4 joint homogeneous subgroups based on 17 significantly different pairs.

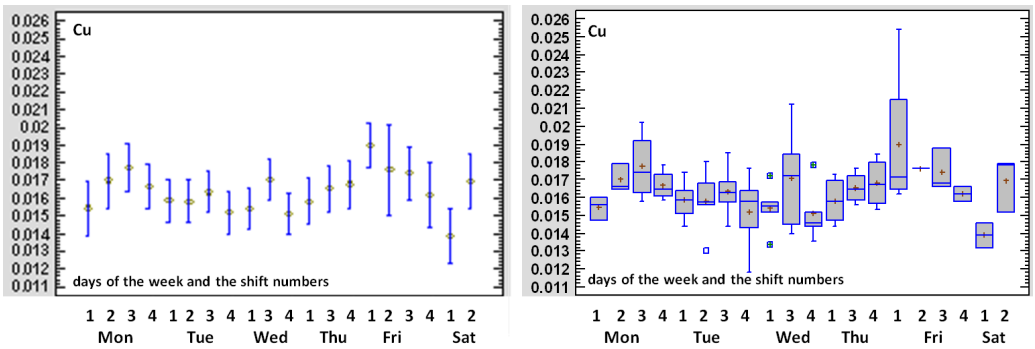

Figure 4.6 Average copper content in the ore transported on the analysed conveyor with 95% confidence intervals and with quartile graph depending on the day of the week and on the shift number

These differences can hardly be logically explained without establishing a connection with production plans and mining face location. In the future, however, a record should be kept and analysed of metal grades in the output stream of mixed ore on the analysed conveyor and/or at the feeding point to OEDs, as the identified statistical differences may be explained by the variation in the quality of ore from different parts of the deposit. Such procedure may serve as the basis for using statistical methods to forecast variation as related to mining face location (feeding point). The procedure may also be used in the DISIRE project.

If neither the shift number nor the days of the week have a significant influence on metal grade in subgroups, the time sequence of ore grade may be possibly analysed as a random sequence.

4.1.3 Conclusions

The analysis of the quality and quantity of ore transported on the transfer conveyor analysed in September 2015 shows that the quantity of the material in separate shifts was not a random process. The most frequent value and median was 3,000 Mg per shift, which indicates that the quantity of material sent from one mine to another via underground transport system was planned and controlled.

The run-of-mine tonnage changed significantly depending on days of the week, number of shifts and days of the week/shift numbers. Eliminating the idle shifts (without ore transport: Wed2, Thu2, Sat2, Sat3, and Sun1-4) allowed to limit the variations. This indicates that during work shifts attempts were made to follow the plan. Reasons for the lack of transport during the second shift on Wednesday and Thursday are not known. Zero load during two shifts on weekends was due to lack of production.

Preliminary analysis of ore grade changes on the analysed conveyor indicates that grade variations may be considered as a random process. Significant grade differences depending on days of the week and shifts may be the result of conducting mining operations in different parts of the mine.

Detail description of the sampling procedure (see chapter 4.1.1) has shown that the Cu content in all ore transported during one shift (c. 3 000 Mg) is estimated based on composite of about a dozen of small subsamples taken randomly during one shift. The subsample size taken from the belt appeared to be too small considering the maximum particle size on the conveyor. Observation indicated some particles in excess of 250x250x100 mm were possible, which would be 30% of mass contained in a typical 30 kg sample cut. Typically a sample of this size should not contain particles greater than about 40 mm. Increasing the sample width even to 1 m width would not improve this situation significantly and would probably result in a sample size unrealistic for manual processing. An automatic belt sampler should be considered if physical samples are required.

Taking into account variable size of ore lumps sometimes greater than 30 cm in diameter and possible big variation of Cu content in extracted ore: from 0.7% Cu in sandstone and dolomite (cut-off grade) up to even 15% Cu in rich shale layer indicate that both the sample mass as well as frequency of subsampling can hardly be representative.

Therefore there is a need to introduce other ways of estimating ore quality (both Cu content as well as composition of ore lithology) what has not been measured till now. A belt analyser (neutron technology) could be considered as well application of special pellets with ore quality information input into ore streams at their beginning in a DISIRE project.

4.2 Variability of the Cu content in copper ore streams on a conveyor belt, in one of processing plants, and mines for the purpose of IPC

One of important and difficult to maintain objectives in real life is ore quality control in feeding point of ore enrichment plants (Tasdemir & Kowalczuk, 2014). In chapter 4.1 it was shown that hitherto procedures of sampling ore from underground conveyor used in KGHM takes a lot of time but can be not fully representative due low frequency of manual sampling and too big dimensions of ore particles in comparison to samples mass. It is hard to even roughly estimate their accuracy due to there is no alternative verification method. Therefore it is not strange that in the event of financial accounting between both mines, despite regular sampling of transported material, both sides have a feeling that something is wrong with quality check results which do not represents real values. Frequently there are also differences between estimates of ore quality created at the beginning of ore streams (on working faces) and checks made in between (e.g. on the transfer conveyor) as well as between estimates made by miners and workers of Ore Enrichment Divisions (OED).

Due to lack of quality data from sampling the same ore stream taken as it moves from mining faces, through long and complicated conveying system with many runoff and flowing points and bunkers to the OED plants it is hard to compare exact levels of Cu content in transported material and notice mentioned above differences. However it is possible to compare results of such research taken in different places and at different times focusing not on Cu content which is not comparable but focusing on Cu content variability which should be comparable because it depends on variability of Cu content within the deposit and it is as it is. Local variability which can be noticed in different geology domains (Holodnik et al, 2015) is reduced by ore mixing

processes within the system of belt conveyors and bunkers. In effect variability of ore stream at feeding points in OED plant is stabilized (Drzymala and Kowalczuk, 2008).

In the Faculty of Geoengineering, Mining and Geology at the Wroclaw University of Technology there were research focusing on modelling of bulk material streams on conveyor belts (Jurdziak, 2008 a & b) however the attention was given to adjust selection of equipment to random loading (Krol, 2013), to estimate required power of conveyors drives (Gladysiewicz & Kawalec, 2006a), to predict durability of idlers under random load (Dworczynska et al, 2013) or to select idlers spacing taking into account random stream of bulk material (Gladysiewicz et al, 2016). Most of research was for surface mine however there were some work also for copper ore mines (Gladysiewicz & Kawalec, 2006b). Now the team is focused on modelling ore streams taking into account quality parameters of transported material in order to build viably prediction of quality of ore feed to OEDs plants. The research is conducted under the DISIRE program but use also results (see next chapter) from other projects ordered by KGHM (Holodnik et al,2015).

4.2.1 Comparison of metal grades at the feeding point, on the conveyor route and at the feed sampling point in OED – averaging from many sources

An assumption may be made that the run-of-mine stream (time series of ore quantity and quality) identified through samples taken at OEDs will be more stable than its counterpart from the analyzed conveyor, which may be considered a transfer point on the route from the grizzly to the concentrating plant. This is because the number of feeding points that contribute to the stream arriving at OEDs is significantly higher and the distance from ore extraction areas is greater, giving many opportunities for the run-of-mine material to be mixed on the way, which eventually leads to limiting grade variability.

Reference was made to the analysis performed in 2010 in one of the concentrating plants, as described in the cited paper (Drzymała and Kowalczuk, 2010), where a set of source data was also provided. Noteworthy is the fact that since the publication of the paper, the average grade has been lowered and no information is available on whether the data relate to the same OED that receives the ore from the analyzed conveyor. Still, the analysis of variable copper content in the feed to OED allows to investigate the quantitative and qualitative character of the variations.

3 streams were compared: on the section conveyor (estimations based on reconciliation from channel sampling) and the analyzed transfer conveyor as well as in one of the OEDs (based on Drzymała and Kowalczuk, 2010).

The first series included 104 values (in the range from 0.01527 to 0.025158, median = 0.01991), the second series included 77 values (in the range from 0.0118 to 0.0254, median = 0,162), the third included 93 values (from 0.0152 to 0.0197, median = 0.0173).

The difference in the number of values results from the fact that concentration plants operate on a 3-shift basis and ore was delivered constantly, while the mine operates on a 4-shift basis and during weekends excavation was practically stopped.

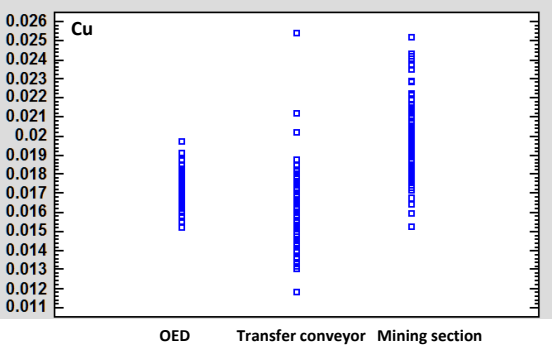

Figure 4.7 Scatter plot of metal grade in each shift during one month in three feed streams: OED, transfer conveyor and section conveyor

Clearly, variation range of Cu content in the ore stream at OED is the lowest (Figure 4.7).

The streams were compared in various tests (Table 4.4). The ANOVA test was used to check whether significant differences occur among the average values (Table 4.5). At 95% significance level, the differences proved to be significant, which is shown in the confidence interval graph for average values (Figure 4.8). The kurtosis value out of +/- 2 range for the transfer conveyor indicates lack of normal distribution for this random variable.

Table 4.4 Summary statistics for the analyzed variables

	Number	***Average***	***Standard Deviation***	***Coefficient of Variation***	***Minimum***	***Maximum***	***Range***	***Skewness***	***Kurtosis***
OED conveyor	93	0.0172581	0.000920459	5.3335%	0.0152	0.0197	0.0045	0.209964	-0.637583
Transfer conveyor	77	0.0163149	0.00193308	11.8485%	0.0118	0.0254	0.0136	4.78786	**10.3165**
Section conveyor	104	0.0199808	0.0020317	10.1683%	0.01527	0.02516	0.00989	0.955587	-0.426594
Total	274	0.0180265	0.00231636	12.8498%	0.0118	0.0254	0.0136	4.24484	1.83402

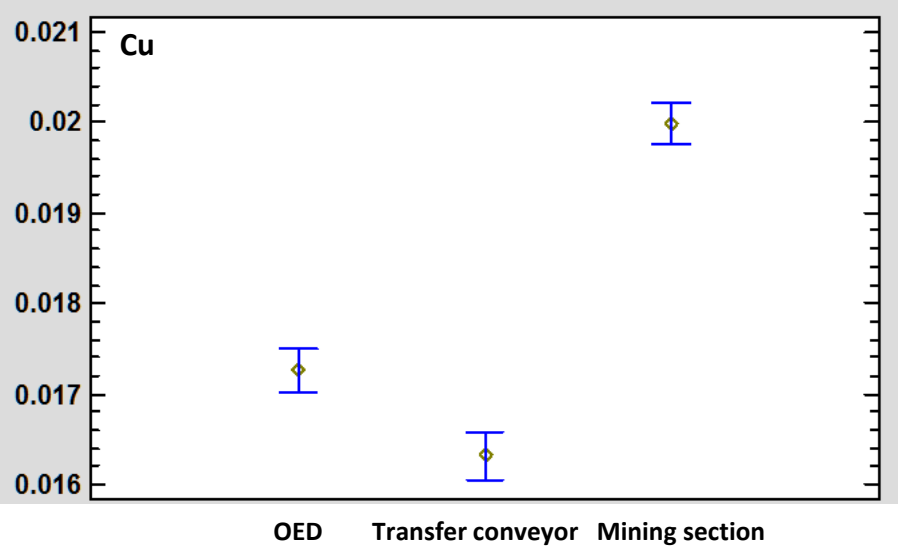

Figure 4.8 Average values for three streams along with their 95% confidence intervals

Table 4.5 Table of ANOVA test

Source	*Sum square*	*Df*	*Average square*	*Ratio F*	*Value P*
Between groups	0.000677677	2	0.000338839	116.66	0.0000
Within the group	0.000787106	271	0.00000290445.		
Total (Corr.)	0.00146478	273			

Table 4.6 The average values and their confidence intervals

			Standard error		
	Number	*Average*	*(pooled s)*	*Lower limit*	*Upper limit*
OED conveyor	93	0.0172581	0.000176722	0.017012	0.0175041
Transfer conveyor	77	0.0163149	0.000194217	0.0160446	0.0165853
Section conveyor	104	0.0199808	0.000167115	0.0197481	0.0202134
Total	274	0.0180265			

ANOVA table (Table 4.5) allows to split data variance into two components: variance between groups and variance within the group. The F indicator, in this case equal to 116.662, is the ratio of inter-group variance to intra-group variance. As the P value of the F test is smaller than

0.05, a statistically significant difference exists between the average values for three variables on the significance level of 5%.

Table 4.6 shows average value for each column of data. The table also shows standard error of the average for each variable, which is a measure of variation in a sample. Standard error is obtained by dividing the total rolling standard deviation by the square root of the number of observations at each level. The table also shows the interval around each average value. The intervals are based on Fischer's Least Significant Difference (LSD). They are constructed so that if two average values are the same, then their intervals overlap for 95% of time. Multi-range tests show that each of the variables creates a homogeneous group (Table 4.7).

Table 4.7 Multi-range test results for the investigated average values

	Number	*Average*	*Homogeneous groups*
Transfer conveyor	77	0.0163149	x
OED conveyor	93	0.0172581	x
Section conveyor	104	0.0199808	x

Contrast	*Signifi-cance*	*Difference*	*+/- Limits*
OED conv. – transf. conv.	*	0.000943129	0.000516966
OED conv. – div. conv.	*	-0.0027227	0.00047885
transf. conv. – div. conv.	*	-0.00366583	0.000504431

* indicates a statistically significant difference

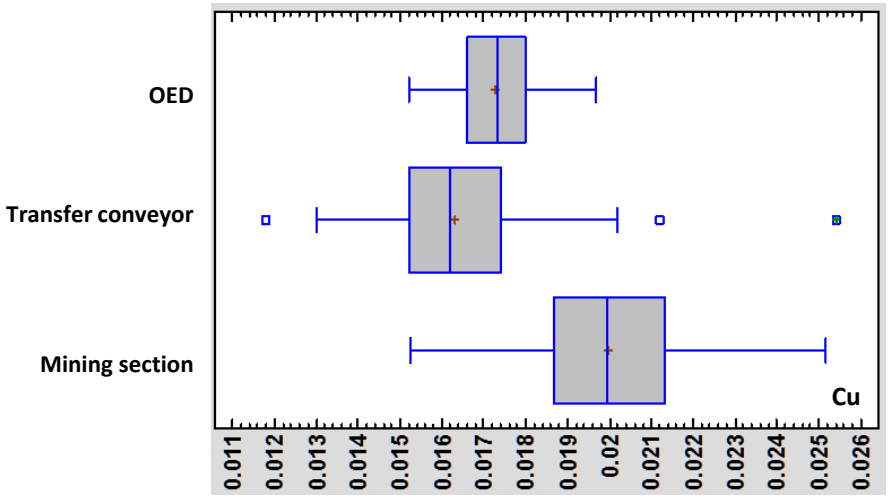

Figure 4.9 Box and whisker graph for Cu content in OED feed, on the transfer conveyor and on the section conveyor

Table 4.8 Variance test results

	Test	*Value P*
Levene's	15.6761	0.0000

Comparison	*Sigma1*	*Sigma2*	*Indicator F*	*Value P*
OED_Cu / T128_Cu	0.000920459	0.00193308	0.226731	0.0000
OED_Cu / L221_Cu	0.000920459	0.0020317	0.205253	0.0000
T128_Cu / L221_Cu	0.00193308	0.0020317	0.905271	0.6512

The statistics shown above in Table 4.8 test the hypothesis that standard deviations in each of the three investigated variables are the same. Of importance here is the P value. It is lower than 0.05, which means a statistically significant difference occurs between standard deviations at 95% confidence level. This observation puts in question one of the most important assumptions underlying variance analysis and challenges the performed standard statistical tests, which were based on the assumption that variance is constant. But at the same time, the observation also confirms variance variability between Cu content on the transfer conveyor and on the conveyor in one of the OEDs, as well as on the section conveyor – which was the object of the study. As no differences occur between the transfer conveyor and the section conveyor, the average values between them may be compared using standard tests.

The table also shows the comparison of standard deviations for each sample pair. Two P values below 0.05 indicate that statistically significant differences occur between the two standard deviations at 5% significance level.

Due to variance variability, standard tests cannot be used to test the hypothesis that the average values are equal and therefore Mood's median test must be used (Table 4.9). The test allows to verify the hypothesis that the median values for all three samples are equal. The test consists in counting those observations whose positions in each group are on both sides of a common median – in this case 0.0176. As the P value for the chi-square test is below 0.05, sample medians are significantly different from each other at the significance level of 95%.

Table 4.9 Median test results

Sample	*Sample population*	*n<=*	*n>*	*Median*	*95.0% lower lim. CL*	*95.0% upper lim. CL*
OED conveyor	93	64	29	0.0173	0.0169523	0.0175
Transfer conveyor	77	63	14	0.0163	0.0166373	-20530.5
Section conveyor	104	11	93	0.01984	0.0194283	0.020879

Test statistic = 108.999 P value = 0

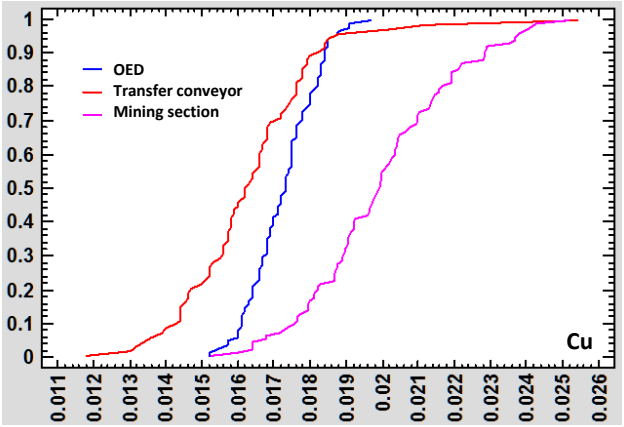

Figure 4.10 Quantile graph for the histograms of the 3 variables

The graph (Figure 4.10) clearly shows the differences in the cumulative empirical distribution functions. Variability range and the inclination of the feed stream on the section conveyor and of the run-of-mine material on the transfer conveyor are similar (both the inclination and the range), but a significantly fatter distribution tail (for the transfer conveyor) in the upper values causes a significant difference. A clear, almost parallel offset can be observed into the area of lower metal content, of about 0.003 (0.3% of percentage point – about -15% as compared to output value). This fact can also be observed on histograms (Figure 4.11 and Figure 4.12) and on “box and whiskers” graphs (Figure 4.9).

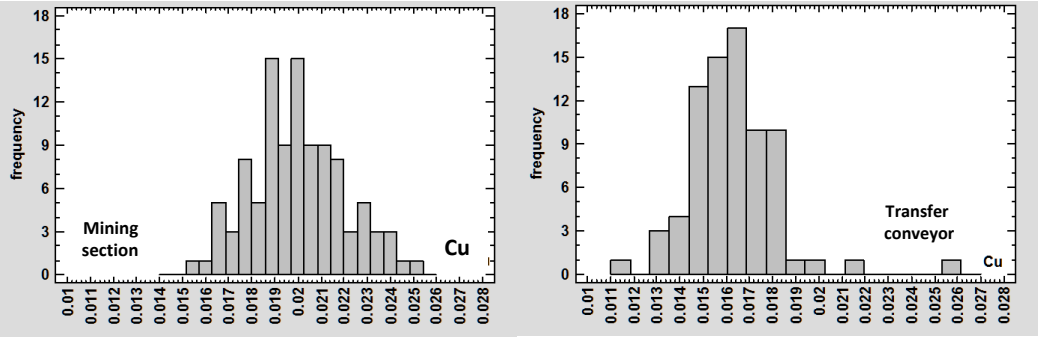

Figure 4.11 Histogram of Cu content variability in the deposit next to conveyor L-221 (on the left) and to conveyor T-128 in September 2015

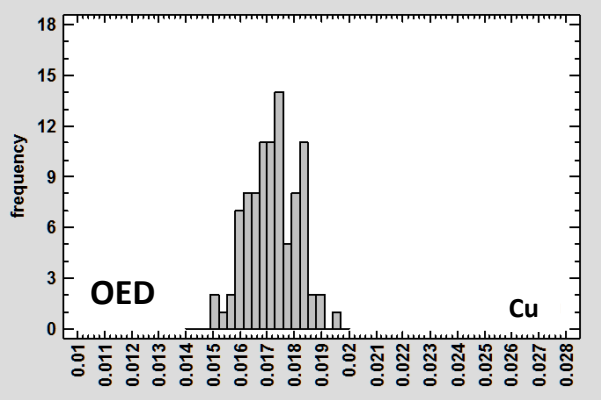

Figure 4.12 Histogram of Cu content variability in the ore on the conveyor in one of the OEDs (based on Drzymała and Kowalczuk, 2010)

The most concentrated and symmetrical distribution can be observed for ore quality in OEDs. Drzymała and Kowalczuk (2010) are confident that the variability of Cu content in ore may be described by Gaussian distribution (Figure 4.13).

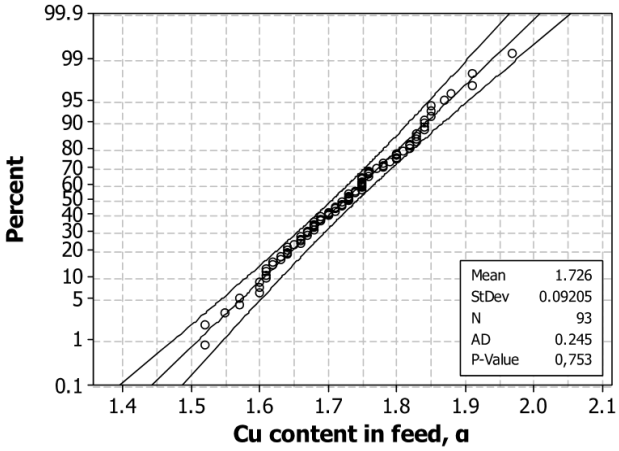

Figure 4.13 Normality graph with 95% confidence intervals for time series data on Cu content in the feed on a conveyor in one of the OEDs (Drzymała and Kowalczuk, 2010)

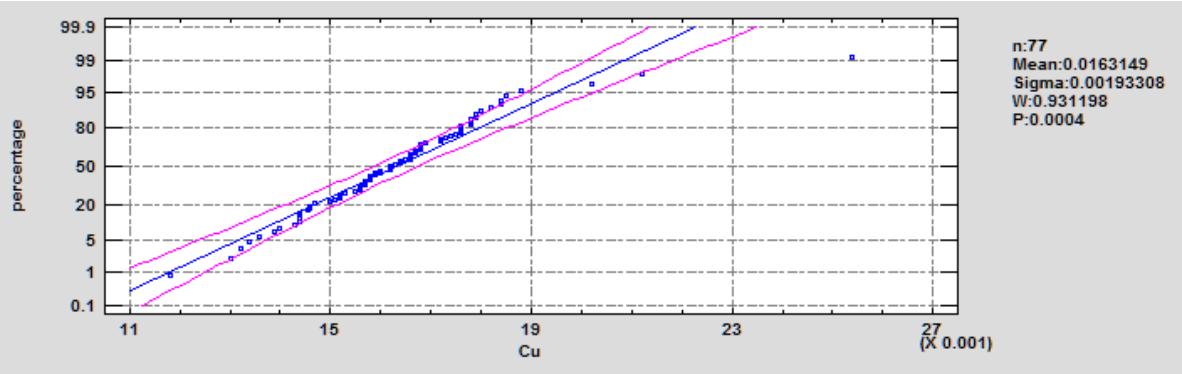

Figure 4.14 Normality distribution graph with 95% confidence intervals for Cu content in the ore on the transfer conveyor in the mine

The graphs indicate that the process of mixing the run-of-mine material in the cumulative stream transported on the gathering transfer conveyor (Figure 4.14) from different feeding points that supply ore of varying grades does not lead to normal distribution. The deviations are visible especially in the “tail” on the right side. This fact may suggest insufficient ore mixing, as higher grades in the feed from sections partially occurred on the transfer conveyor, although they should have been reduced due to mixing with lower grade ore from other feeding points. High Cu mineralization in the run-of-mine material (2.54% on shift no. 97) may hence be due to error. Possibly, the number of feeding points was insufficient (only 7 section conveyors feed to the gathering transfer conveyor from which samples were taken) with 3 to 4 dominated in terms of ore fed, (conveyors: A, B, and C). A separate issue is whether feed mineralization levels in the sections supplying the run-of-mine material to the transfer conveyor can be treated as fully independent variables (the process of summing the values of independent random variables would meet the conditions of a limit theorem indicating normal distribution of such variations). Components of the variability of Cu content in the deposit (in the ore fed to the conveyors upstream of the transfer conveyor) are normal, at least some most important ones (Figure 4.15). The sum of those components does not show as normal distribution, and this fact might imply either that the mixing process is not perfect or that dependent variables exist (spatial correlation of this parameter is actually used in geostatistics). The Cu content in the run-of-mine material fed to grizzlies located in proximity to each other may be correlated.

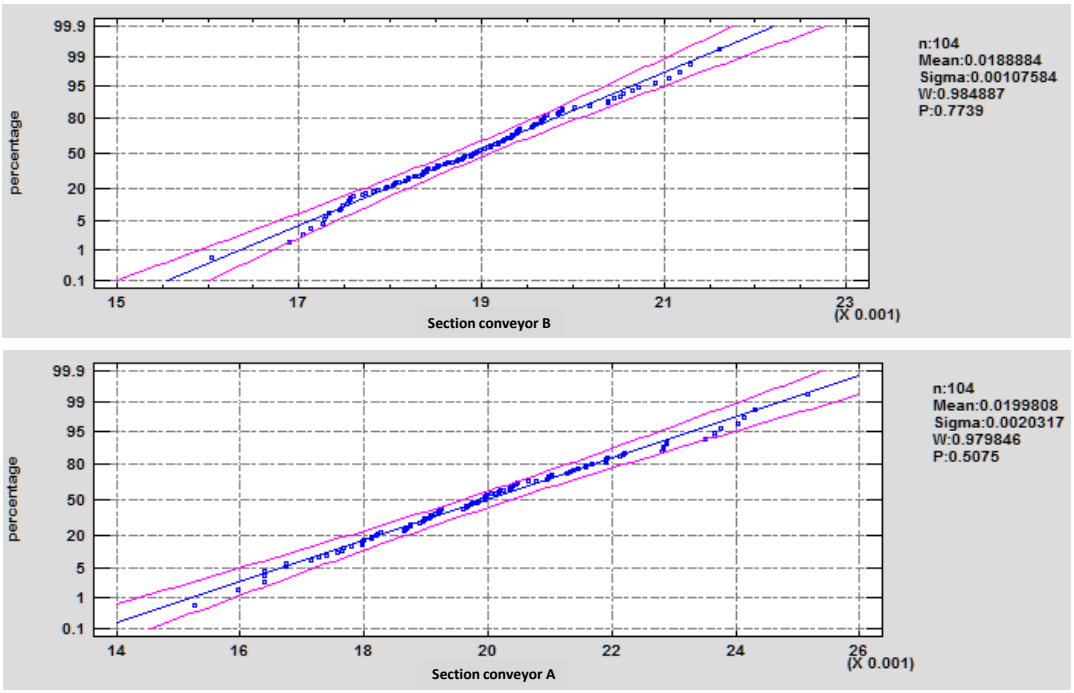

Figure 4.15 Normality distribution graph with 95% confidence intervals for Cu content in the ore on section conveyors A and B feeding to the transfer conveyor

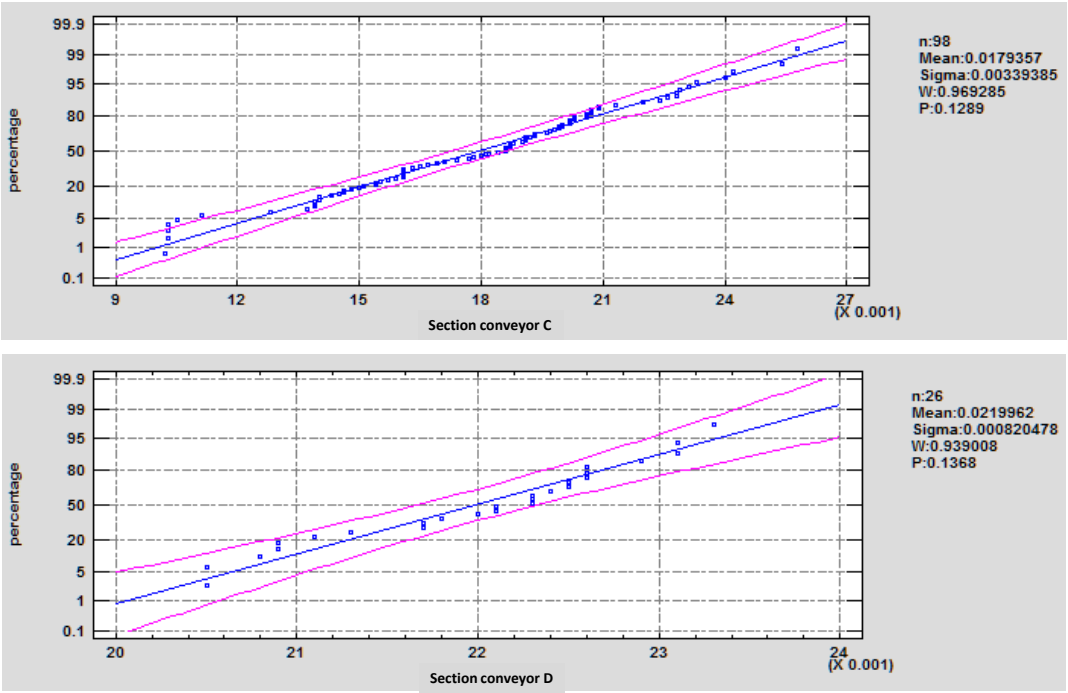

Figure 4.16 Normality distribution graph with 95% confidence intervals for Cu content in the ore on conveyor C and D feeding to the transfer conveyor

The frequency with which especially extreme Cu content values occur may thus deviate from normal distribution, as the same high values will occur simultaneously in several feeding points and are transferred to the cumulative stream. Hence, the mixing process does not allow to obtain sufficient average values. The best distribution for grade levels on the transfer conveyor during the 1st shift was maximum value distribution (Figure 4.17), which might indicate that when samples are taken, maximum instantaneous mineralization value is recorded. This is impossible, however, due to randomly selected sample collection times. In addition, during other shifts the distribution is not the best fit (during shift no. 2 the distribution is uniform, during shift no. 3 it is inverse Gaussian and during shifts no. 4 it is Weibull). The best distribution for all shifts was logarithmic-logistic distribution (Figure 4.18).

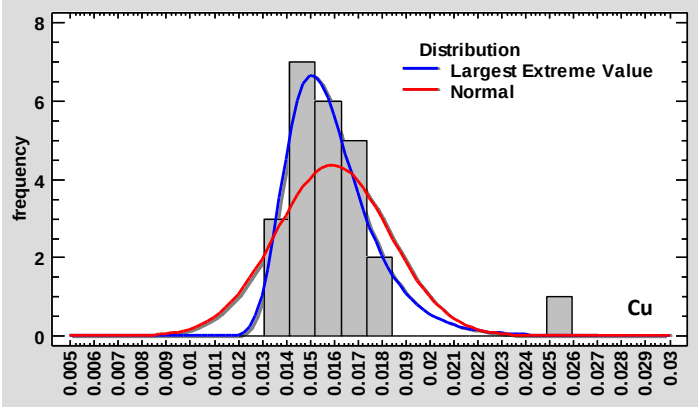

Figure 4.17 Combined extreme (maximum) value distribution and normal distribution for Cu content during shift no. 1, on the gathering transfer conveyor

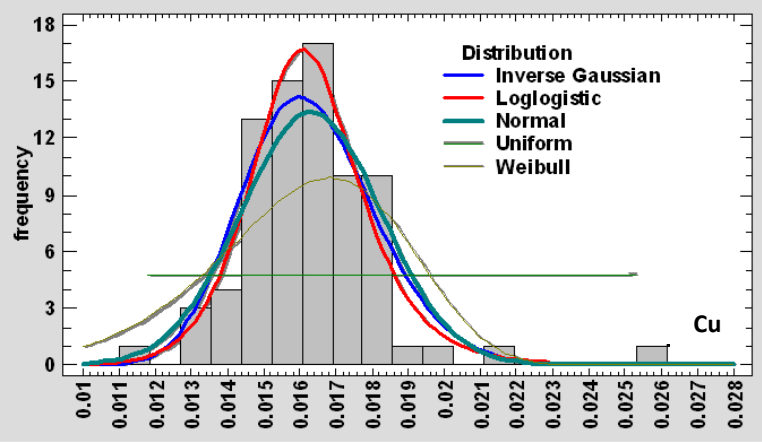

Figure 4.18 Combined distributions for Cu content on the gathering transfer conveyor

The fact that in the analyzed period normal distribution was not suitable for use in describing the variability of Cu content on the analyzed gathering transfer conveyor might be due to insufficient number of feeding points. The transfer conveyor was at that time supplied from a maximum of 7 conveyors (usually 3-4), which is not enough to achieve satisfactory convergence to normal distribution. A spatial correlation also exists of the quality of the run-of-mine material fed on the neighboring grizzlies. The range for this correlation may be determined using geostatistical methods and autocorrelation. The run-of-mine material may be insufficiently mixed. If the conveyors are fed sequentially, then the random samples might not represent many distributions, but instead only a small number of distributions and this can lead to the transfer of extreme values to the cumulative distribution. The averaging effect will not occur. Both the range and the variability will be similar to those at feeding points (on section conveyors).

4.2.2 Conclusions

Investigation into the variability of Cu content in three ore streams – on the section conveyor labelled as A) at the transfer point on the gathering conveyor and in one of the conveyor in OED – allowed to confirm the variability of the means and variances. The average value of Cu content on the gathering conveyor underground (at the transfer point) is significantly lower. The fluctuation (variance) of Cu content in the feed sent to the processing plant is also lower than at the transfer point and on the section conveyor.

The analysis of the variability of Cu content in the stream of feed sent to OED is of qualitative character (due to lack of data of September 2015), as the reference data were of 2010 and no information is available whether they are related to the same OED. Since that time, the average grade levels significantly decreased, not allowing to make quantitative estimations on Cu content in ore.

Analytical works should be continued, however, in order to compare time series of Cu content variability in various regularly assayed locations, as the process of reducing variability due to increased mixing of various streams may be represented quantitatively, thus aiding forecasts

based on multidimensional statistical and simulation models. The results of such analysis may also be used in the DISIRE project.

The findings indicate that normal distribution may be used to describe the distribution of Cu content in the ore transported to OED and on the section conveyors. The situation is different at the transfer point on the analyzed conveyor, which may be the result of insufficient mixing, of the relationship between ore quality in the streams of run-of-mine material fed to neighboring grizzlies or of insufficient number of feeding points (maximum 7 conveyors).

It is worth to compare three run-of-mine ore streams considering them as random time series of consecutive values rather than random variables to check if there are autocorrelations between them (Tasdemir & Kowalczuk, 2014). It seems that due to on next shifts excavation is continued in the very close area to the previous place the average values should be correlated with next ones. Of course it depends on the rate and scale of grade changes within the deposit. So we can expect the greatest changes in mining sections du to advances of faces but average values from more sources od ore shoud change less rapidly and correlation should be stronger what should allow on better ore grade predictions in feeding point to OED what is the aim of research.

4.3 Modeling of ore lithology compound on delivery to the ore concentrating division

The productivity of metal ore processing depends on the identification of its parameters as they are key factors of the effectiveness of implemented technology of concentration. The variability of ore parameters is determined by the geological structure of the deposit. An uniform structure means relatively stable physical and chemical parameters of the ore which facilitates the appropriate adjustments of the concentrating processes. In a case of more complicated geology of a mined ore, finding the best solutions of ore processing is becoming a challenge.

The renowned copper ore lode in the South-West Poland mined by KGHM S.A. company in underground mines belongs to the most complicated deposits. As stated in (Bazan et al, 2014): “The Polish resources are among the most complex in the world, and these resources are additionally the most difficult to be processed. The main reasons for rating the Polish copper deposits as among the so-called difficult ones are due to the following factors:

- the relatively long flotation times as a result of slow kinetics of sulphide mineral particles,
- three lithology forms occur at the same time, but in different proportions, thus having a significant influence on the grinding and flotation conditions,
- fine and ultra-fine sulfide mineral particles require a fine grinding process.”.

The generalised structure of the deposit within the balance seam is presented on Figure 4.19. The texture presents Figure 4.20.

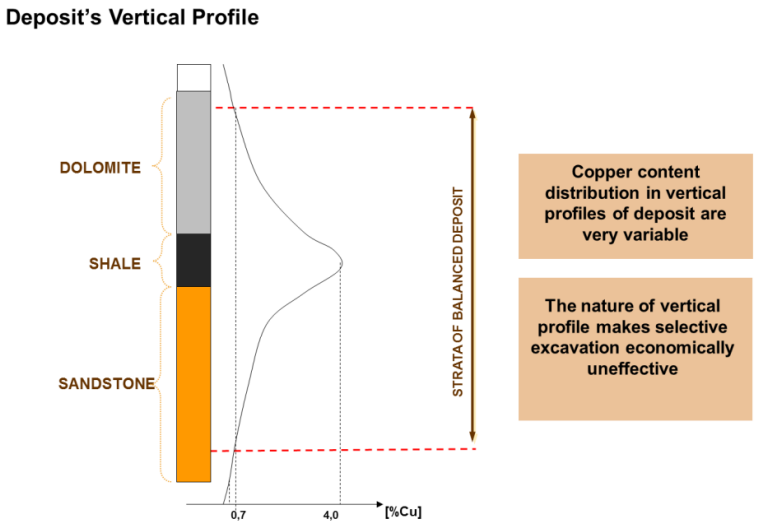

Figure 4.19 Structure of copper ore deposit in the KGHM S.A. underground mines in Poland

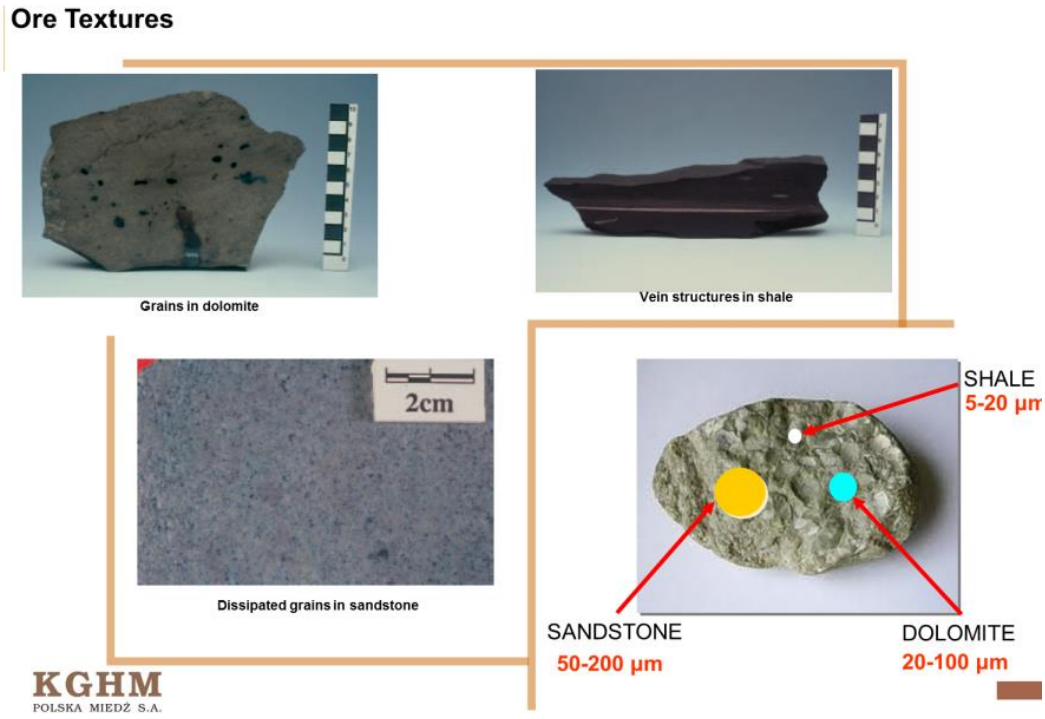

Figure 4.20 Types of texture of copper ore

As shown on the above figures, the particles of copper ore are significantly differentiated in size according to the given lithology. Due to the available, non-selective mining technology these particles are blended when supplied to the processing plant. The average proportions of the ore lithology (see Table 4.10) do not reflect the actual differences in mining fields (see Figure 4.21).

Table 4.10 KGHM S.A. deposit's changing of lithology structure (Bazan et al, 2014)

Concentrator Name	Sandstone		Shale		Carbonates	
	Years 1985-91	Years 2009-11	Years 1985-91	Years 2009-11	Years 1985-91	Years 2009-11
Lubin	54%	77.545	8.1%	0.94%	37.9%	21.52%
Polkowice	9.9%	22.67%	5.9%	5.28%	84.2%	72.05%
Rudna	43.3%	54.11%	5.5%	11.56%	51.2%	34.33%

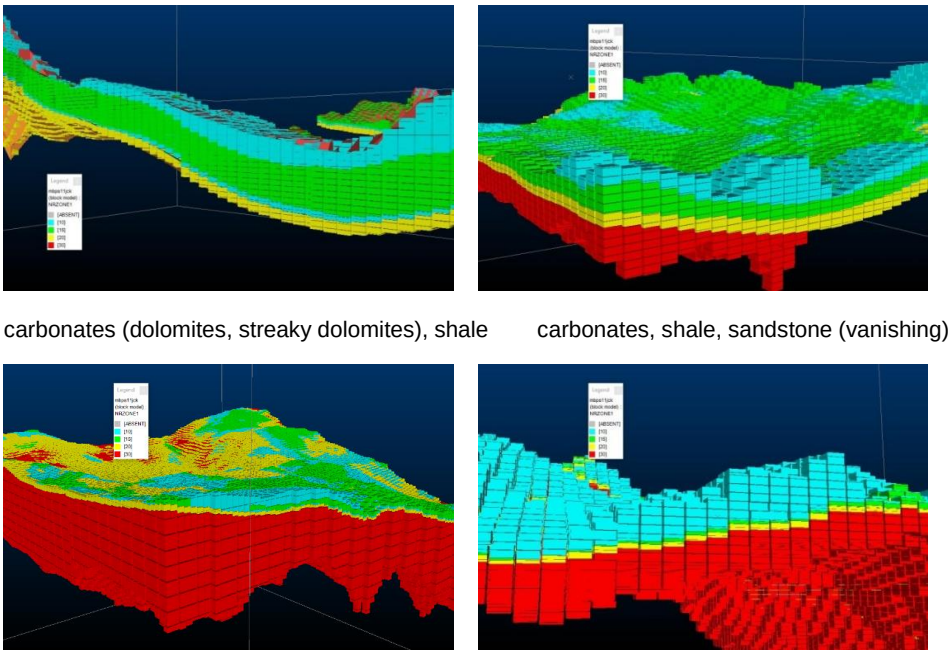

carbonates (dolomites, streaky dolomites), shale

carbonates, shale, sandstone (vanishing)

shale, sandstone

carbonates, shale, sandstone

Figure 4.21 Visualisation of the structural block model of the balance ore from four mining fields of two KGHM S.A. mines (applied legend of ore lithology: blue – dolomites, green: streaky dolomites, yellow:shale, red: sandstone)

4.3.1 An idea of identification of copper ore with the use of Process Analyser Technology sensors

The DISIRE technology is targeted for the enhancement of existing information systems already implemented in a company – that could either provide required information to be embedded into pellets or process and analyse the information extracted thereafter.

4.3.1.1 Prerequisites

The KGHM S.A. successfully implements advanced information systems for supporting the complex processes of copper ore enrichment - FloVis, MillVis, ConVis (Konieczny et al 2011). Especially the last one – ConVis, built for the optimisation of managing and grinding of ore supplied from various mining fields needs information about the lithology of ore to achieve the main targets of ConVis: stabilization of ore granulation, optimisation of grinding and maintaining the stable crushed material flow onto mills feeders.

The second reason for considering the implementation of DISIRE technology is the fact that KGHM S.A. undertook a project to upgrade the existing geological and mine planning systems into the full 3-D geological modelling and mine planning digital environment. The consulting division of CAE Mining (developer and distributer of Datamine software) was commissioned for this work and the training and implementation project was launched in 2015. It is expected to lead to a change in methods used for data handling and to provide accurate, regularly updated information about the orebody as well as advancing mining fields (Figure 4.23).

The last vital element of the existing information environment is the managing and control system that supports underground belt conveying (see Figure 4.22). These systems (containing also weights on selected conveyors) can provide with the information about the actual operation status and load of each object of the transportation system.

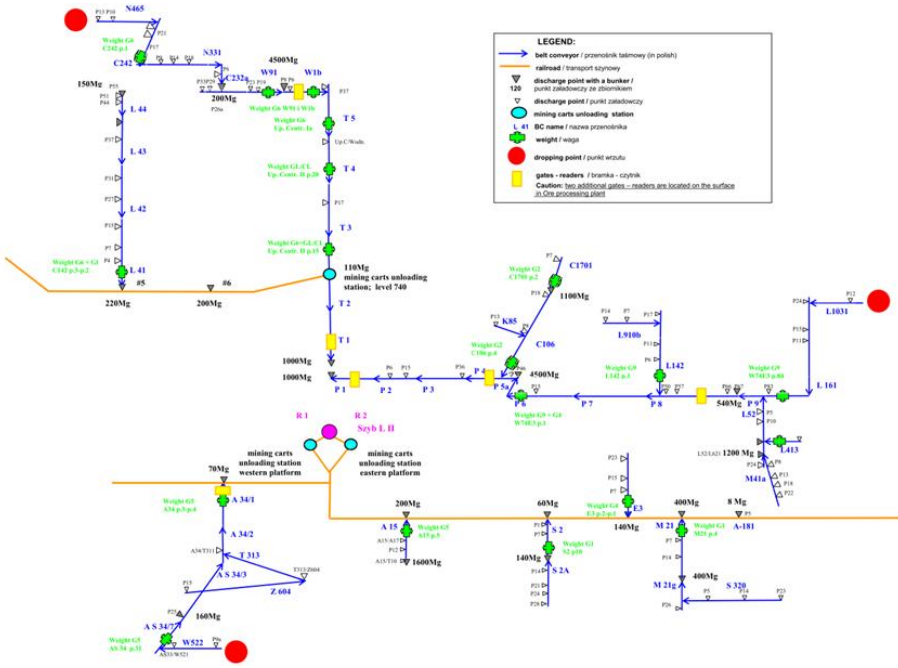

Figure 4.22 The underground transportation system in the “Lubin” KGHM mine with the proposed locations of pellet dropping points (red bullet points) and pellet readers (yellow squares, 2 others are located on the surface on the entrance to the Processing Plant)

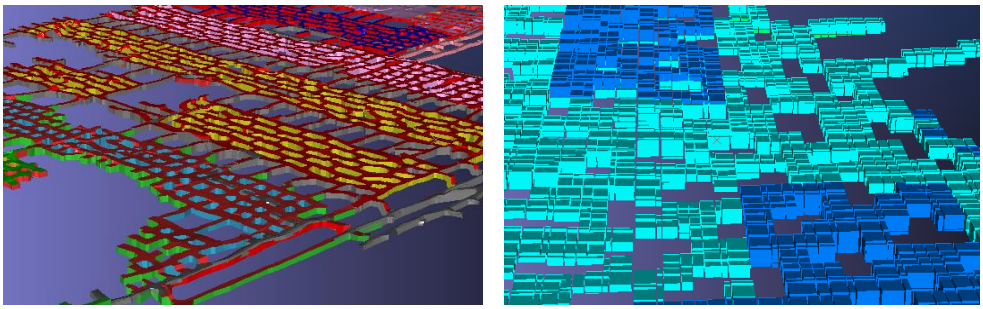

Figure 4.23 Typical visualisation of a digital 3-D model of underground room-and-pillar developments: left panel: solid wireframes, right panel: block model cells coloured by mining fields numbering (source: Datamine Studio)

4.3.1.2 Proposal of the DISIRE concept for tracking the ore lithology

The proposal of the use of DISIRE pellets for tracking the ore in order to provide the suitable information to the processing plants assumes the following:

- Pellets will be used to provide the information about lithology of the ore,
- Pellets are dropped into the copper ore bulk material while it is being discharged by trucks or loaders onto the division belt conveyor loading point (Figure 4.22),
- Pellets denote the place of mining (mining field) and the consecutive number of discharging,
- Pellets are read instantly after the portion of ore is hoisted by a skip from the shaft bunkers onto the surface (Figure 4.22).

The practical use of DISIRE pellets requires the interaction between the existing, currently being implemented and planned information systems. The 3-D geological modelling and mine planning system should provide the information about the lithology (Figure 4.21 and Figure 4.23) on the basis of actual orebody structural model and location of the mining field. It is expected that the system would be on-line interrogated with the annotation of the mining field read from the pellets delivered on the surface to return with the actual lithology composition at the mining faces obtained from the orebody model.

However, the composition of lithology of the ore hoisted on the surface depends on blending of the ore from several mining fields. The assessment of this will be achieved with the use of read-in several pellets as well as the information about the work of the underground transportation system.

Nobody assumes that all pellets can survive the transportation from the division belt conveyor to the surface in the difficult operational conditions of underground mines. The in-situ tests will allow to predict the percentage of pellets that are lost but it is obvious that the variance of “losses” will be high. Therefore the result lithology based only on the (weighted) data from pellets should be compared with the results of simulations of ore flow within the belt conveyor system.

The Convis system is expected to be fed with the data of lithology of ore that will be soon conveyed to the processing plant. The time delay caused by its transportation can be utilised for the proper adjustment of machinery equipment.

The planned workflow of process of identification of ore lithology with the use of modeling the ore and simulation of the ore flow in the BC system is presented below on 3 consecutive sheets (Figure 4.24) with the use of IDEF0 scheme (explained in the black frame in the bottom of the figure).

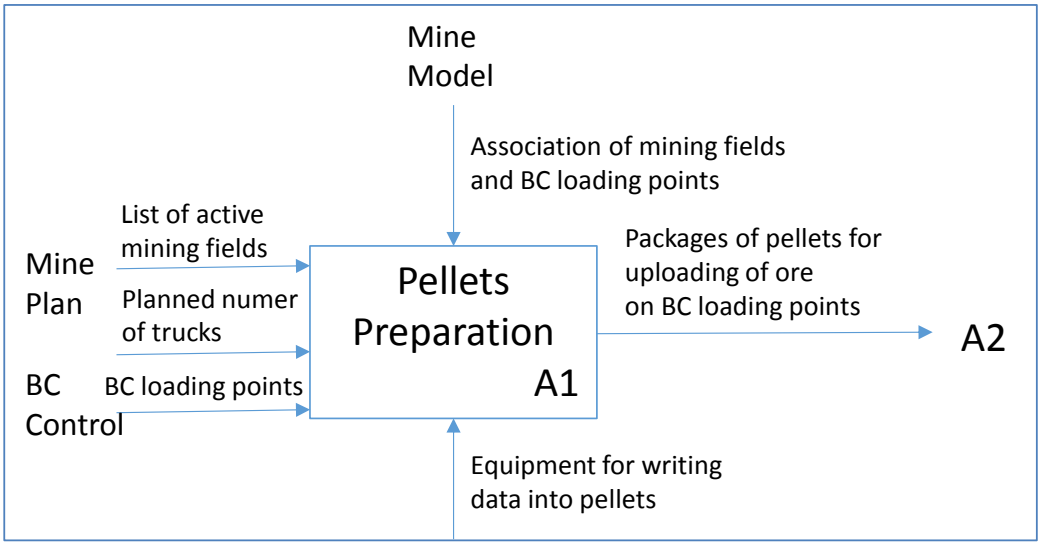
Mine
Model
Association of mining fields
and BC loading points
List of active
mining fields
Mine
Plan
Planned numer
of trucks
BC
Control
BC loading points
Pellets
Preparation
A1
Packages of pellets for
uploading of ore
on BC loading points
A2
Equipment for writing
data into pellets

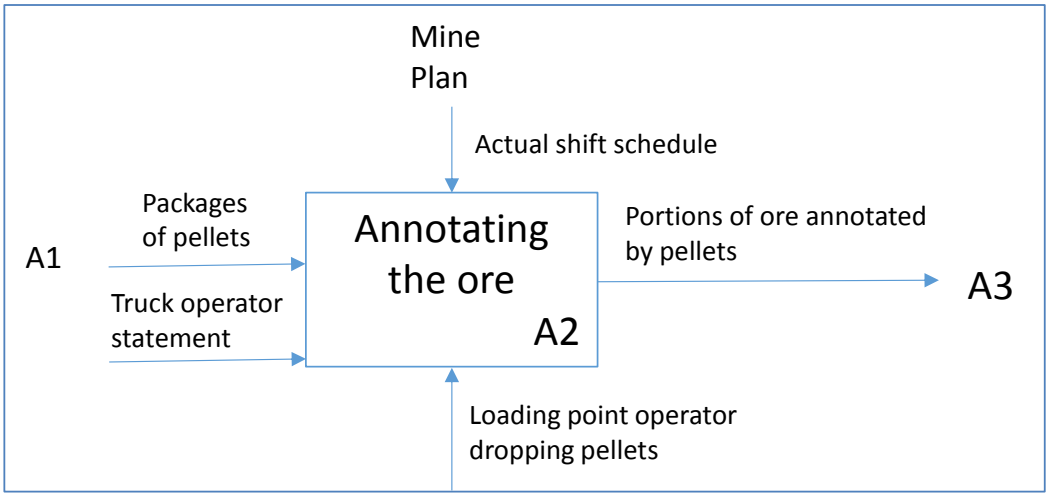
Mine
Plan
Actual shift schedule
Packages
of pellets
A1
Truck operator
statement
Annotating
the ore
A2
Portions of ore annotated
by pellets
A3
Loading point operator
dropping pellets

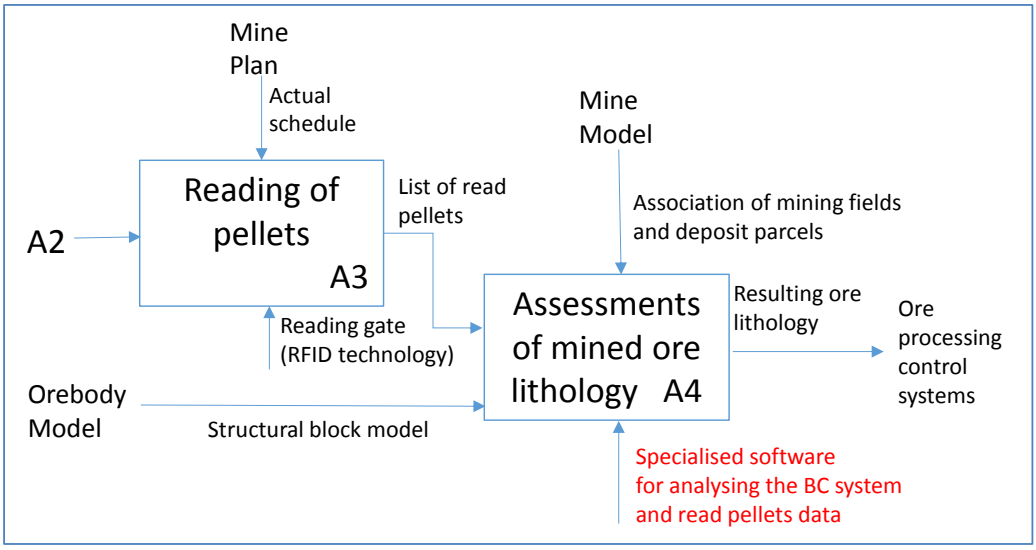
Mine
Plan
Actual
schedule
Mine
Model
A2
Reading of
pellets
A3
List of read
pellets
Association of mining fields
and deposit parcels
Reading gate
(RFID technology)
Assessments
of mined ore
lithology A4
Resulting ore
lithology
Ore
processing
control
systems
Orebody
Model
Structural block model
Specialised software
for analysing the BC system
and read pellets data

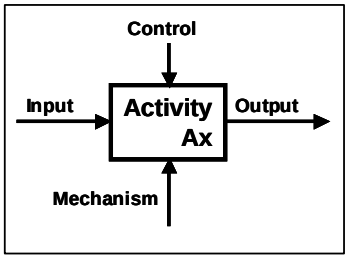

Figure 4.24 The workflow of identification of ore lithology with the use of DISIRE PAT sensors; in the bottom the IDEF0 scheme of annotation

The specialise software for analysing the BC system and read pellets data (in red on fig.4.24) has to provide with the information even in the case of loosing of some pellets. The simulation module helps to make the assessment of resulting ore compound. These elements are under development yet.

4.3.2 Conclusions

The problem of identification of the differentiated lithological compound of copper ore mined in the KGHM S.A. underground mines on its delivery to the ore concentrating divisions is presented. This identification can be achieved by the complex use of existing or being implemented information systems supported by the DISIRE Process Analyser Technology (PAT) pellets embedded into the conveyed ore for annotating each particular portion of mined material when uploaded onto a conveyor.

The flow of information and methods of its processing is proposed. The planned in-situ experiments as well as theoretical investigations including digital simulations and testing of necessary workflow od processed data are under development within the DISIRE project.

The description of the module will be presented in the next deliverables of the DISIRE Project.

References

[1] Tasdemir A., Kowalczuk P.B., 2014, Application of Statistical Process Control for Proper Processing of the Fore-Sudetic Monocline Copper Ore. Physicochem. Probl. Miner. Process. 50(1), 249−264 (2014).

[2] Hołodnik K., Jurdziak L., Kawalec W., Krysa Z.,Milczarek W., Paszkowska G., Pattinson G., Simpson R., 2015. Principles and recommendations for the system of quality assurance and control of analytical data with verification of current sampling procedures for the deposit, run-of-mine ore and feed (in Polish). Raport from ordered work (archive material)

[3] Drzymala J., Kowalczuk P.B., 2010, Problems with Statistical Evaluation of Separation Results, Proc.off the XIIth International Mineral Processing Symposium, Cappadocia, Turkey, 1191– 1202

[4] Dworczyńska M., Gładysiewicz L, Król R., 2013. Conveyed bulk material model for the needs of idlers durability assessment, (In Polish) Transport Przemyslowy i

Maszyny Robocze (Industrial Transport and Heavy Machinery), 1(19)/2013; ISSN 1899-5489.

[5] Gładysiewicz L., Kawalec W., Król R. Selection of carry idlers spacing of belt conveyor taking into account random stream of transported bulk material. Eksploatacja i Niezawodnosc – Maintenance and reliability 2016; 18 (1): 32–37, http://dx.doi.org/10.17531/ein.2016.1.5.

[6] Gładysiewicz L., Kawalec W., 2006a, Optimised selection of a belt conveyor loaded by a BWE. Continuous surface mining. 8th International symposium. ISCSM 2006. Proceedings, Aachen, September 24th-27th 2006. Aachen : Mainz, 2006.

[7] Gładysiewicz L., Kawalec W., 2006b. Selection of distance belt conveyors for underground copper mine. Proceedings of the Fifteenth International Symposium on Mine Planning and Equipment Selection, Torino, Italy, 20-22 September Vol. 1. Ed. by M. Cardu [et al]. Galliate, (NO) : FIORDO, 2006]. s. 101-106.

[8] Jurdziak L., 2008a. Application of extreme value theory for joint dimensioning of BWEs and long distance belt conveyors in lignite mines. Bulk Europe 2008. International Conference on Storing, Handling and Transporting Bulk, Prague, Czech Republic, 11-12 September. Wurzburg: Vogel Industrie Medien, p. 17.

[9] Jurdziak L., 2008b. Reactivation of the model of transported material distrubution on conveyor belt (in Polish). Górnictwo i geologia VIII (Mining and Geology VIII). Wrocław: Oficyna Wydaw. PWroc., 2005. s. 99-109.

[10] JURDZIAK L., KAWALEC W., KRÓL R., 2016. Current methods and possibilities to determine the variability of the Cu content in copper ore on a conveyor belt in one of KGHM PM mines. MEC 2016.

[11] Król R., 2013. Methods of testing and selection of the belt conveyor equipment with regard to random loading of a transported bulk material (in Polish). Monograph, Wroclaw University of Technology Press.

[12] B. Bazan B., Kasinska-Pilut E., Garbacki M., Bazan-Krzywoszanska A., 2014, Propulsion Investigation of the impeller radial velocity and copper mineralogy influence of the Cu scavenger flotation recovery in KGHM Polska Miedz S.A. Concentrators (Proceedings of the Mineral Engineering Conference MEC2014, 2014)

[13] Konieczny A. et al., 2011, Application of visualisation systems for controlling operating parameters of flotation machines in KGHM S.A. division of concentrators, Górnictwo i geologia 2011, tom 6, zeszyt 2 (in Polish)

[14] Konieczny A., Bazan B., 2012, Challenges and difficulties of comminution processes in KGHM PM S.A. Division of Concentrators (MEI Conference Comminution 2012)

Chapter 5

Belt conveyor (BC) energy efficiency

5.1 Idle work of BC system

As stated in chapter 2.3, the main goal of managing the BC systems in KGHM S.A. underground mines is to maintain the high level of the total output of ore supply. The firm requirement of mining divisions is to avoid delays of discharging mining trucks and LHDs because of any stoppages of the receiving BCs. Such delays result in decrease the number of trucks' courses – less ore is then hauled from a mining panel. Due to the following reasons:

- an inevitable random process of uploading the BCs by the cyclical transport - trucks or LHDs (as modelled in chapter 3),
- the required high instantaneous capacity of BC receiving the load of copper ore bulk onto its feeding point,
- the long and tedious procedure of switching on a BC after it has been stopped (due to rigorous safety precautions)

the BCs that receive ore from the cyclical transport are generally expected to run throughout the whole period of a working period of a shift.

Despite there is a possibility of the use of numerous ore bunkers (see Figure 5.10) to temporarily store the transported ore in order to switch off the sequent BCs (in the case of their low load work), such approach is avoided because it declines the reliability of the transportation network. The full capacity of ore bunkers is needed to allow on any unpredicted stoppages of BCs (see the chapter 6) without holding the ore delivery from mining panels.

Summing up, the idle work of BCs in the underground ore transportation is not a result of a bad, careless management of the transportation system but it is caused by putting the high output of mining panels on the top of the priority list. Therefore in order to achieve the significant energy savings of ore conveying in the underground transportation system, the efforts should be put into the decrease of specific energy consumption of BCs by the lowering their idle work energy consumption. This can be achieved by an improvement of BC design aiming the low energy consumption. This goal can be achieved due to:

- careful choice of a conveyor belt, with special regard to rubber mix parameters, selected individually for the planned operational conditions at the users' site,
- modernised idlers with reduced rotational resistance to motion,
- precise dimensioning of a conveyor units (which requires the use of advanced, computer assisted design tools).

The only possible way of the successful improvement of the elements of a BC designed to work in the harsh operational environment of underground mines is the extensive support of in-situ tests combined with the accurate calculations of the BC drive power requirements with regard to alternative BC equipment selection. The applied solutions are described below.

5.2 Modeling of a belt conveyor drive power requirements

Modeling of a belt conveyor drive power requirements bases on the calculations on its resistances to motion. Commonly used and well established standards for calculation belt conveyors (ISO5048, DIN22101) employ the concept of rolling resistance of the belt on idlers. Determining the coefficient of the main resistance ***f*** based upon indications provided by standards is more a matter of experience than of a calculation supported by theoretical and experimental scientific research (Gladysiewicz and Kawalec 2000). Such simplified methods, though regarded as out of date, can be successfully applied to typical belt conveyors only. They fail, however, when a deeper improvements of a conveyor equipment are considered and no previous operational experience is available.

The method of precise calculation the main resistance of belt conveyor has been developed in the Institute of Mining Engineering of the Wroclaw University of Technology (Gladysiewicz 2003). The method bases on the analysis of the energy dissipation processes in a conveyor belt and in the material load stream, as well as the analysis of the interaction between the belt and idlers. Physical properties of the belt and bulk material and the geometry of the conveyor have been employed in the algorithm to identify main resistance of a belt conveyor: rolls turning resistance, indentation resistance, flexure resistance of a belt and bulk material and sliding resistance of a belt on the idlers (Figure 5.1).

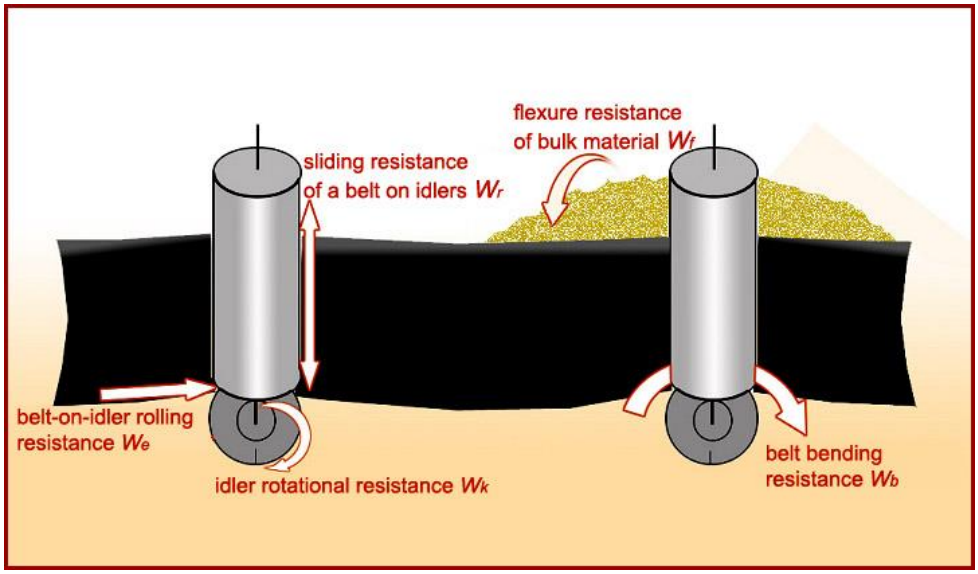

Figure 5.1 Components of belt conveyor main resistances to motion

Based on the algorithm, a computer program called Tasmtest was then developed (Gladysiewicz & Kawalec, 2000, 2001, 2005).

The resistance to motion is calculated for each object on the conveyor route (loading point, pulley, idler, cleaning device, etc.) with regard to the actual belt tension, actual normal loading (caused by actual conveyed material capacity) and all available specific parameters of the object and the belt, with the use of inheritance of objects and virtual methods. This object model is ready to deal with any concept of a belt conveyor (Figure 5.2). A given conveyor type

is modelled with the use of a composition of objects and definition of triggers (Gladysiewicz and Kawalec 2006).

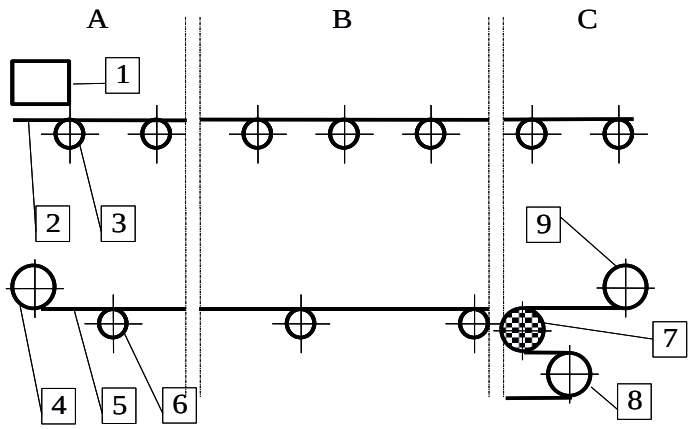

Figure 5.2 The general layout of the main belt conveyor objects: 1: loading point, 2 and 5: top and return belt, 3 and 6: idler sets in top and bottom belt, 4, 7, 9 and 10: tail, drive, take-up and head pulley respectively, section A: tail head, section B the route, section C: head station

The methods are programmed on the basis of the developed algorithm (Gladysiewicz, Hardygora, Kawalec 2009) and implemented into the in-house software Tasmtest and then into the comprehensive, specialized program for belt conveyor modeling and calculation – QNK-TT, already used by domestic and foreign (German and Russian) companies (Kawalec & Kulinowski 2007). QNK-TT is a suitable tool for the multi-purpose studies of belt conveyor design. Its library of procedures for calculating resistance to motion, forces and wear is being continuously improved and verified. Thus, there is a possibility of analysing various modernized elements of a belt conveyor as their individual characteristics are used as virtual methods in the module for calculation the conveyor movement resistance – method of primary resistances QNK-TT software. These characteristics are being developed upon the series of tests that are carried out both in a laboratory and in-situ. The last ones allow to take into consideration the influence of BC operational parameters.

5.3 Testing belt conveyor resistance to motion in underground mine condition

The conservative approach to the design of belt idler set support systems has long been observed. This conservatism is partly due to uncritical acceptance of standards specifying safe ranges. The latter often have an excessive margin of safety, whereby they are not always optimal. The pilot industrial installations of long-distance belt conveyors constructed both worldwide (Antoniak 2001, 2003) and in Polish mining industry (Antoniak 2010, Lutynski and Kozubek 2010) contradict some of the accepted and commonly used design solutions. This contradiction is also highlighted by the results and economic effects of research and development studies dealing with the optimization of belt conveyor designs carried out for PGiE KWB Belchatow S.A., which led to implementation of the designs in 2010 (Stefaniak et al, 2014). The main aim of the research was to indicate possibilities for the reduction of belt conveyor drives' energy consumption and to present the technical means for achieving them (Antoniak

2001, 2003, Bukowski et al. 2011, Gladysiewicz and Krol 2012, Gladysiewicz, Krol and Kisielewski 2012, Krol 2013).

The belt conveyors that are operated in the underground mines of KGHM Polska Miedz S.A. were mostly designed in the 1990s. The planned mining of new copper ore deposits situated deep and far off the existing main (transportation) shafts, creates a need to create new efficient and economically viable belt conveyor solutions.

It should be noted that the final solution of continuous transport system will be equipped with modern automation and monitoring systems with decision support algorithms. These issues have been widely presented in the literature, among others in (Mazurkiewicz 2014, Stefaniak, Zimroz and Krol 2012, Stefaniak, Wlomanska and Obuchowski 2014, Zimroz, Hardygora and Blazej 2014). However, one of the solutions which fit into the Company's innovation strategy is the use of belt conveyors with significantly reduced resistances to motion. Since the experience acquired from the research on optimal solutions for opencast brown coal mines cannot be directly applied to much smaller underground belt conveyors, mainly due to different types of belts employed, different (more compact) belt conveyor structure and more difficult installing and operating conditions, a project to develop a new energy saving belt conveyor was launched in KGHM PM S.A. The modernization efforts were divided into three main areas and consisted in the use of energy saving belts, idlers with reduced rotational resistance and drive units with enhanced efficiency. A schedule of research aimed at reaching the established goals was drawn up. The results of the investigations were published in (Kawalec and Wozniak 2014, Krol and Kisielewski 2014).

In case of horizontal and quasi-horizontal belt conveyors, main resistances constitute the biggest part of conveyor resistance to motion. Main resistances consists of: idler rotational resistance Wk, indentation rolling resistance We, belt bending resistance (flexure resistance of a belt) Wb, flexure resistance of bulk material Wf, sliding resistance of a belt on idlers Wr. Idler rotational resistance and indentation rolling resistance have a significant impact on energy consumption of belt conveyors (Gladysiewicz and Kawalec 2008). The conducted analyses showed that the sum of these two components can account for up to 70% of total belt conveyor resistance to motion (Antoniak 2001, Blazej, Jurdziak and Kawalec 2013). Greatest energy consumption reductions may result from adequate belt and idler selection, from optimal spacing of carrying idler sets, and in some cases also from unconventional solutions used in the design of routes, take-up arrangements and transfer chutes (Gladysiewicz and Kawalec 2003). The results of research and development works carried out at the Wroclaw University of Technology, Machinery Systems Division have shown that one of the conditions for successful reduction of the energy consumption of belt conveyor drives is to use high-quality idlers characterized by low rotational resistance under a wide range of working loads (Bukowski et al. 2011, Gladysiewicz and Krol 2012) and energy-saving conveyor belt characterized by low indentation rolling resistance (Bajda and Hardygora 2009, Bajda 2008).

5.3.1 Measuring method

Figure 5.3illustrates the concept behind the measurement of a single carrying idler set's resistances to motion. The term "carrying idler set" is here used in accordance with its common definition as a set of rolls supporting the belt and the material on the belt and will be later in this article referred to as "the idler set". The measuring idler set thus defined comprises a set of three carrying idlers and is installed on a specially constructed measuring unit of belt conveyor route equipped with six strain-based force gauges. The tested idler set is suspended from a special crossbar and is hinge-supported on two gauges measuring vertical forces F1 and F2, and registering the tensile force.

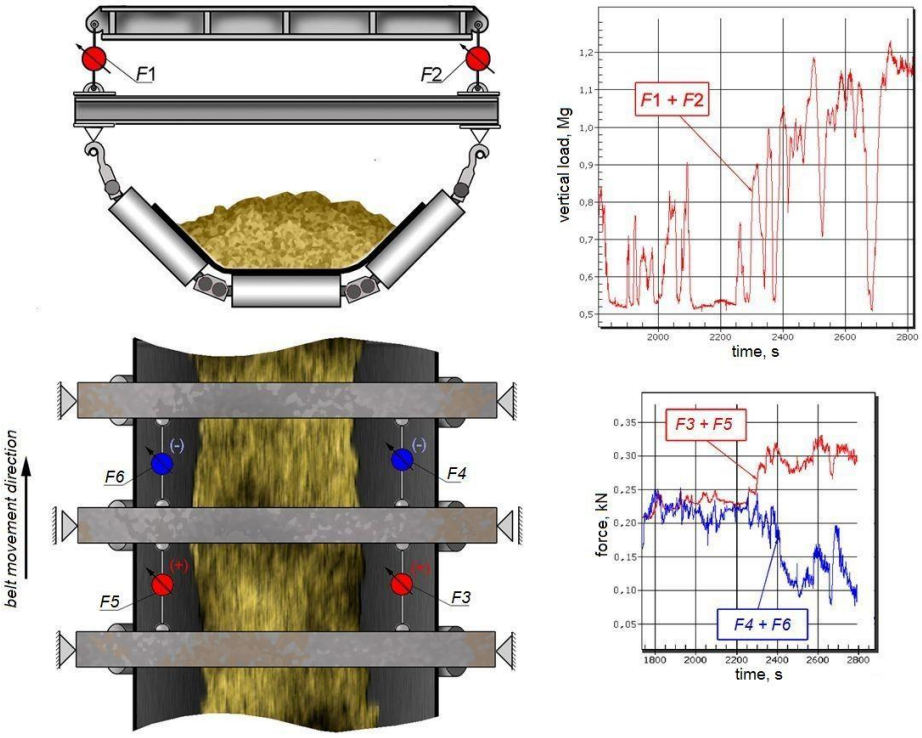

Figure 5.3 Measuring idler set with force gauges

During measurements, the sum of the two forces represents the resultant vertical load acting on the idler set. The load is composed of the idler set belt weight and the instantaneous weight of bulk material. This means that instantaneous conveyor output is also measured. Before each measurement, the crossbar with the hinge-supported set is lowered (using rigging screws) below the belt to register the gravity force of those elements of the set, which must be later deducted from the total reading of the force gauges. The neighbouring idler sets installed on the measuring unit are also suspended from crossbars and it is possible to adjust the suspension height on each side. Owing to this, prior to the experiment all the idlers can be precisely positioned in one plane, which eliminates any additional loading on the idlers. The bars holding suspended idler sets can be differently spaced from one another, which allows the spacing of the upper idler sets to be changed. The measuring set is held with articulated joints on both sides and supported in the horizontal plane by two pairs of narrow-range force gauges.

Differences between the readings given by the four force gauges are the basis for determining the instantaneous horizontal force at the belt/idlers contact area while the belt is running. The total resistance to motion per idler set is measured by two pairs of force gauges (F3 and F4, F5 and F6) located on both sides of the set and fixed to the horizontal elements. It should be noted that during belt movement horizontal forces registered by the gauges change as follows:

- forces F3 and F5 increase by respectively ∆F3 and ∆F5, due to the direction of the horizontal force of mutual interaction between the belt and the rollers:

$$F_3 = F_{30} + \Delta F_3 \tag{5.1}$$

and

$$F_5 = F_{50} + \Delta F_5 \tag{5.2}$$

- forces F4 and F6 decrease relative to their initial values, due to the horizontal force of mutual interaction between the belt and the rollers:

$$F_4 = F_{40} - \Delta F_4 \tag{5.3}$$

and

$$F_6 = F_{60} - \Delta F_6 \tag{5.4}$$

In order to determine the total resistance to motion per measuring set, one should add all the force increments registered by the horizontal gauges, i.e.

$$W_g = \Delta F_3 + \Delta F_4 + \Delta F_5 + \Delta F_6 \tag{5.5}$$

Thus, using relation (5.5), one can determine the instantaneous motion resistance values on the basis of the traces recorded by the four force gauges.

If belt tensioning force does not occur, which is the case when the neighbouring idler sets are aligned with the measuring set, the resultant horizontal force measured by the four gauges may be assumed to represent the total motion resistance of a single idler set. During the experiment, two preceding idler sets and two succeeding idler sets of the measuring stand were levelled relative to the measuring stand. Therefore, no effect of weight component is observed on the measured resistance to motion.

5.3.2 Testing and calibration of mobile measuring stand

In order to test the resistance to motion, which occurs on a single three-roll idler set, a mobile measuring stand was designed and built. Figure 5.4 shows a 3D model of the mobile measuring stand while the assembly drawing is shown in Figure 5.5. Owing to its design, the stand can be easily and quickly assembled at any point along the conveyor route, without disturbing the structure of the conveyor's load-bearing elements. Moreover, the design fits both 1000mm and 1200mm conveyors. The whole measuring set is equipped with two symmetrically located load gauges measuring the vertical load acting on the idler set and with four gauges in the horizontal plane, measuring the resultant horizontal force acting along the longitudinal axis of

the belt (the resultant motion resistance of the idler set). The measurement frame design allows for quick adjustment, and can be adapted to specific operating conditions, such as belt width and idler set load., As a result, resistances to motion can be measured on any belt conveyor under its typical operating conditions.

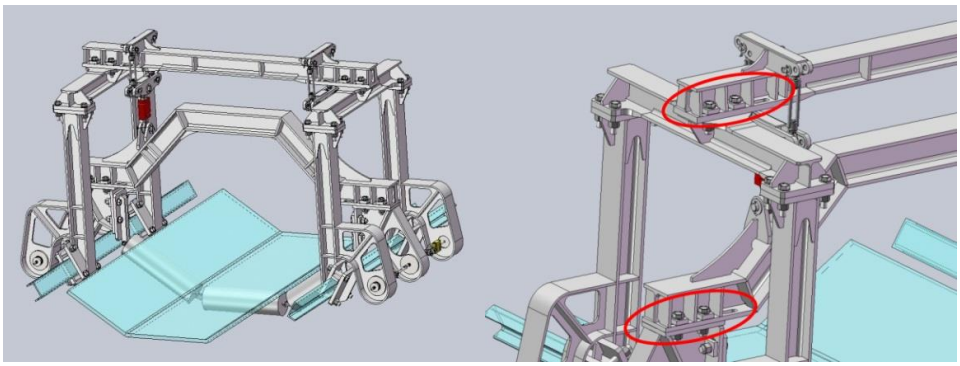

Figure 5.4 3D model of mobile measuring unit: a) general overview, b) view of the universal mounting flange

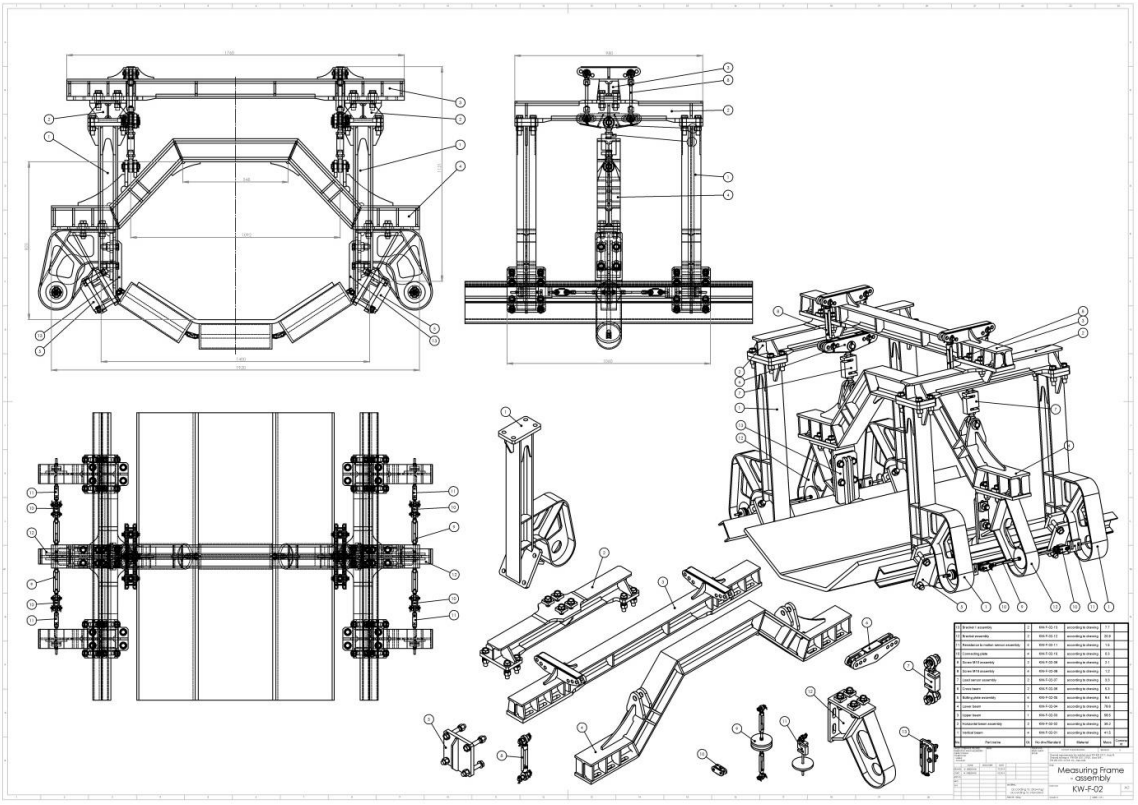

Figure 5.5 Assembly drawing of the measuring unit structure

When designing the measurement frame, several technical requirements were taken into account. The required features included:

- suitable stiffness of the frame, adaptable to the 1000mm and 1200mm wide conveyor route structure,

- the possibility to disassemble the device into conveniently small parts to be easily transported and assembled at any point along the belt conveyor route,
- the possibility to level the measuring set and suitably position it relative to the neighbouring idler sets.

The measurement frame of the mobile measuring stand was manufactured and then assembled on the production floor of KGHM ZANAM Sp. z o.o. Figure 5.6 shows a view of the assembled frame with gauges. The measuring signal was registered and transmitted from the force gauges using a SPIDER 8.0 amplifier connected to a computer equipped with Hottinger Catman Easy software, which enables recording, processing and analysing measurement signal changes. Hottinger S9 gauges with a measuring range of 20 kN were used to register vertical forces, while S2 gauges with a measuring range of 500 N were used to register resistance to motion.

Figure 5.6 Measuring unit view with force gauges

During the design stage of the measurement frame, the kinematic diagram of the system was analyzed. The examination involved active forces generated by the weight of a three-roller idler set and the reactions they caused.. The system's kinematic diagram is shown in Figure 5.7. The sum of the forces originating from the suspended set, the belt weight and the weight of the transported bulk material is denoted as F_v, while the forces connected with the motion resistance of the single three-idler set are represented by F_H. Assuming that the forces acting in the vertical plane and in the horizontal plane are in equilibrium and that particular elements are connected with articulated joints, the following equation of equilibrium for the vertical forces may be established:

$$F_V = F_1 + F_2 \tag{5.6}$$

where:

F_v – the resultant vertical loading force, kN,

F1, F2 – the registered vertical forces, kN.

In the horizontal plane, there is assumed equilibrium of the forces originating from the motion resistance of a single idler set and from the reaction forces measured by gauges F3 to F6 is

assumed. Before measurements, the gauges were preloaded to half of the measuring range. For the measuring plane, the following equation of the equilibrium of forces is obtained:

$$F_H = F_3 - F_4 + F_5 - F_6 \qquad 5.7)$$

where:

F_H – the force of the motion resistance of a single idler set, N,

F3, F4, F5, F6 – the horizontal forces being registered, N.

Three possible cases of different loading were analyzed, with attention paid to the effects of the phenomena that might occur along the belt conveyor route in real operating conditions (e.g. side movement due to mistracking). A view of the measuring system during calibration is shown in Figure 5.8. Accuracy of the readings from the installed force gauges was analyzed in the following cases:

- the application of vertical load, shown in Figure 5.8a,
- the lateral displacement of the crossbar, shown in Figure 5.8b,
- the action of applied vertical force and of horizontal force, shown in Figure 5.9.

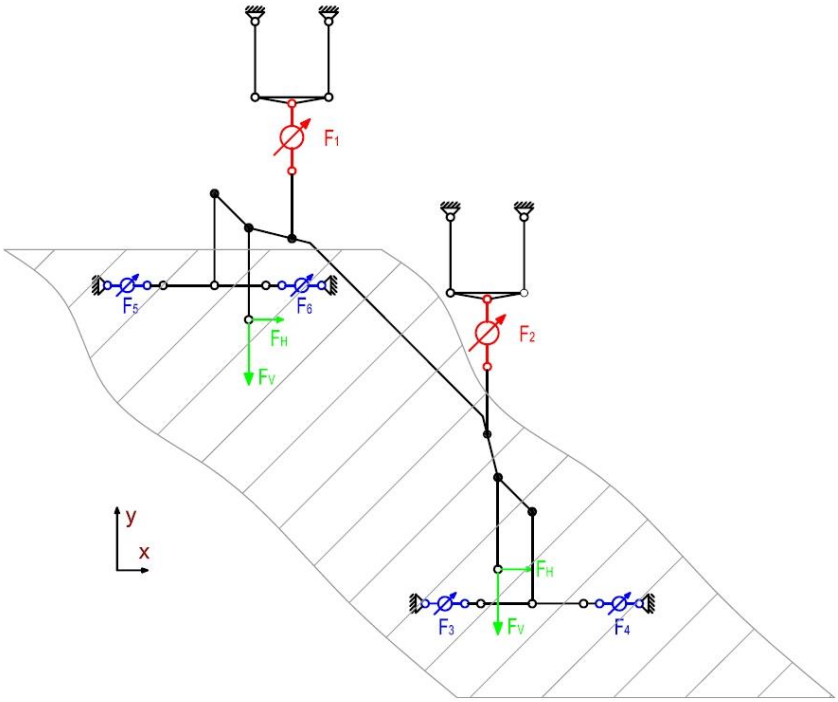

Figure 5.7 Kinematical diagram of measuring system

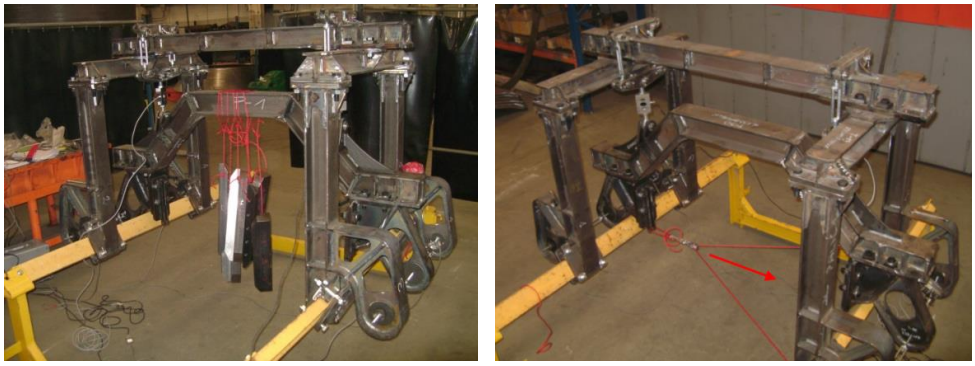

Figure 5.8 View of calibration of measuring system:
application of the vertical load (left), lateral displacement of the crossbar (right)

During the first two stages of calibration, reading accuracy of the mounted vertical and horizontal force gauges was tested due to applied vertical force and lateral displacement of the crossbar separately . The impact of applied vertical force on the reading accuracy of force gauges was analyzed with the use of known applied vertical force; this stage of calibration is shown in Figure 5.8a. The impact of the lateral displacement of the crossbar on the reading accuracy of force gauges was analyzed with the use of applied lateral displacement of the crossbar; this stage of calibration is shown in Figure 5.8b.

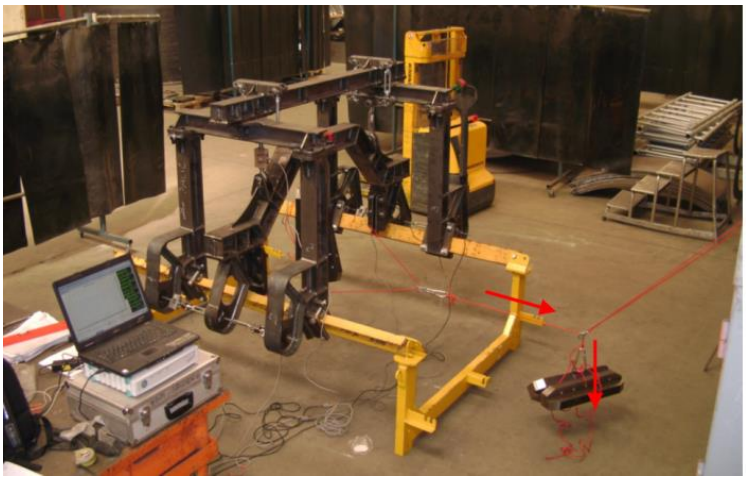

Figure 5.9 View of calibration of measuring system with use of applied vertical and applied horizontal force

Table 5.1 Effect of the action of applied vertical force and applied horizontal force on vertical force gauged reading accuracy

Applied force	Force gauges		Calculated force	Calibration error		Absolute error	Total absolute error	Total Relative Error
$F_{V\ App}$	F_1	F_2	F_V	-		$\Delta F_1, \Delta F_2$	$\Delta F_1 + \Delta F_2$	$\delta F_1 + \delta F_2$
[N]	[N]	[N]	[N]	[N]	[%]	[N]	[N]	[%]
269.7	819	911	274	4.30	0.02	10.00	20.00	0.023
539.5	962	1052	558	18.50	0.03			0.020
696.5	1043	1129	716	19.50	0.03			0.018

Table 5.2 Effect of the action of applied vertical force and applied horizontal force on horizontal force gauged reading accuracy

Applied force	Force gauges				Calculated force	Calibration error		Absolute error	Total absolute error	Total Relative Error
$F_{H\ App}$	F_3	F_4	F_5	F_6	F_H	-		$\Delta F_3, \Delta F_4, \Delta F_5, \Delta F_6$	$\Delta F_3, \Delta F_4, \Delta F_5, \Delta F_6$	$\delta F_3 + \delta F_4 + \delta F_5 + \delta F_6$
[N]	[N]	[N]	[N]	[N]	[N]	[N]	[%]	[N]	[N]	[%]
269.7	347.1	218.4	325.4	177.5	276.6	6.90	1.23	0.25	1.00	0.004
539.5	425.2	168.9	395.9	132.2	520.0	-19.50	3.19			0.005
539.5	426.8	170.2	397.5	132.5	521.6	-17.90	3.17			0.005

The third stage of calibration was carried out having regard to the level of forces acting on the elements of the belt conveyor during normal operation. During this stage of calibration, the accuracy of both vertical and horizontal force gauges was tested simultaneously. Results are presented in Table 5.1 and Table 5.2. For this purpose, possible force system acting on the measuring idler set was analyzed. According to the measuring unit's design, all of the force gauges are connected with articulated joints. This type of connection allows to perform calibration making allowance for friction forces occurring on. The calibration process was therefore conducted in conditions simulating operating conditions of the belt conveyor.

Calculation of resistance to motion and vertical load of the single carrying idler set on the basis of force gauges readings is made with some accuracy, which is connected with the uncertainty of the measurement. For measurement of vertical force (Figure 5.3), S9 type force gauge was used, manufactured by Hottinger Baldwin Messtechnik GmbH with measuring range up to 20 kN and accuracy class of 0.05. Measurements of horizontal forces were made with the use of S2 type gauge from the same manufacturer. Measurement range of S2 type gauge is up to 500 N, the accuracy class is the same as in the case of S9 gauges. Before the measuring process, horizontal gauges were preloaded up to 50% of measuring range (Figure 5.3). In

addition, the measuring range of the gauges is bigger than the expected value of the measured horizontal forces. An important requirement for the gauge is to withstand the peak loads that can appear during normal operation of belt conveyor and have a negative impact on, or even destroy the force gauges. Therefore horizontal force gauges with the range up to 500 N are necessarily used, despite the relatively small calculated resistance to motion (20 – 45 N). During downtime of the belt conveyor, all horizontal force gauges are preloaded up to approx. 250 N, although during belt conveyor's normal operation readings from horizontal force gauges change within the range of 150 – 350 N. Resistance to motion is calculated on the basis of readings from horizontal force gauges according to equation 5.5. Absolute error (Δ) of a single S9 type force gauge is 10 N For two S9 gauges located in the measuring system, the total absolute error is the sum of absolute errors of each force gauge ($\Delta F1+\Delta F2$) and reaches up to 20 N. Absolute error of single S2 type force gauge is 0.25 N, thus for four S2 gauges installed in the measuring system the total absolute error is sum of absolute errors of four gauges ($\Delta F3+\Delta F4+\Delta F5+\Delta F6$) and reaches up to 1 N. Absolute and relative errors calculated for vertical and horizontal force gauges are shown in Table 5.1 and Table 5.2.

5.3.3 Tests on standard belt conveyor

The operational measurements were carried out on the L-1031 standard conveyor with a 1000mm wide belt, working in the EAST region of the KGHM Lubin mine, whose specifications are as follows:

- Belt conveyor type Legmet H1000
- Length, L 530 m
- Conveyor belt width, B 1000 mm
- Speed of conveyor belt, v_t 2,0 m/s
- Idlers spacing, l_k 0.83 m
- Drive system specification :
- number of electric motors 2
- type of electric motors 2SIE 315M6D
- power of electric motors 2 x 160 kW 50 Hz, 500 V
- clutch type VOITH TVVSN
- gear type PLC40 – R10-G12-25
- gear ratio 1:25
- Brake type Disk brake OMEGA 200
- Average slope 1°39′
- Expected load 400 Mg/h

Location of L-1031 belt conveyor within KGHM Lubin mine transportation network is indicated in Figure 5.10.

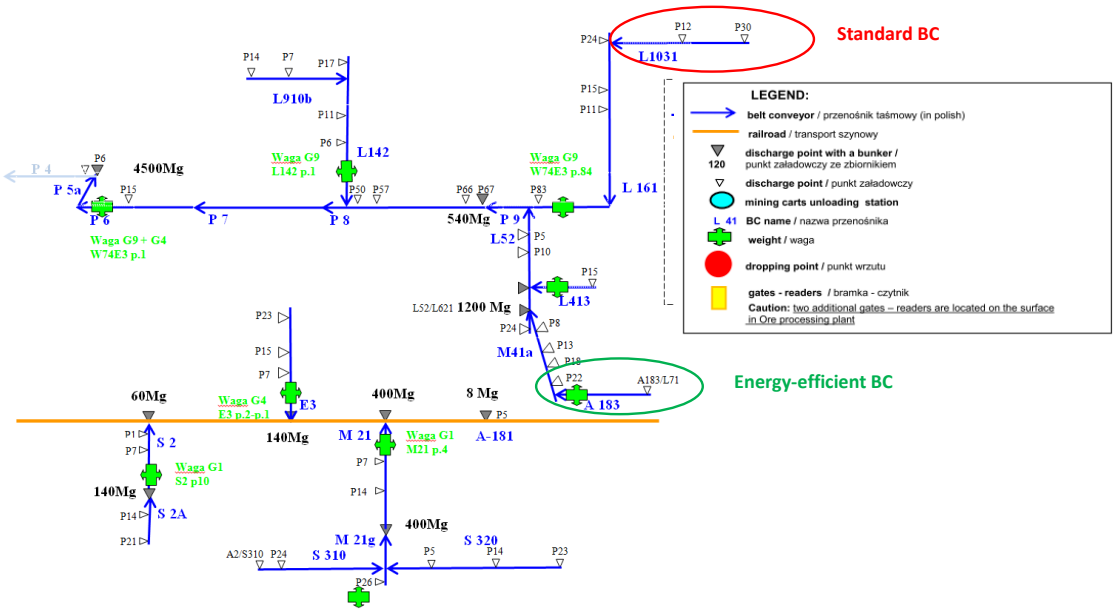

Figure 5.10 KGHM Lubin mine transportation network

Figure 5.11 shows a view of the belt conveyor and the mobile measuring unit on which the motion resistance of a single carrying idler set was measured.

Figure 5.11 View of the conveyor and the assembled measuring unit

During the measurements, records were taken of the trace of the resultant vertical force, which is the sum of the readings from the two side force gauges F1 and F2 (Figure 5.12),and the trace of the resultant horizontal force, as the total signal from the four force gauges: F3, F4 (Figure 5.13) and F5, F6 (denotations consistent with Figure 5.3). The vertical resultant force is a measure of the instantaneous output of the belt conveyor, while the horizontal resultant force is the measured motion resistance per idler set.

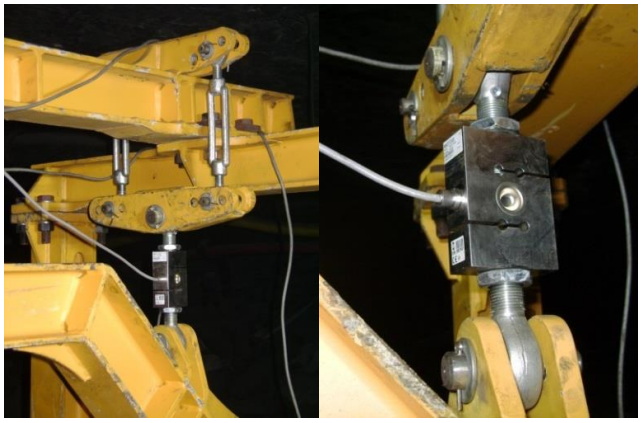

Figure 5.12 Gauges registering resultant vertical load Fv

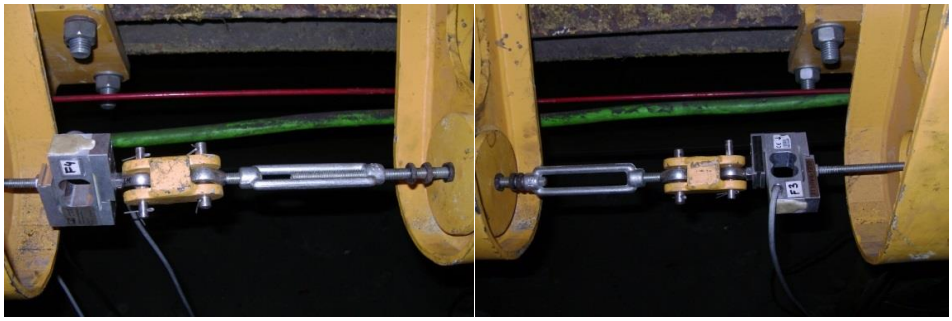

Figure 5.13 Gauges registering horizontal forces F4 and F3

Measurements carried out in mine conditions allowed to record the real forces that exert load on the tested measuring set and to determine the motion resistances of the set. The variation in the vertical forces over time is shown in Figure 5.14. The resultant vertical force is a measure of the instantaneous output of the conveyor, while the resultant horizontal force is a measured resistance to motion per idler set (Figure 5.14Figure 5.15).

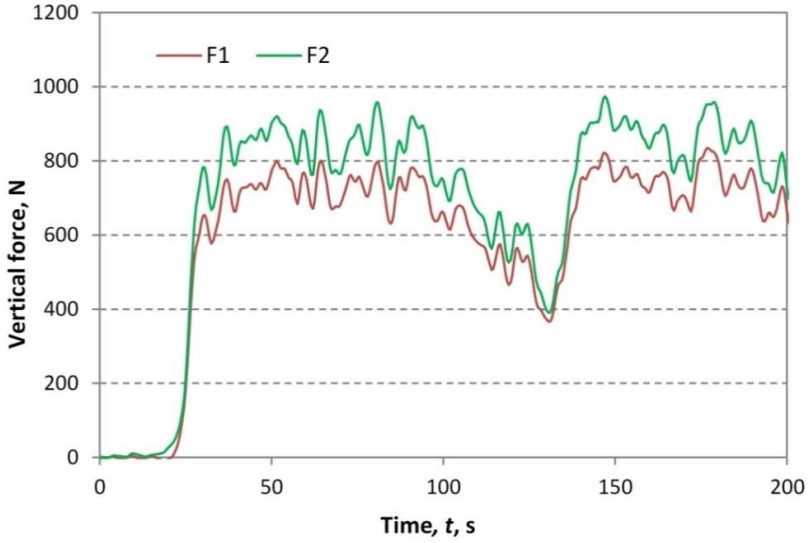

Figure 5.14 Exemplary traces of instantaneous vertical forces

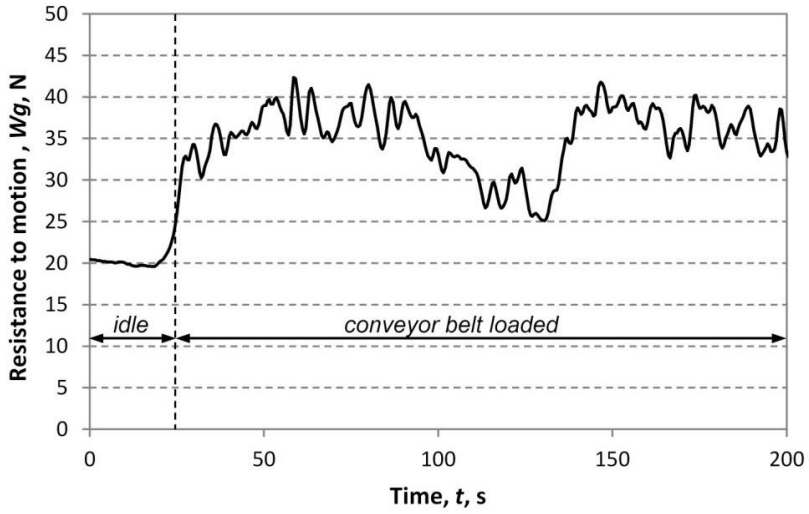

Figure 5.15 Exemplary variation in resistance to motion of idler set

The indications of the force gauges were continuously recorded during one working shift. The results were then screened by selecting time intervals with characteristic variations in load, resulting from variations in the stream of bulk material. Figure 5.16 shows the idler set's motion resistance, according to the research results, as a function of recorded vertical load F_V. The measurements are contained within the vertical force range of up to about 2 kN – the value corresponding to the rated loading of the belt with bulk material. This allowed to obtain a number of measuring points, showing a distinct functional dependence.

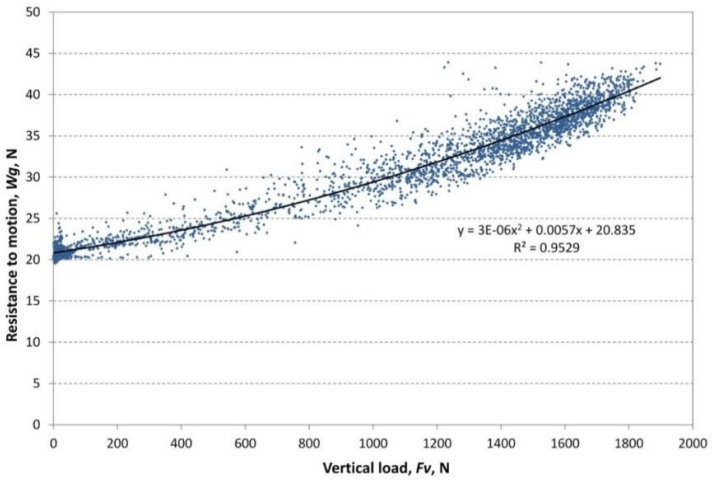

Figure 5.16 Set of measuring points illustrating dependence between motion resistance of single idler set and vertical load Fv

In order to determine the energy consumption of the base (reference) belt conveyor, against which energy saving effects will be compared, it is necessary to convert resultant vertical force F_V into mass capacity Q_m. Recorded resultant vertical force F_V acting on the idler set, induced by the deadweight of the belt and the instantaneous output weight, amounts to:

$$F_V = l_k \cdot g \cdot \left(B \cdot m_t + m_u\right) \quad \text{in N,} \tag{5.8}$$

where:

l_k– the spacing of the upper idlers, m;

B – the width of the belt, 1.00 m;

m_t – the specific weight of the belt, 21,74 kg/m2;

g – gravitational acceleration, 9.81 m/s2;

m_u–the linear weight of the output, kg/m.

The instantaneous conveyor belt capacity amounts to:

$$Q_m = m_u \cdot v_t \quad \text{in kg/s,} \tag{5.9}$$

or:

$$Q_m = 3{,}6 \cdot m_u \cdot v_t \quad \text{in Mg/h,} \tag{5.10}$$

where:

vt– the belt speed, m/s.

Hence the mass capacity expressed in Mg/h, determined on the basis of the resultant vertical force, is calculated from the relation:

$$Q_m = 3{,}6 \cdot \left(\frac{F_V}{l_k \cdot \mathrm{g}} - B \cdot m_t \right) \cdot v_t \tag{5.11}$$

The nature of the variations in idler loading was described as a linear regression function. For this purpose a polynomial trend line of the 2nd degree was determined for the recorded measurement series. Fit coefficient R2 obtained for the trend line was very high and amounted to 0.95.

The visible changes in the resistance to motion of the tested idler set are due to changes in the amount of the stream of material on the conveyor. Therefore, changes in instantaneous motion resistance values need to be always analyzed in correlation with the random variation in the bulk material stream. The determined dependence between single idler set motion resistance W_g and mass capacity Qm is shown in Figure 5.17.

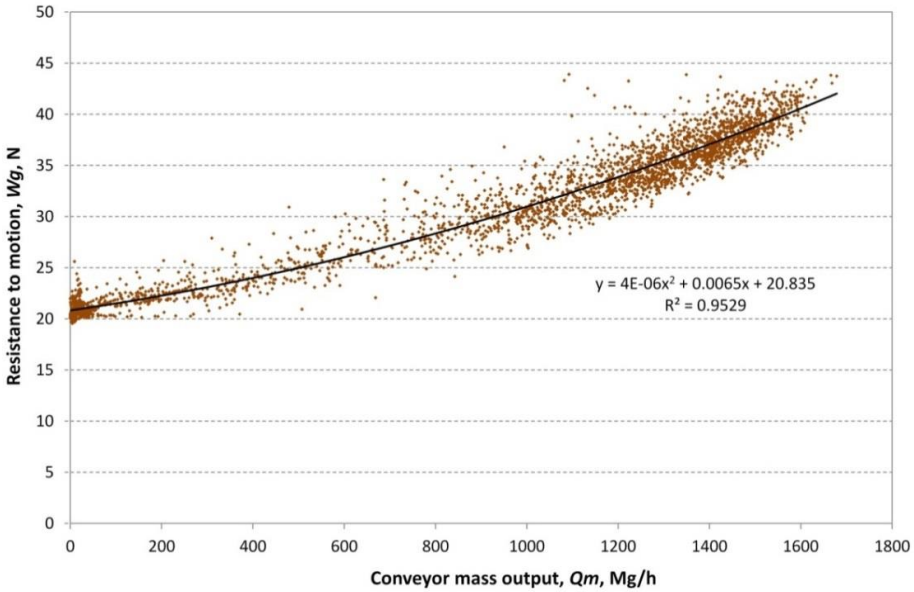

Figure 5.17 Single idler set motion resistance versus mass capacity

5.3.4 Tests on energy-efficient belt conveyor

After the operational measurements carried out on the L-1031 belt conveyor the mobile measuring unit was moved to the energy-efficient belt conveyor which location within KGHM Lubin mine transportation network is indicated in Figure 5.10. The energy-efficient belt conveyor was developed and manufactured with use of components (idlers, belt) which were selected based on their laboratory tests aimed at resistance to motion (energy consumption). Moreover the conveyor belt in energy-efficient belt conveyor is supported by “stiff” idler sets which are shown in Figure 5.18.

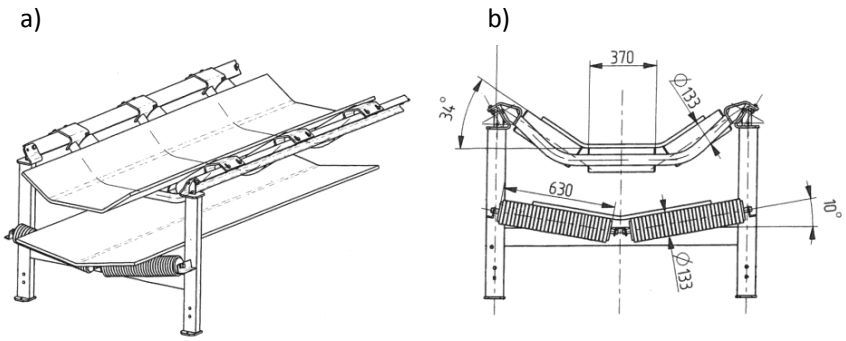

Figure 5.18 Scheme of the energy-efficient belt conveyor route: a) side view, b) crossection

The range of operational measurements carried out at energy-efficient belt conveyor was identical as at the standard belt conveyor. The results of operational measurements carried out at energy-efficient belt conveyor are shown below. Fragment of determined instantaneous vertical forces trace is shown in Figure 5.19.

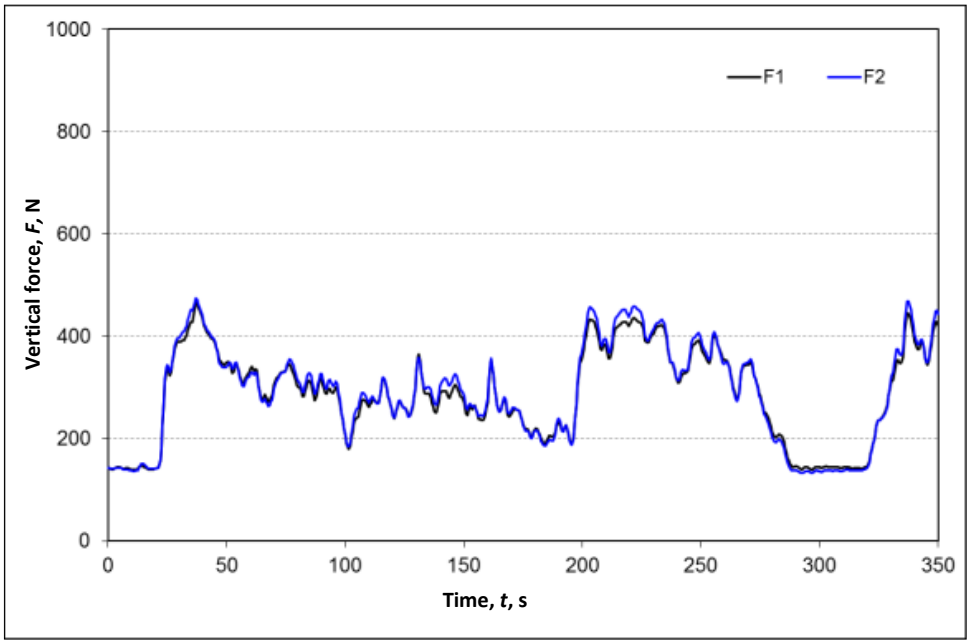

Figure 5.19 Exemplary traces of instantaneous vertical forces

Fragment of determined instantaneous resistance to motion of idler set is shown in Figure 5.20.

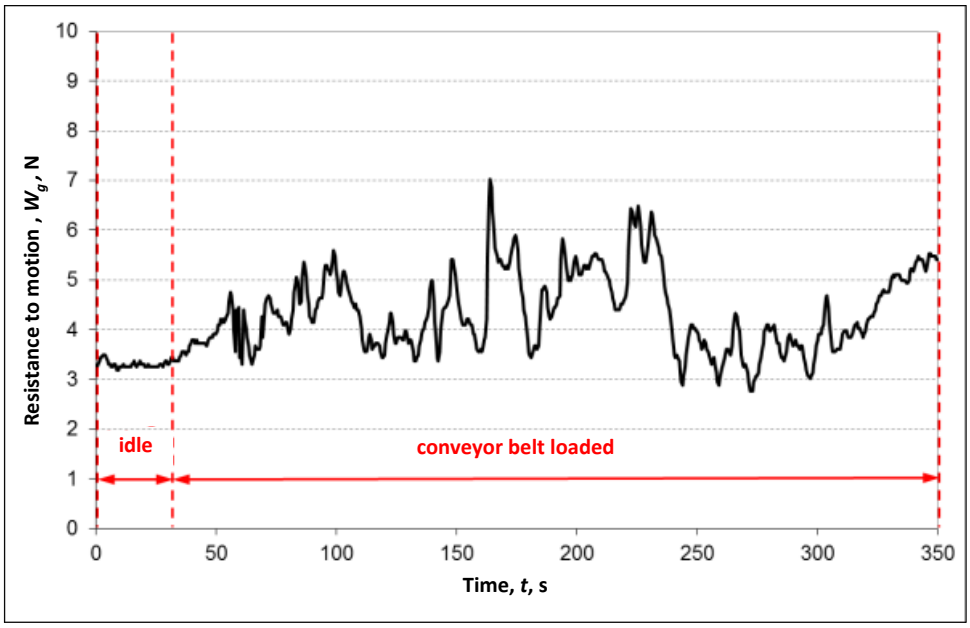

Figure 5.20 Exemplary variation in resistance to motion of idler set

The determined dependence between single idler set motion resistance W_g of energy-efficient belt conveyor and it's mass capacity Qm is shown in Figure 5.21.

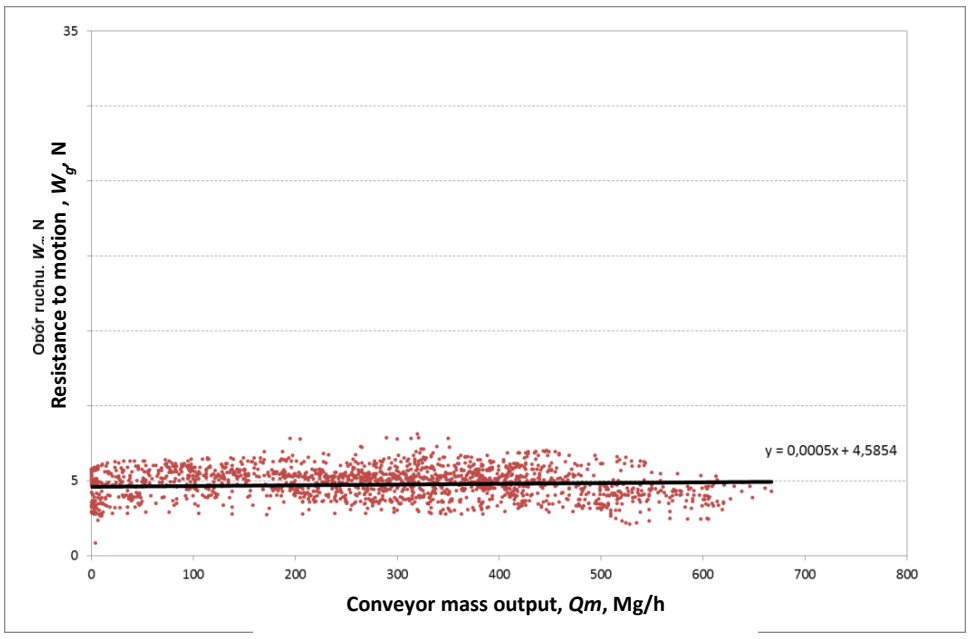

Figure 5.21 Single idler set motion resistance versus mass capacity

5.3.5 Conclusion

The accuracy of the available computing methods is vital in analyses aimed at determining the effect of belt conveyor design parameters on its resistances to motion. In order to verify the methods, measuring belt conveyor resistances to motion appears a necessity. The proposed

measuring method, based on registering forces in a hinged system supporting the measuring crossbar, was found to be useful in the operational testing of a belt conveyor in underground mine conditions. Calibration confirmed high accuracy of the proposed measuring method and the recording-measuring apparatus proved to be fully useful. The research allowed to determine resistances to motion of a single idler set of the belt conveyor in the whole range of the randomly variable stream of bulk material. A distinct effect of the degree of belt conveyor filling on the values of was observed. The amount of bulk material on the conveyor belt was observed to have significant influence on the registered values of motion resistance.

The results of tests carried out in industrial conditions at two belt conveyors confirmed the rightness of components selected for new energy-efficient belt conveyor. Selected components allowed to achieve the significant reduction of main resistance of energy-efficient belt conveyor in relation to standard belt conveyor (resulting in lowering the drive's energy consumption). It has been shown that the proper development of new generation of belt conveyors to be used in KGHM PM S.A. should take place primarily through careful selection of energy saving conveyor belt and idlers with low rotational resistance. During components selection the construction and reliability issues should be defined with particular attention and taken into account. On the basis of determined vertical forces F1 and F2 the symmetrical load of measuring idler set was observed which indicates low misalignment of conveyor belt (lateral belt movement) and symmetrical loading of transported material on the belt. The use of energy saving conveyor belt manufactured with use of properly selected rubber compound for bottom cover (non-carrying side) and idlers with low rotational resistance with "stiff" support allowed to reduce the average idler set motion resistance (main resistance) from 20N for standard belt conveyor to 5N for energy-efficient belt conveyor (for mass output up to 700 Mg/h which reflects approximate 0.45 loading coefficient k_z). The comparison of tests results for standard and energy-efficient belt conveyor is shown in Figure 5.22.

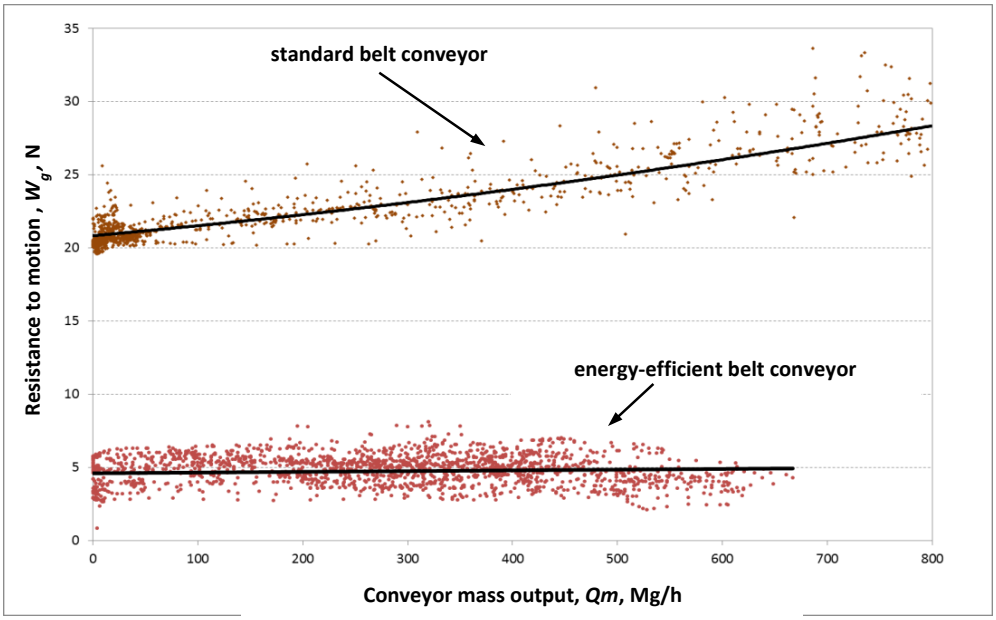

Figure 5.22 Comparison of tests results for standard and energy-efficient belt conveyor

Current operating conditions of Energy efficient belt conveyor made impossible to carry out tests for full range of conveyor's mass output. However, low main resistance within the range of small mass output allow for the assumption that the main resistance will remain low within the range of large mass output.

The test results will be analysed in order to build modified characteristics of the modernised, energy-efficient BC in order to model the BC drive power requirements in various operational conditions, typical for various positions of a BC in the transportation system. This will allow to make the reliable assessment of the energy savings of the whole BC transportation system due to the available BC design improvements regardless on any optimisation of the transportation system management.

Acknowledgements:

The above chapter 5.3 is mostly based on the paper: Robert Król, Waldemar Kisielewski, Damian Kaszuba & Lech Gładysiewicz (2016): Testing belt conveyor resistance to motion in underground mine conditions, International Journal of Mining, Reclamation and Environment, DOI: 10.1080/17480930.2016.1187967.

The design, calibration and manufacture of the mobile measuring stand was financed by courtesy of KGHM ZANAM Sp. z o.o.

Further research carried out into belt conveyor resistance to motion in underground mine condition was supported by the Framework Programme for Research and Innovation Horizon 2020 [under grant agreement n. 636834 (DISIRE)].

References

[1] Antoniak J.: Resistances to the motion in mining belt conveyors. Acta Montanistica Slovaca,roč. 6,č. 2, 2001, s. 150 – 157.

[2] Antoniak J.: Theoretical basis and industrial applications of energy – saving and increased durability belt conveyors. Acta Montanistica Slovaca, roč. 8, č. 2-3, 2003, s. 106 – 117.

[3] Antoniak J.: Technical undertakings to decrease in energy consumption of mining belt conveyors (in Polish):

[4] Przedsięwzięcia techniczne zmniejszające energochłonność górniczych przenośników taśmowych). Mechanizacja i Automatyzacja Górnictwa, 3(48)/2010, s. 42 – 51.

[5] Bajda M., The impact of the conveyor belt rubber cover on its rolling resistance over idlers. Dissertation Wroclaw University of Technology (not published), 2009.

[6] Bajda M., Hardygóra M., 2007. Determination of the conveyor belt's resistance to rolling on idlers. Proceedings of the Sixteenth International Symposium on Mine Planning and Equipment Selection, MPES 2007, Bangkok, 59-67.

[7] Błażej R., Jurdziak L., Kawalec W., Energy saving solutions for belt conveyors in lignite surface mines. Proceedings of the 13th IAEE European Conference, Duessedorf, August 18-21, 2013.

[8] Bukowski J., Gładysiewicz L., Król R.: Tests of belt conveyor resistance to motion. Eksploatacja i Niezawodność - Maintenance and Reliability, 3/2011, s. 17–25.

[9] Gładysiewicz L., Belt conveyors theory and calculations (in Polish: Przenośniki taśmowe Teoria i obliczenia), Oficyna Wydawnicza Politechniki Wrocławskiej, 2003, ISBN 83-7085-737-X.

[10] Gładysiewicz L., Hardygóra M., Kawalec W. 2009, Determining belt resistance. Bulk Handling Today 2009; vol 5: 23-28.

[11] Gladysiewicz, L., Kawalec, W., 2000, Object modelling of a belt conveyor. Mine Planning and Equipment Selection 2000. Athens

[12] Gładysiewicz L., Kawalec W., The possibilities of decreasing the belt conveyors main drive power demand, Proceedings of the Conference Bulk Europe 2008, Prague, September, 2008.

[13] Gładysiewicz L., Król R.: Operational tests of resistance to motion and load of idlers in the belt conveyor.(in Polish: Badania eksploatacyjne oporów ruchu i obciążeń krążników na przenośniku taśmowym). Problemy bezpieczeństwa w budowie i eksploatacji maszyn i urządzeń górnictwa podziemnego: monografia. 2012, s. 95-107

[14] Gładysiewicz L., Król R., Kisielewski W.: Experimental studies on the resistance to motion in an overbunden belt conveyors system. World of Mining, 6/2012.

[15] Kawalec W.: Long-distance belt conveyors (in Polish: Przenośniki taśmowe dalekiego zasięgu). Transport Przemysłowy, 1(11)/2003.

[16] Kawalec W., Kulinowski P., 2007, Computations of belt conveyors. Transport Przemyslowy 1(27), 2007 (in Polish)

[17] Kawalec W., Woźniak D.: Energy efficiency of the bottom cover of a conveyor belt – the first step to the new classification of belts (in Polish: Energooszczędność okładki bieżnej taśmy przenośnikowej – wstęp do nowej klasyfikacji taśm). Mining Science, 21(2)/2014, s. 47 – 60.

[18] Król R.: Methods of testing and selection of the belt conveyor equipment with regard to random loading of a transported bulk material (in Polish: Metody badań i doboru elementów przenośnika taśmowego z uwzględnieniem losowo zmiennej strugi urobku).Oficyna Wydawnicza Politechniki Wrocławskiej, 2013, ISBN 978-83-937788-1-2.

[19] Król R, Kisielewski W.: The influence of idlers on energy consumption of belt conveyor (in Polish: Wpływ krążników na energochłonność przenośnika taśmowego). Mining Science, 21(2)/2014, s. 61 – 72.

[20] Lutyński, A., Kozubek A.: Operation of rising conveyor on transport/haulage dip-heading in „Marcel" Hard Coal Mine (in Polish: Eksploatacja przenośnika wznoszącego upadowej odstawczo-transportowej w KWK "Marcel"). Maszyny Górnicze, 2(28)/2010, s. 13 – 18.

[21] Mazurkiewicz D.: Computer-aided maintenance and reliability management systems for conveyor belts. Eksploatacja i Niezawodnosc- Maintenance and Reliability, 3/2014, s. 377 – 382.

[22] Stefaniak P., Zimroz R., Krol, R., et al.: Some Remarks on Using Condition Monitoring for Spatially Distributed Mechanical System Belt Conveyor Network in Underground Mine - A Case Study . 2nd International Conference on Condition Monitoring of Machinery in Non-Stationary Operations (CMMNO), Hammamet, TUNISIA, MAR 26-28, 2012.

[23] Stefaniak P., Wyłomańska A., Obuchowski J., at al.: Procedures for Decision Thresholds Finding in Maintenance Management of Belt Conveyor System - Statistical Modeling of Diagnostic Data. PROCEEDINGS OF THE 12TH INTERNATIONAL SYMPOSIUM CONTINUOUS SURFACE MINING – Aachen SEP 21-24, 2014, Book Series: Lecture Notes in Production Engineering.

[24] Zimroz R., Hardygóra M., Błażej R.: Maintenance of Belt Conveyor Systems in Poland - An Overview. PROCEEDINGS OF THE 12TH INTERNATIONAL SYMPOSIUM CONTINUOUS SURFACE MINING – Aachen SEP 21-24, 2014, Book Series: Lecture Notes in Production Engineering.

Chapter 6

Modeling of data relations in application to fault detection

6.1 Temperature and electric current relation modelling

6.1.1 Introduction

Trouble-free operation of mechanical systems is of high importance in many industries. Automotive, chemical, aerospace and mining industries are prominent examples of branches, where condition of mechanical systems plays an important role (Jardine, Lin, and Banjevic 2006; Randall 2011; Yin et al. 2015). Any unexpected break might result in problems with fulfilment of the production schedule. Today's technological opportunities give possibility to monitor a lot of informative features related to operational condition of machinery systems. This raises a need to develop models for continuous-time fault detection systems that would help to maintain complex systems that consists of many machines. Surely, mining networks of belt conveyors are illustrative examples of such systems. Belt conveyors, especially these that are connected serially, are exposed to unexpected downtimes due to fault of their elements. One of the most crucial components of the belt conveyor is the conveyor belt. There are many systems that quantify condition of the belt. Each type of conveyor belt is related to specific approaches which can be beneficial in terms of fault detection. For instance, belts with steel cord might be diagnosed using systems that measure magnetic disruptions (Błażej, Kirjanów, and Kozłowski 2014; Mao et al. 2011). Condition of fabric conveyor belts might be assessed using X-ray imaging or other non-destructive methods (Fourie et al. 2005). Both of these approaches require advanced methods of signal processing (Obuchowski, Wylomańska, and Radosław Zimroz 2014; Xian-Guo et al. 2011). Another crucial part of belt conveyor network is the drive train, which usually consists of electric motors, shafts, gearboxes and pulleys. In this case, monitoring systems are often equipped with sensors that measure vibrations, temperatures, weight of the transported material, electricity consumed by motors, etc. (Stefaniak et al. 2016; Radoslaw Zimroz, Hardygóra, and Blazej 2015). Fault detection systems require not only to monitor the acquired data, but the main purpose is to provide decisions whether the considered part of the conveyor is faulty or not. In this section we propose a model of the relation between electric current and temperature on the gearbox. When the new measurements are available, the model parameters are estimated and compared to the healthy-case parameters. It is presented that the electric current of engines and temperature measured on gearboxes might provide a reliable diagnostic information that might help to minimize stall time of the belt conveyor network in the underground mine. The methodology presented in this section is based on the concept presented in (W Bartelmus and R Zimroz 2009; Radoslaw Zimroz, Walter Bartelmus, et al. 2014), where similar kind of relations are found for vibration data.

6.1.2 Analyzed data description

In this report temperature and current records acquired by commercial, multichannel low frequency data logger are analyzed. The measurement systems operates continuously in an underground copper ore mine. Data is collected on four gearboxes and electric motors installed within a drive station on a single belt conveyor. Size of the belt conveyor system causes that the monitoring system measures a lot of signals. In order to avoid overwhelming size of the data

files, readings are quantized into predefined, finite set (denote $T = \{\tau_1, \tau_2, , \tau_{n_t}\} : \tau_j < \tau_{j+1}$ for temperature, $I = \{i_1, i_2, i_{n_i}\} : i_j < i_{j+1}$ for current) and the system saves a particular reading if it differs from previous one more than a given threshold. Each record possesses information of time (year, month, day, hour, minute and second) and related physical quantity. Unfortunately, this storage-saving solution comes with difficulties in signal processing. During specific time interval each channel might possess different amount of values recorded in different time points. Therefore, integration of data from different channels might be difficult. Thus, signal interpolation is strongly recommended and can solve this problem. Moreover, in analyzed observation one can notice some outliers. Let τ_j be a temperature recorded at the k-th time point, and assume that it corresponds to j-th value from the predefined set of quantized temperature data, namely $x_k = \tau_j$. Due to nature of temperature and continuous work characteristic of a system, x_{k+1} should belong to $\{\tau_{j-1}, \tau_{j+1}\}$. However, some records do not fulfill this pattern. According to historical data, they might take values from a set 30^oC, 129^oC for a few seconds or minutes and afterwards return to usual values of temperature. Such observations are recognized as errors and should be removed from the data sample, since temperatures of transmission in this mine are not lower than 20^oC nor higher than 90^oC (even for overheated faulty gearbox). In the Fig. 6.1 the exemplary conveyor belt gearbox and the temperature sensor are presented.

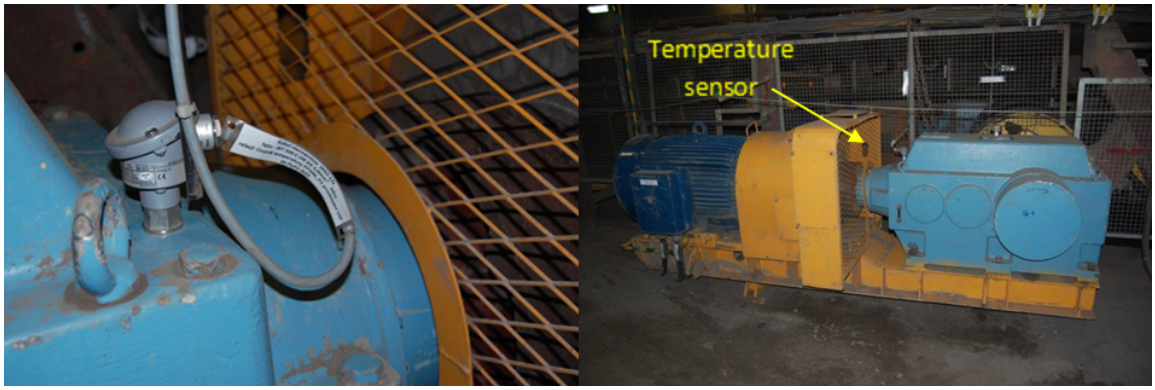

Figure 6.1: Conveyor belt gearbox and the temperature sensor

6.1.3 Data pre-processing

As it was mentioned in previous section, analysis of relation between raw temperature and electric current signals are difficult since sampling is time-varying and it is different for each channel. Firstly, error values should be erased from data and both temperature and current have to be interpolated at identical time axis for each channel in order to make analysis simpler. It was decided to interpolate data at equally spaced time points with one minute time intervals. It is worth mentioning that in Section 6.2 similar problem was discussed. Here we use one-minute long time intervals in order to better fit the relation between electric current and temperature. Due to physical properties of analyzed quantities it was decided to use linear interpolation of temperatures and stepwise for electric current. Linear interpolation of temperature is motivated by its slow variation in time. Jumps and periods with constant value of the electric current (engine is switched off) lead to stepwise interpolation (known also as piecewise constant interpolation).

The procedure of such data pre-processing is presented in Fig. 6.2. The linear interpolation is curve fitting by the first order polynomial. Namely, the interpolated values between two records are calculated from fitted linear function. The stepwise method is even simpler. All of the interpolated variables are equal to the last recorded quantity.

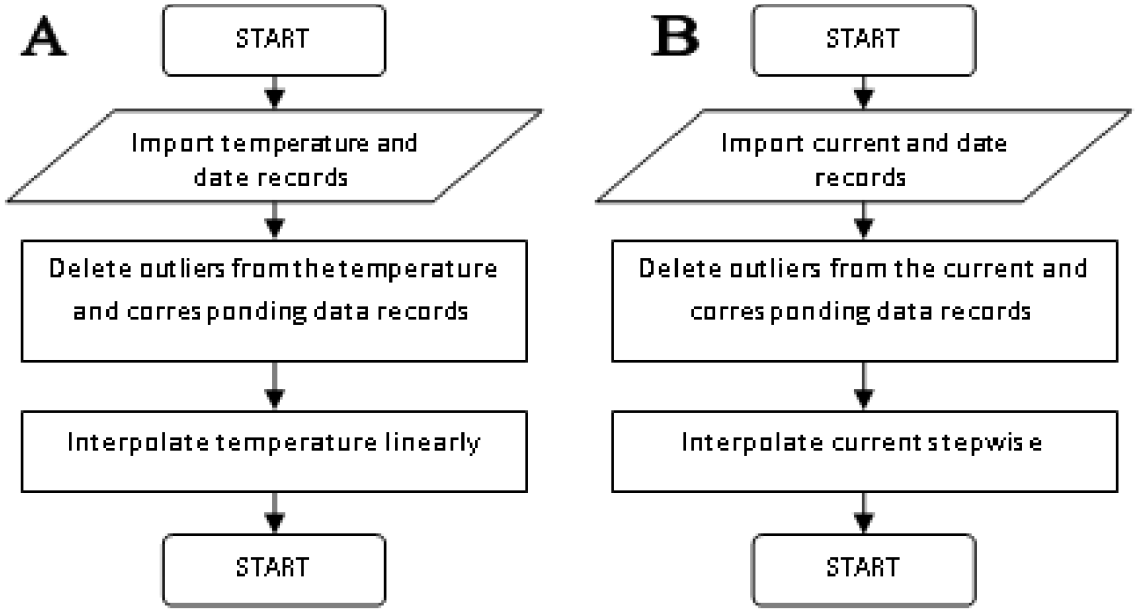

Figure 6.2: Outliers and interpolation data pre-processing for temperature (**A**) and electric current (**B**)

6.1.4 Data smoothing

It is expected that the temperature depends rather on past current values measured through some period than on its instantaneous value. In order to process the real data the smoothing algorithms can be used. They provide somehow averaged time series corresponding to a given time horizon. There are many well-known methods that can be applied. In this analysis we present two of them. The first one is moving average (MA) and the second one is exponential smoothing.

Moving average

This method is based on averaging the data over the given time period with the series of weights. The formula for signal X_t, smoothing horizon k and weights w_i, $i = 1, \ldots, k$ is given:

$$Y_t = \sum_{i=1}^{k} w_i X_{t-i}.$$

In this approach we use the equal weights for all $i = 1, \ldots, k$, i.e. $w_i = \frac{1}{k}$. Then all past k electric current recorded values have the same influence on the averaged temperature Y_t.

Exponential smoothing

In the second method the impact of historical electric current data on temperature decreases with respect to time (according to the smoothing parameter m), what might be more relevant for real data than the previous approach. The formula for given smoothing parameter $m \in (0, 1)$ and signal X_t is presented below:

$$Y_t = mX_t + (1-m)Y_{t-1}, \quad t > 1$$

$$Y_1 = X_1.$$

Moreover the explicit form of smoothed signal can be expressed by following equation:

$$Y_t = \sum_{j=0}^{t-2}(1-m)^j X_{t-j} + (1-m)^{t-1}X_1.$$

In this method the smoothing parameter m has to be specified. Smaller value of m results in slow decrease of weights, thus past values have relatively large influence on current Y_t. Higher value of m stands for high influence of latest values on the smoothed signal. Thus, the output of the smoothing procedure might still contain some high-frequency variations. The parameter m equal to 1 results in $Y_t = X_t$ for each t. One can derive the sum $S_{m,l}$ of weights applied to l latest recordings:

$$S_{m,l} = \sum_{j=0}^{l} m(m-1)^j = \sum_{j=1}^{l+1} m(m-1)^{j-1} = 1 - (1-m)^{l+1}.$$

From above equation one can estimate the influence of the l latest observations on Y_t for given m. Moreover, the formula for smoothing parameter m depending on given sum $S_{m,l}$ can be derived:

$$m = 1 - \sqrt[l+1]{1 - S_{m,l}}.$$

Therefore, one can require that latest l observations are responsible for $p\%$ of currently calculated Y_t. Alternatively, one can arbitrary set the smoothing parameter and calculate the influence of l latest weights on Y_t. For example, for sampling interval of data equal to 1 minute and smoothing parameter $m = 1/120$, the sum of weights related to 120 latest recordings (2 hours) is $S_{1/120,120} \approx 0.6367$. Therefore, 120 latest recordings account for about 64% of Y_t. In further analysis we exploit temperature signals interpolated linearly at equally spaced on one-minute intervals and stepwise-interpolated current signals smoothed using both mentioned methods, i.e. moving average with equal weights and exponential smoothing.

6.1.5 Diagnostic methodology

The analysed data is sampled on one minute basis. In the first step the pre-processed signals are separated into 24 hour groups starting at 6 a.m. This is motivated by the fact that the working day in the mine starts at 6 a.m. and it consists of 4 complete shifts of equal duration. Due to the work cycle, the belt conveyors usually do not work from Saturday, 6 a.m. till Monday, 6 a.m.

Moreover, signals obtained on Mondays (Mon, 6 a.m. to Tue, 6 a.m.) are significantly different from the rest of the week, since on Mondays the machines start working after a long brake. Therefore, signals from 4 working days (Tuesday 6 a.m. - Saturday 6 a.m.) are considered here.

From the diagnostic point of view, the most crucial parts of the monitored signals are related to periods with high load or operation without load - increasing energy consumption during idle state might indicate increasing resistance. The monitoring system covers the most important conveyors among the network. These conveyors operate usually under high load, thus there might be insufficient amount of data to perform idle state analysis. In order to select data related to high load, the proper thresholding for smoothed electric current might be used. Namely, we investigate relation between electric current and temperature for which the averaged current is higher than a given threshold. The methodology flowchart is presented in Fig. 6.3. In the analy-

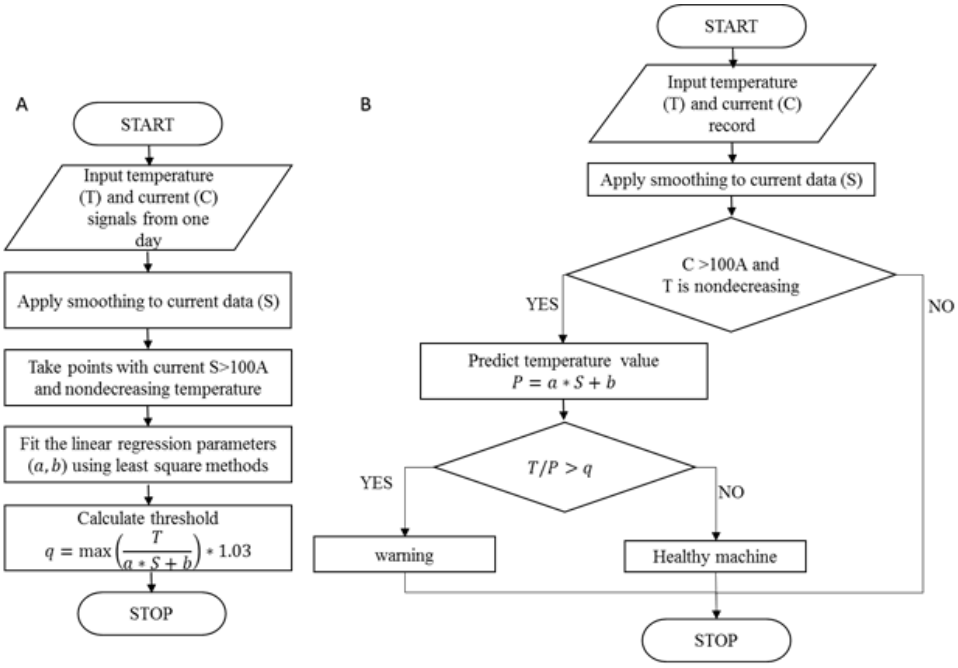

Figure 6.3: **A** Model fitting flowchart, **B** Damage detection flowchart

sis different values of thresholds are being tested, thus the best one can be chosen. Clearly, the data records can be separated into two groups with respect to temperature trend. The authors decided to consider only data for which the temperature does not decrease, since it corresponds to non-decreasing load. The last stage is focused on the proper model selection. Authors observed that for such pre-processed data the linear regression is suitable. Namely, the following static model might be applied:

$$T_t = aS_t + b$$

where T_t is temperature, S_t smoothed electric current at time t and a, b are the model parameters to be estimated. The model of smoothed electric current and temperature is static, thus the

model of raw electric current and temperature is dynamic. In order to test the goodness of fit the R^2 measure is applied. Linear regression can explain the relation between variables. The estimation is done via least squares method. Having model parameters a and b the prediction can be performed. We take smoothed current record and the model parameters, and calculate the prediction of temperature P_t. Finally the relation between observed value T_t and predicted P_t is tested. The crucial part is an indication when the real data does not follow the forecast, i.e. when the acquired data does not meet the fitted model. We propose a simple method, based on relation between observation and fitted model. Namely, the ratio P/T is being observed. The significance threshold is arbitrary set as $q = k \max\{P/T\}$, where $k = 1.03$. Clearly, the value of the parameter k is crucial. The smaller k, the higher chance to indicate the abnormal machine condition, but more false alarms can be obtained. On the other hand, using high values of k can prevent us from false alarms, but some faults can be omitted. Such tradeoff can be often found in automatic damage detection systems. In our data we tested that $k = 1.03$ is the most suitable. Changes of the model parameters during machine operation might indicate damage, similar to the methodology presented in (W Bartelmus and R Zimroz 2009) for wind turbines condition monitoring. To wit, faulty machine would reach higher temperature than the healthy one, for a given load. Moreover the model is simple, does not require time-consuming calculations and it is easy to interpret. In order to diagnose a machine the regression line parmeters (namely slope and intercept) can be analysed. The results of the application of proposed method for real signals are presented in the next section.

6.1.6 Real data application results

The analysed data consists of temperature and electric current recorded on 4 gearboxes from one belt conveyor. Signals are pre-processed as it is described previously. Furthermore, one of the machine (no. 54) was damaged and repaired during the analysed period. The main goal is to show capability of damage detection with proposed methodology of temperature and electric current relation modelling. Thus, the model was applied to faulty gearbox. The comparison of the result with transmission in good condition is also provided. First of all, the signal of electric current and temperature recorded on gearbox 54 are presented in the Fig. 6.4.

Clearly, before the faulty component was replaced, the anomaly temperature is observed. After the repair the temperature returned to normal level. Additionally, one can be interested in developing an automatic procedure for detection of such anomaly. As it was mentioned in previous sections the model parameters are estimated on the smoothed electric current instead of the raw signal. The comparison of two introduced averaging methods is depicted in Fig. 6.5. Furthermore, the corresponding values of temperature are also plotted. The exponential smoothed parameter was set to $1/120$ and MA parameter is equal to 180 (180 minutes, half of one shift). One can observe specific relation between current and temperature. The increase of smoothed electric current implies increase of the temperature.

In order to compare the smoothing methods the linear regression was applied. Then the R^2 measure provides information, which averaging procedure is more suitable for the real signals. The whole data can be divided into three subgroups, depending on the stage of damage development. First one, before the damage appeared, corresponds to relatively low tempera-

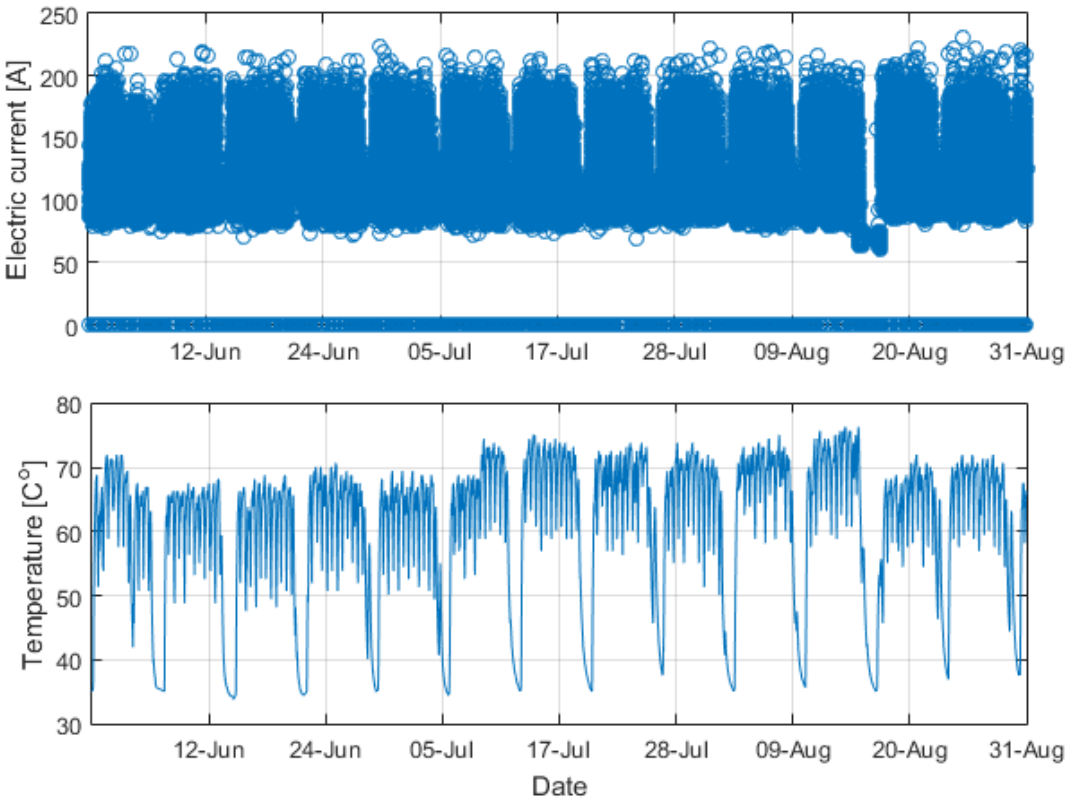

Figure 6.4: Current and Temperature signals recorded on damaged gearbox. Red box marks the period, when the temperature increased significantly. The green box shows the period when the machine was repaired

ture (usually below 70^oC). When the temperature rises, the second subgroup can be noticed - it stands for damage development. Finally, the third subgroup consists of signals acquired after repair, which corresponds to a good condition. In Fig. 6.6 there are presented the linear regression results for selected days. The plots on the top are related to the day before the temperature grown and they can be observed in the Fig. 6.4. The middle plots represent the day after the anomaly increase. The temperature-current relation is presented on the bottom panel. Furthermore, two electric current averaging methods are also compared. One could expect that the exponentially smoothing is more adequate, because the weights decrease with respect to time. Indeed, the goodness of fit for this smoothing method is much better. All R^2 are higher than 0.7 and for good condition they are even higher than 0.9. It means that temperature data, during heating periods, can be well explained by exponentially smoothed electric current. On the other hand, one can easily observe that moving average method is not good enough. The R^2 are much smaller (except one day) and the linear regression should not be applied for such data. Once the smoothing method is chosen, the performance of the proposed diagnostic method can be examined. Apparently, the differences between healthy and faulty machine can be observed. Plots for days before temperature growth and after repair looks similarly (Fig. 6.6). On the contrary, the middle plot is almost shifted in parallel, with the higher value of intercept b and similar slope a. Fig. 6.6 presents only exemplary results from the analysed time horizon. In

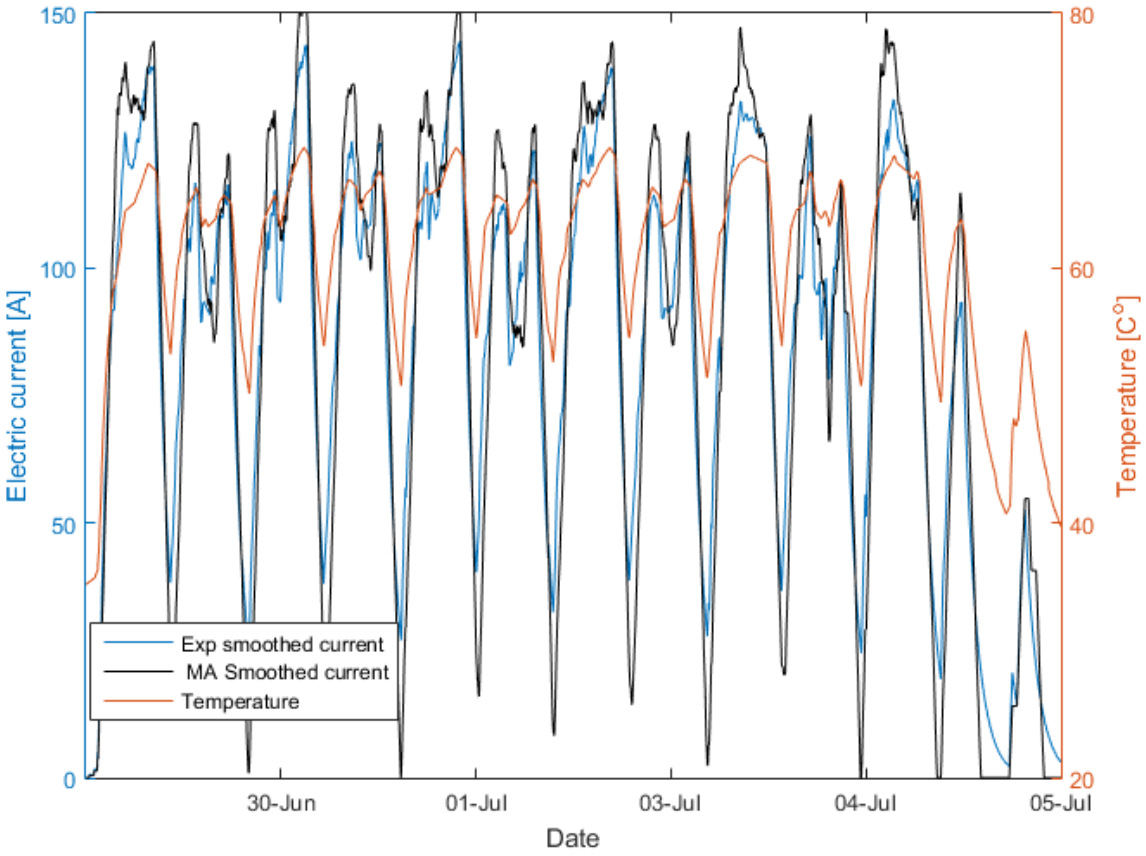

Figure 6.5: Smoothed electric current and temperature comparison

Fig. 6.7 there are presented the outputs of the fitted models for each analysed day. As it could be expected, the difference between healthy and faulty condition states is clear. The parallel shift of regression lines is noticeable, the ones from the damage development period are much above the other ones. Thus, the linear models fitted to conveyor belt data can be considered as an indicator of machine condition. The presented results are obtained for the exponential smoothing parameter equal to $1/120$. The lower bound for smoothed electric current was arbitrary set to 100 A - it indicates that the load is applied to the system. Moreover, only the data acquired during temperature increase is analyzed and signals during weekends and one day after them are not considered. Thus, the data from different days are comparable and it can be concluded that the changes in fitted model parameters are related to change of machine condition. The comparison of the outputs of the model fitted to different gearboxes is presented in Fig. 6.8. Condition of each gearbox is represented by value of the fitted regression line at electric current equal to 100 A (diagnostic feature). The damage of gearbox no. 55 can be clearly noticed therein. After the repair, the value of the proposed diagnostic feature returns to the level before damage development. Clearly, only on the gearbox no. 55 the diagnostic feature changes significantly. Furthermore, the proposed feature does not increase significantly during the entire considered period. Thus, the proposed model that combines smoothed interpolated data of temperature and electric current is able to detect abnormalities in technical condition of the gearbox.

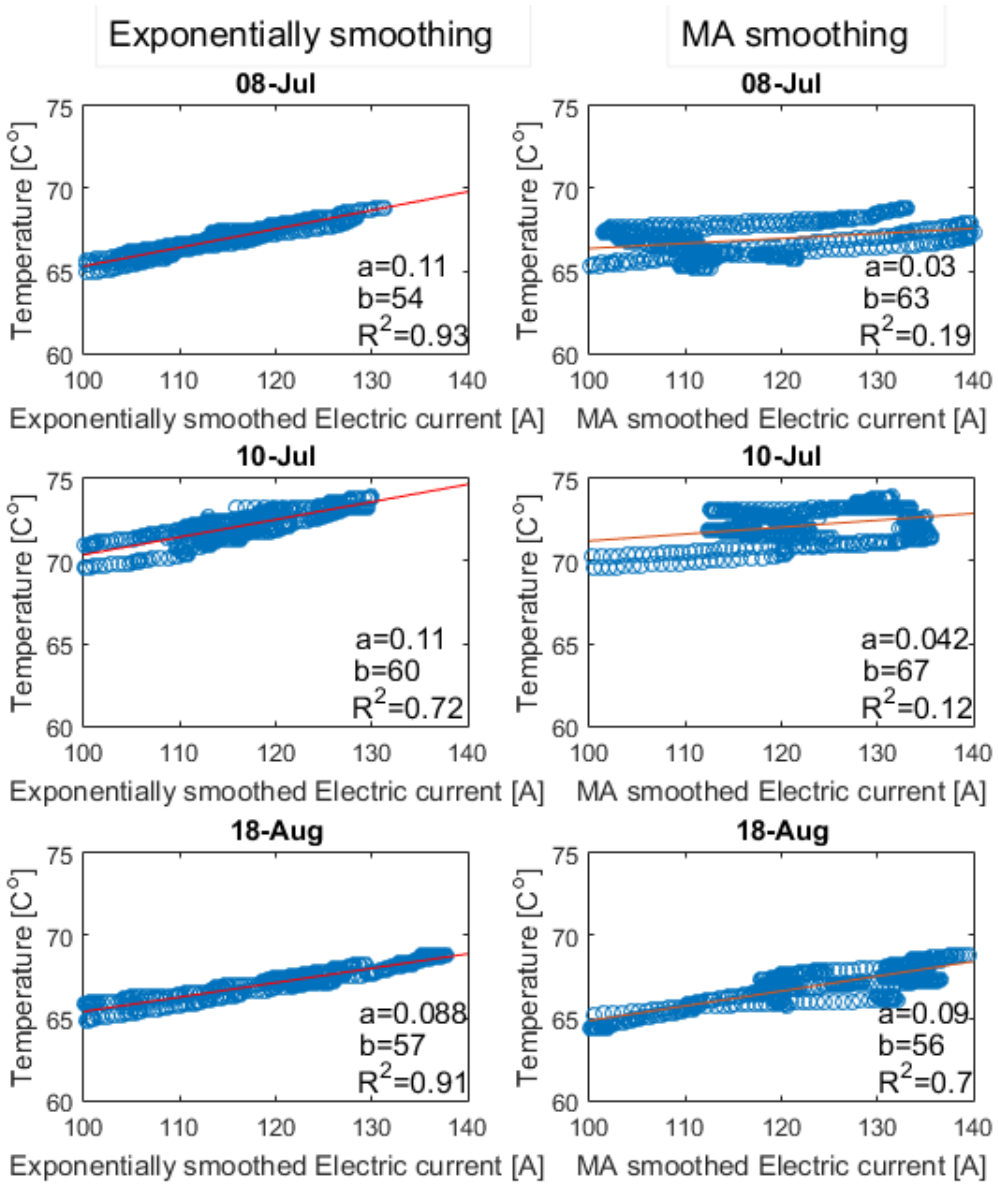

Figure 6.6: Linear regression applied to temperature versus electric current. A day before damage (top panels), during damage (middle panels) and after repair (bottom panels). The results are presented for exponentially smoothed (left side) and MA smoothed (right side) data

Finally, let us present the results of the prediction application (Fig. 6.9). Model was fitted on 10 of June, when the machine was working properly. One can observe that the proposed method is able to detect the abnormal situation. Once the temperature is rising and current is on the normal level, the model marks the warning (black circle). The algorithm precisely indicates the moment of fault occurrence. Before the damage occurred only a few false alarms were obtained (between June 20 and 30). Moreover, after repair the model marks the good condition of the machine, but after a few days the second fault was detected, thus many black circles can be found in the following days. Lower plot from Fig. 6.9 depicts the threshold and the test statistic (ObservedTemperature-to-Prediction ratio). If the test statistic is above the calculated

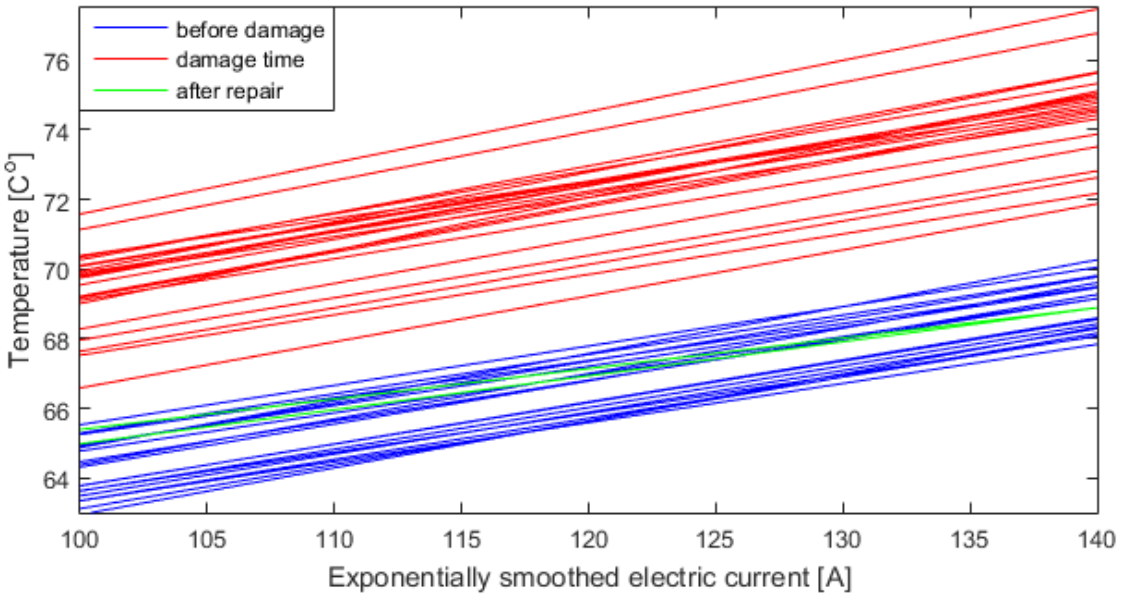

Figure 6.7: Regression lines for days divided into 3 groups with respect to machine condition

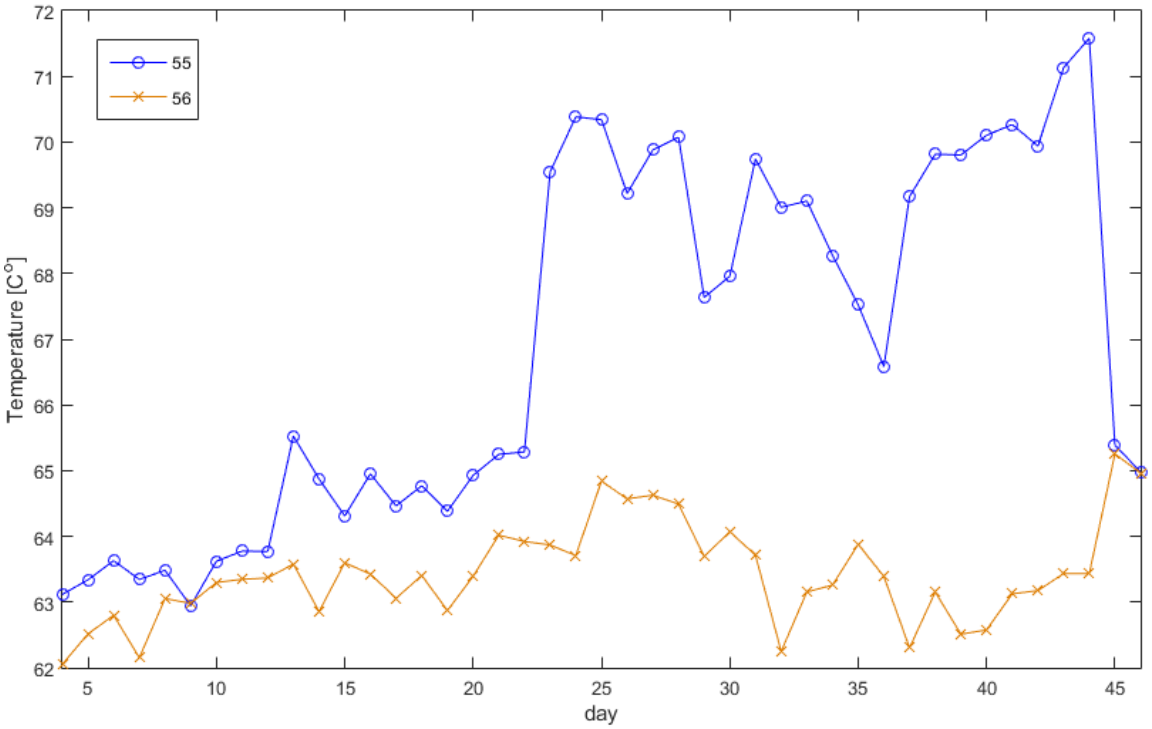

Figure 6.8: Values of the regression lines at smoothed electric current equal to 100 A, two different gearboxes. The damage one is no. 55. Red box marks the period, when the machine was in faulty condition

threshold the alarm is raised. In order to minimize the number of short lasting alarm states one can apply some additional rules, e.g. consider only the alarms lasting for more than 2 following days.

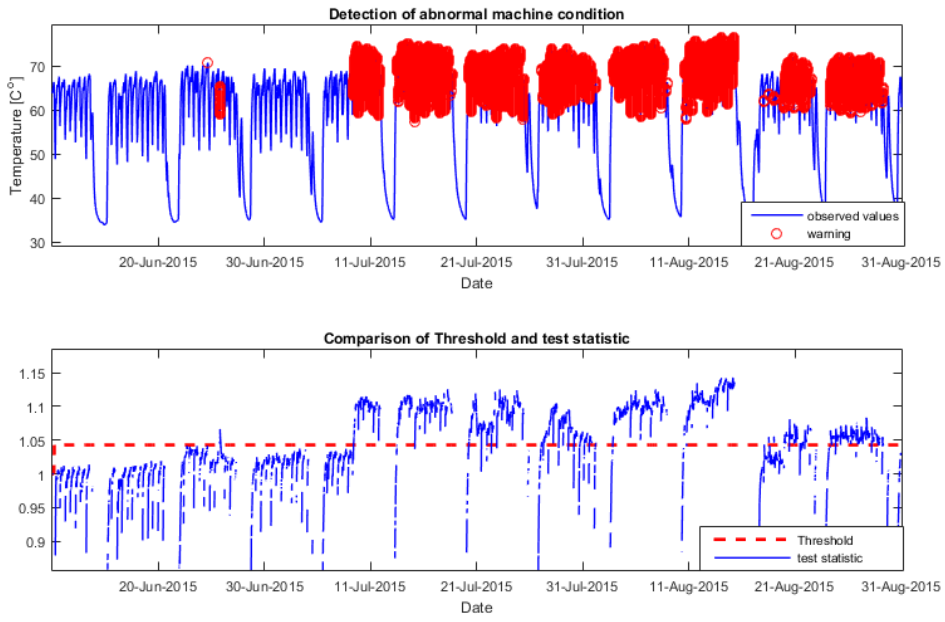

Figure 6.9: The results of the damage detection based on prediction (top panel). Test statistic and the threshold (bottom panel).

6.1.7 Conclusions

Belt conveyors are responsible for ore transportation in the mine. Thus, their trouble-free operation is highly desirable. One of the most important thing in maintenance of transportation system is avoidance of unpredicted break downs. The standard drive unit damage detection methods is based on the temperature observation and once it exceeds an a priori assumed level the operator is warned. The focus of this analysis is extraction of additional information from temperature and electric current relation modelling. It was shown that the exponentially smoothed electric current is beneficial in temperature analysis. The detection method based on the linear regression was proposed. It is important to fit the model on appropriate data acquired during the most crucial operation period. Thus, the fitting process was performed only for data, where temperature was non-decreasing and electric current was higher than 100 A. The detection of abnormal machine technical condition is based on the relation between real temperature and predicted one. The proposed methodology was applied to real data recorded on the belt conveyor operating in underground mine. According to the result, the proposed methodology is able to assess the machine technical condition. The benefits from the multivariate data analysis in fault detection is shown. The analysis of two variables and application of linear regression can provide satisfactory results.

6.2 Model of gearbox temperature as a mixture of different sources - Independent Component Analysis

6.2.1 Introduction

Information extraction is a very important topic in many branches of the field of signal processing. It is not easy for singular signals, but multivariate (multichannel, multidimensional) signals can provide some interesting opportunities. For example, we can assume that information is hidden and distributed among many input channels and/or measured signal is a mixture of different sources. Blind Source Separation (BSS) methods come in handy in that case (Cichocki, Zdunek, and Amari 2006; Roan, Erling, and Sibul 2002; Wang et al. 2014). The idea is the separation of a set of source signals from a set of mixed signals, without the aid of information (or with very little information) about the source signals or the mixing process. In that case we consider a model of temperature data in which the input channels are mixtures of some underlying sources, processes or events. This problem is in general highly underdetermined, but useful solutions can be derived under a surprising variety of conditions. One of very useful methods is called Independent Component Analysis, and its approach can be particularly effective if one requires not the whole signal, but merely its most salient features (Hyvärinen and Oja 1997; Li and Qu 2002). It is a computational method for separating a multivariate signal into additive subcomponents. This is done by assuming that the subcomponents are non-Gaussian signals and that they are statistically independent from each other. This section presents the usage of ICA to extract feature carrying information about non-typical failure-related signal changes over time.

6.2.2 Methodology

In this section we present the methodology which we use to real temperature signals from the set of heavy duty gearboxes of belt conveyor driving station used in mining industry. Functional scheme of the procedure is presented in Fig. 6.10. Temperature data acquired from SCADA systems are frequently used for condition monitoring purposes especially for mechanical systems with relatively hard access as wind turbines farm, off shore or mining machines operating underground (Astolfi, Castellani, and Terzi 2014; Nembhard et al. 2013; Wilkinson et al. 2014; Radoslaw Zimroz, Wodecki, et al. 2014). However, in our case, due to several factors influencing variability of temperature, raw data are difficult to process and decision making process related to damage detection is problematic. In previous work we have tried to simplify structure of the signal by segmentation, data driven or model based decomposition etc., It is well known that segmentation is commonly used as pre-processing stage in many applications (speech, seismic, physics, radiation etc (Crossman et al. 2003; Radoslaw Zimroz, Wodecki, et al. 2014)) where one can extract information related to event, cycle, or specific signal properties. In our case such segment might be related to week or shift related cycles. However, it is believed that optimal procedure should be quick and exploit information hidden in all channels simultaneously. It was proved in condition monitoring, especially for nonstationary context, that multidimensional analysis (for several channels or for several variables) might be very powerful in the context of

removing redundancy and environmental influence (e.g. loading conditions) (Bartkowiak and R Zimroz 2014). It is worth mentioning that validation of signals acquired in harsh underground mining conditions is often a critical stage. In our case we have tried to minimize all indirect stages of processing, however some basic data cleaning and resampling were required. Pre-

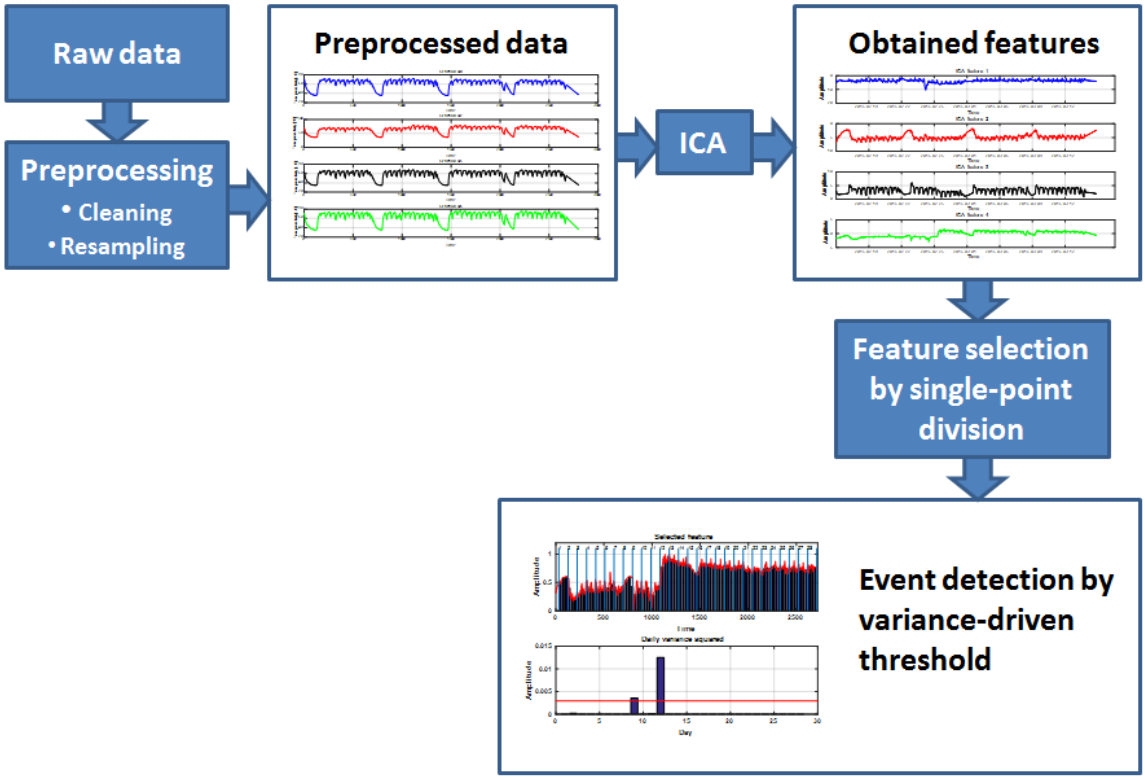

Figure 6.10: Functional scheme of the algorithm

sented method consists of four main steps: preprocessing of the raw data, feature extraction with Independent Component Analysis, selection of desired informative feature, and event detection according to selected feature.

Preprocessing

Firstly, outliers have been removed. It turned out that there were several samples of negative values, which clearly are measurement errors. They were replaced with the previous value for simplicity. There is no practical reason to apply more sophisticated procedures dealing with missing data, since variability of the temperature signal is low in this case. Moreover, the minimum temperature increment is relatively high (approx. $0.5C$), thus more complex missing data solutions could result in a temperature value that cannot be logged by the system. The second challenge is non-uniform sampling of the data. This saves the storage, but makes time series analysis more complicated. Raw data are sampled with time-varying period depending on dynamics of the signal (i.e. temperature variability). If temperature is nearly constant, sampling frequency becomes small, and if temperature is changing significantly - sampling of signal becomes more frequent. Data vectors have been resampled using linear interpolation, which is a way of curve fitting with first-order polynomial. Although it is the simplest way of interpolation, it

is very appropriate for this application, since we know that newly created sample between two already existing is going to take value between them. Otherwise, change-sensitive acquisition system would have register it in the first place. It also matches the character of the signal with its other property: slow variations of value.

Independent Component Analysis (ICA)

Independent component analysis was originally designed to solve so called 'cocktail party problem'. Consider two people speaking at the same time, being captured by two microphones positioned in different places, that capture two different records and producing two time signals. Lets denote those signals by $x_i(t)$ and original speech signals by $s_i(t)$. This situation can then be expressed as a linear combination:

$$\begin{bmatrix} x_1(t) \\ x_2(t) \end{bmatrix} = \begin{bmatrix} a_{11} & a_{12} \\ a_{21} & a_{22} \end{bmatrix} \begin{bmatrix} s_1(t) \\ s_2(t) \end{bmatrix}$$

Where a_{ij} are coefficients related to distances from microphones to speakers. Those coefficients are not known, so the problem cannot be dealt with by solving the equation with traditional methods. ICA is designed to estimate those coefficients based on statistical independence of original sources. In our problem we treat measured signals as mixtures $x_i(t)$, and we hope to obtain distinct features from the ICA. If we assume that the set of measured signals $X = \{x_1(t), x_2(t), , x_n(t)\}$ is the linear combination of independent sources $S = \{s_1(t), s_2(t), ,_s m(t)\}$ where $m \geq n$, then matrix form of the ICA problem is

$$X = AS$$

Where A is the coefficient matrix consisting of a_{ij} elements, and we do not know either A or S matrices. We regard the noise to be one of the sources. ICA method attempts to estimate a separating matrix $W^T = A^{-1}$ to be able to obtain the sources S by solving the equation:

$$S = A^{-1}X = W^T X$$

From the Central Limit Theorem we know that the distribution of a sum of independent random variables tends to the Gaussian distribution. Hence, since sum of sources is expected to be more Gaussian than the sources, maximizing the non-Gaussianity of $W^T X$ will result in independent components. There are many measures of non-Gaussianity. In this application, the one proposed by Hyvarinen and Oja (Hyvärinen and Oja 2000) based on maximum-entropy principle is used, where negentropy is defined as follows:

$$J(y) \propto [E\{G(y)\} - E\{G(y_{gauss})\}]^2$$

where y_{gauss} has ideal Gaussian distribution, y_{gauss} and y are centered and have unity variance, $E\{\}$ is an averaging operator, and G is nonlinear function. This application of ICA algorithm uses approximation where $y = W^T X$ and $G(y) = tanh(y)$. Unfortunately the ICA method

cannot identify uniquely neither correct ordering of the source signals, nor their proper scaling and sign, as well. The sign issue however can be managed if our understanding of type and character of signals permits us to modify the unmixing matrix W^T.

Selected properties of ICA:

- ICA can separate only linear combinations of sources;
- Order of input signals is irrelevant;
- ICA separates sources basing on maximization of non-Gaussianity, so perfectly Gaussian sources cannot be separated;
- Even if sources are not perfectly independent, ICA finds such space, in which they are maximally independent.

In the case analyzed here physical meaning of sources is obviously different than for original cocktail party context. We assume that the acquired signals are mixtures of four sources (processes) that describe: a) weekly variation and show weekly drops of value; b) change of state in the process. possibly failure of a machine; c) oscillating character of signal during the days and shifts; d) additive white Gaussian noise.

Feature selection

Afterwards, algorithm selects feature that carries viable information about the failure-related changes in the process. For every ICA feature we search for such point in time, that splits the data into two parts of the highest difference in mean. Then the feature of interest (i.e. this realted to change of process) is the one with the highest mean difference. After that, correlation of selected feature with all acquired signals provides us with information for which signal (alternatively - for which gearbox) the misbehavior occurred.

Event detection

As a last step, selected feature is segmented into individual days. After that, daily variance is calculated. To emphasize differences in values even more, variance is squared. At the end, threshold for variance is defined to enable automatic event detection and localization.

6.2.3 Application to real data

Described method was exploited to analyze temperature data measured on set of four heavy-duty gearboxes used in belt conveyor drive station in KGHM underground mine.

Description of real data

The data acquisition system used for performing measurements is a commercial, multichannel low frequency data logger that is operating continuously. The system stores the value of a variable only if it changes by some predefined value $\pm\Delta T$. This allows to reduce amount of data being recorded, which is convenient for very low frequency processes. On the other hand it can lead to some difficulties from the signal processing point of view. Measurement channels will have a different amount of samples for the same time period. Because of this such signal

cannot be considered as time series, and it has to be preprocessed before any further actions (Sawicki et al. 2015).

Although signals originate from different physical sources, gearboxes drive the same conveyor within a single station, so their behavior is heavily related. Basing on this assumption we can consider the signals describing (modeling) one process in a multidimensional manner (Fig. 6.11). It was proven by Cempel and other authors that multidimensional analysis for condition monitoring, especially under nonstationary operations is a very interesting approach (Bartkowiak and R Zimroz 2014).

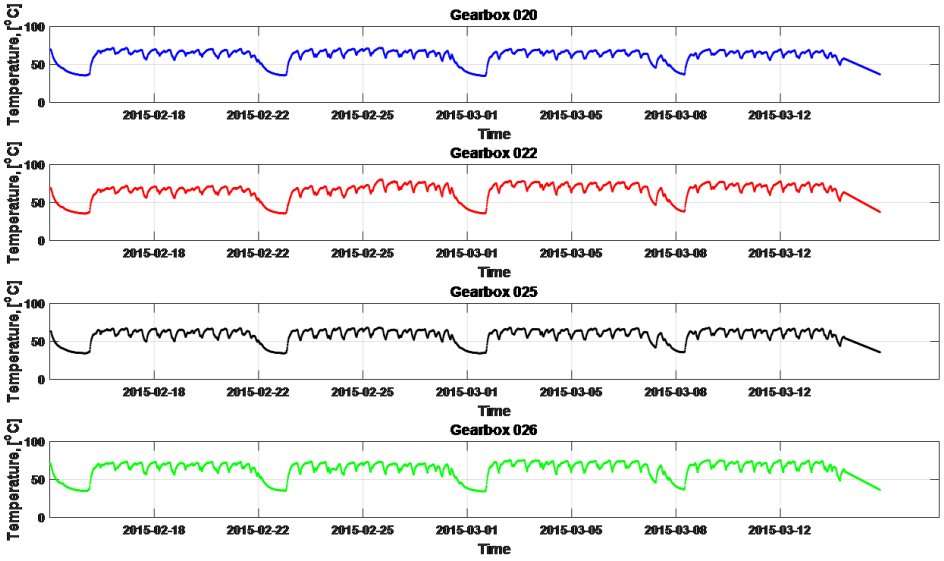

Figure 6.11: Preprocessed input signals

Results

At first, signals had to be preprocessed according to methodology described in section 6.2.2. The output sampling period was set to 15 minutes. In order to better visualize relative changes in signal behavior, four data vectors are presented together in Fig. 6.12.

First conclusion after comparing Fig 6.11 and 6.12 is that looking on each signal separately is non-effective from diagnostic point of view. It is hard to notice change in the signal, but even simple presentation all signals together shows that there is a change in the middle of week 2.

However, we are looking for an automatic technique that will exploit the considered model in which several sources influence the acquired signal. So, ICA approach was used. In our case ICA returns four features. For reasons described in section 6.2.2 arrangement of output features will be different at every execution of the ICA algorithm. As we can see in Fig. 6.13 features 1 and 4 carry information about common factors of signals behavior, feature 2 presents high frequency details, and feature 3 informs about trend of behavior change, so in this case third feature is selected for further fault analysis. Besides, correlation analysis provides the information that selected feature is connected with behavior of signal coming from gearbox 022.

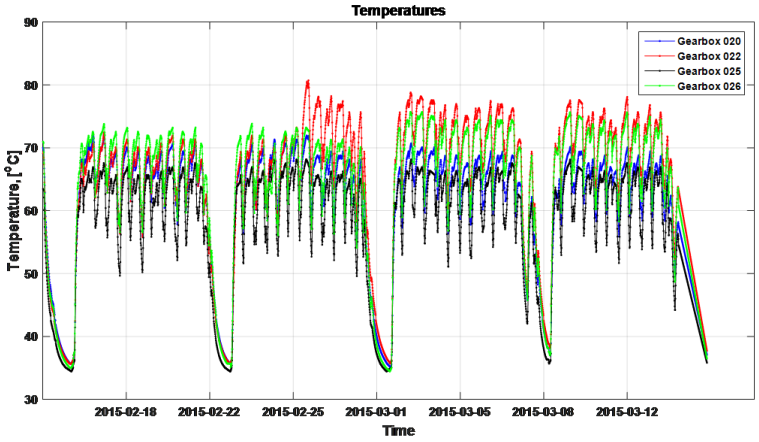

Figure 6.12: Raw signals presented together

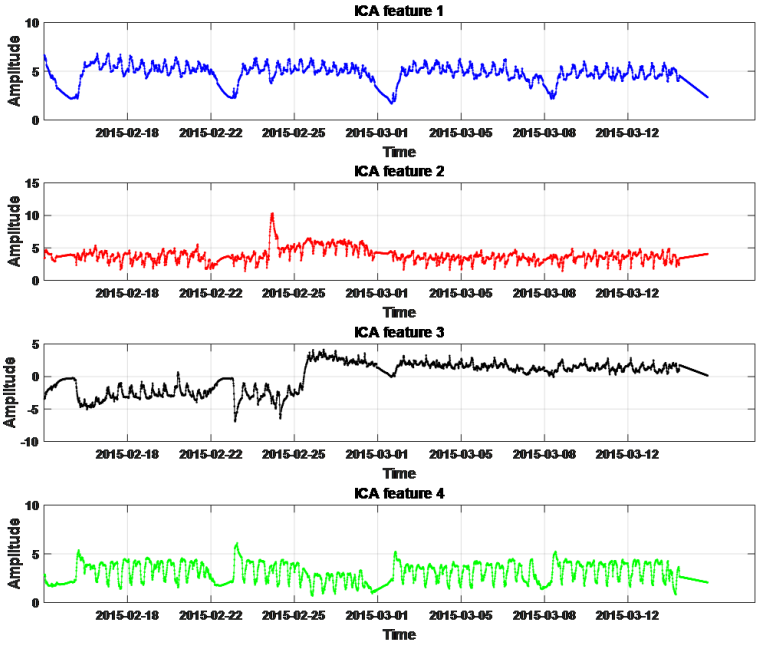

Figure 6.13: Four features obtained after ICA

Selected feature along with daily variances is presented in Fig. 6.14. One can see that two events can raise the alarm. Event occurring during 12th day can be clearly seen in Fig. 6.12 (gearbox 022). On the other hand, event occurring during 9th day is not easily visible. Fig. 6.15 presents this situation. One can see that during 24th of February, temperature of gearboxes 026 and 022 dropped unusually compared to behavior from previous work cycles. This might be caused by temporary external source of cool air (e.g. air condition system fan placed near the gearbox) which can be easily neglected by the monitoring personnel.

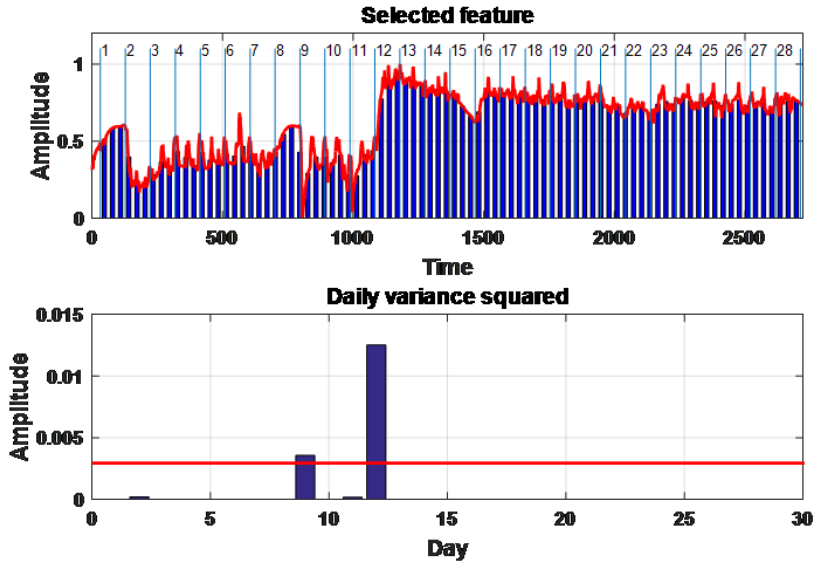

Figure 6.14: Selected feature with consecutive days indicated. Daily variance squared has been proposed as event selector

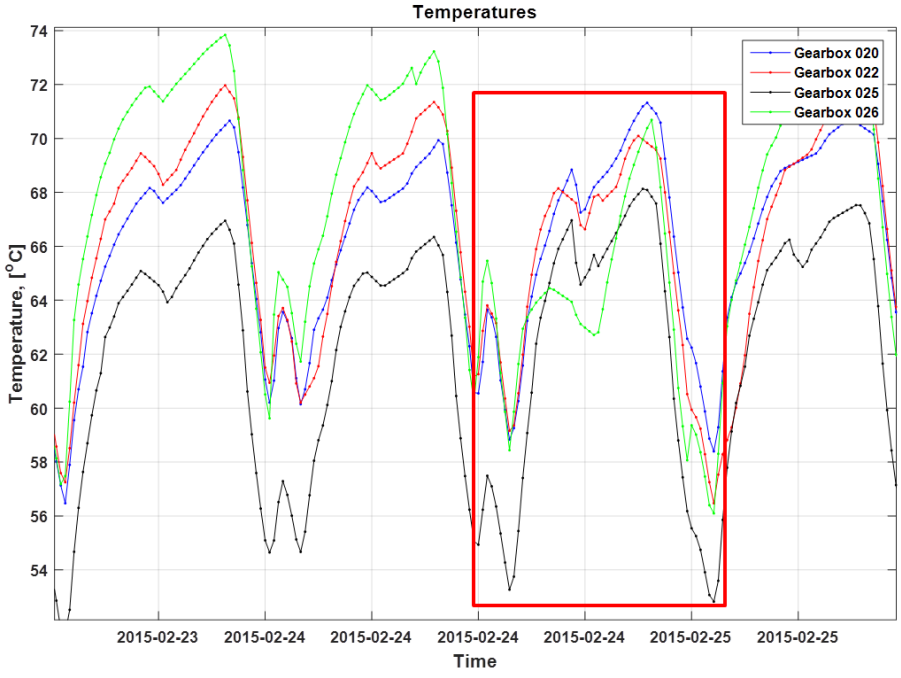

Figure 6.15: Event from day 9

6.2.4 Conclusions

In this section we have presented application of Independent Component Analysis for signal feature extraction applied to real temperature signal from set of heavy duty gearboxes used in mining industry. The methodology is based on the analysis of multichannel time series. In order to extract information about the damage we analyze the features obtained by applying the ICA to four-channel input signal. The introduced technique applied to real data allowed to compare four gearboxes which is more certain than fault detection using a single signal. Extracted features allow to detect unusual behavior of gearboxes, identify misbehaving device and provide behavioral feature for further analysis and interpretation. By using ICA we are able to separate different sources influencing shape of measured temperature signal, or in other words, we are able to remove from signal contribution related to operational factors. Thus, modeling of the temperature signal and application of ICA allowed not only to extract the relevant content of the signal, but it enabled a possibility of fault detection in belt conveyor network.

6.3 Cyclic modulation spectrum - an online algorithm

6.3.1 Introduction

In this section we investigate a model of vibration signal from a rotating mining machinery, namely a gearbox operating in an underground mine. The model states that the signal from such machine (operating under almost constant rotational speed) is a second-order cyclostationary signal, if only the fault occurs. Thus, extraction of amplitude modulation properties (number of harmonics, modulation depth etc.) could be crucial in fault detection. Rolling element bearing damage detection is widely studied topic and many different methods have already been introduced. The local damage of the bearing entails impulses, which can be detected in the vibration signal measured on the machine (McFadden and Smith 1984). In order to indicate presence of these impulses, the vibration signal can be analyzed in several domains. A universal tool used for detection of impulses is kurtosis, which can be applied in e.g. time, frequency and time-frequency domains (Jerome Antoni 2007; Barszcz and JabŁoński 2011; Radoslaw Zimroz, Obuchowski, and Wylomanska 2016). On the other hand, the theory of cyclostationarity can be applied to address cyclic character of this impulsive signal. Vibration responses acquired on rotating machinery (e.g. bearings and gearboxes) are considered as cyclostationary signals. The theoretical background and application methods are already well explained in the literature (Jérôme Antoni 2009; Hurd and Miamee 2007). In (Raad, Jerome Antoni, and Sidahmed 2008) the Authors presented indicators which can quantify cyclostationarity of the considered signal. Moreover in (Borghesani et al. 2013) there are described statistical tests for testing second order cyclostationarity with non-white noise. Such tests could be applied to signals from rotating machinery in order to examine whether the machine is faulty or not. In (Urbanek, Barszcz, and Jerome Antoni 2013) the Authors propose a method for extracting second-order cyclostationary components from a vibration signal. This method called Averaged Instantaneous Power Spectrum (AIPS) is a time-frequency representation and its benefits are illustrated using a simulated signal, test-rig experiment and real vibration signal from a wind turbine. Cyclostationarity gives also tools to model a signal from rotating machinery. For instance, periodic autoregressive time series can model a vibration signal from a planetary gearbox operating in a bucket wheel excavator (Wyłomańska et al. 2014). Cyclostationarity of vibration signals from the bucket wheel excavator has been also investigated in (Radoslaw Zimroz and Walter Bartelmus 2009) where a Spectral Coherence Map is proposed as a tool for fault detection. A comprehensive discussion on modeling of vibration signal from gears and bearings can be found in (Jérôme Antoni et al. 2004).

One of the most popular, simple and powerful cyclostationary tools is cyclic modulation spectrum (CMS). It was introduced in 2009 by (Jérôme Antoni 2009) and described thoroughly in (Julia Antoni and Hanson 2012). CMS can be considered as double DFT applied to the signal or, alternatively, DFT of the spectrogram. It was developed in order to overcome the high computational cost of cyclostationary tools. Its computational cost as well as main advantages and drawbacks are discussed in (Borghesani 2015).

However cyclostationarity based analysis is powerful, it claimed to be computational inefficient, in general. It is a crucial drawback, which impede the commercial application. There are many

articles analyzing the complexity of this approach (Liu, Qiu, and Sheng 2012; Roberts, Brown, and Loomis Jr 1991). In this report we would like to propose a novel, computationally efficient online algorithm for CMS. The idea is based on the sliding discrete Fourier transform (SDFT), which was proposed in 2003 (Jacobsen and Lyons 2003).

6.3.2 Cyclic modulation spectrum

The Cyclic modulation spectrum (CMS) was introduced in 2009 by Antoni (Jérôme Antoni 2009). The idea is based on double usage of the DFT to the signal. The procedure consists of two stages. Firstly, the spectrogram with N-sample long DFT from the given signal $\mathbf{X}_{0,L} = (x_0, \ldots, x_{L-1})$ with M-sample long window and S-sample step between the adjoining windows has to be computed:

$$\begin{aligned} \mathbf{Spec}(n,f) = |STFT(n,f)|^2 = \\ = \left| \sum_{m=0}^{N-1} w(m) x(n+m) e^{-2i\pi f m/N} \right|^2, \end{aligned} \tag{6.1}$$

where $w(\cdot)$ is a window function, $n = 1, \ldots, \lfloor (L-M+S)/S \rfloor$ is the time index, f is a frequency bin and $N \geq M$. Then let $K = \lfloor (L-M+S)/S \rfloor$ be the number of time points in which spectrogram is calculated (the number of windows). In order to compute CMS, the DFT of the spectrogram slices for each f separately has to be calculated

$$\begin{aligned} CMS(\alpha, f, \mathbf{X}_{0,L}) = DFT(\mathbf{Spec}(n,f)) = \\ = \sum_{n=0}^{K-1} \mathbf{Spec}(n,f) e^{-2i\pi n\alpha/K}. \end{aligned} \tag{6.2}$$

In the above formula there are two different frequencies - α is called cyclic and f - carrier frequency. This procedure is one of the most useful tools in cyclostationary signal analysis. For stationary data all energy would be distributed near $\alpha = 0$ (Jérôme Antoni 2009). On the other hand a signal which consists of an amplitude modulated components would have cyclic modulation for $\alpha \neq 0$. Moreover it is useful in estimation of cyclic frequency magnitude for given f, α, where f can be treated as a carrier frequency and α is modulation frequency (Borghesani 2015). The CMS is simple and provides important information about cyclostationary properties of the signal. One of the main drawbacks of this method is the upper bound for the cyclic frequency α. Indeed, there is a limitation which links carrier and modulation frequencies:

$$\alpha < f. \tag{6.3}$$

Moreover maximum α is equal to reciprocal of the time resolution in the spectrogram (Jérôme Antoni 2009).

The naive algorithm for calculating CMS is via double FFT procedure. In such case the computational complexity is equal to $O(KN \log_2(KN))$. CMS for a single signal does not require time consuming computations, although naive algorithm for online CMS calculation requires one

N-sample long FFT for spectrogram update and N FFT's for update of spectra corresponding to frequency bins. Thus, the time for CMS update could be longer than the sampling interval, even if CMS is being updated at every S samples arrival, for $S > 1$. Thus, it is worth to investigate an alternative algorithm which decreases the computational complexity of CMS update and makes it possible to incorporate CMS in embedded industrial condition monitoring systems.

In Fig. 6.16 there are presented spectrogram and CMS for a signal recorded on the faulty pulley bearing operating in a belt conveyor driving station. The sampling frequency is equal to 19200 Hz and the measurement time is 2.5 seconds. The spectrogram is obtained for Kaiser 250-sample long window with 240 overlapping samples and 1024 FFT points. One can notice several wide-band excitations on the spectrogram at carrier frequency band 1-5 kHz. These excitations are cyclic, thus wide spectral lines can be also noticed on the CMS at carrier frequencies 1-5 kHz and modulation frequency of 12.7 Hz (and its multiples). This stands for outer race local damage.

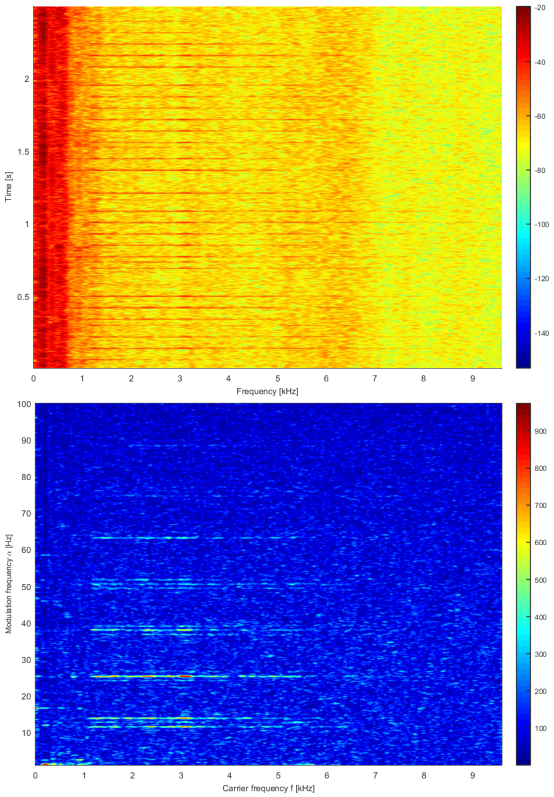

Figure 6.16: The spectrogram (top panel) and cyclic modulation spectrum (lower panel) generated for the signal recorded on the pulley bearing operating in a belt conveyor driving station

6.3.3 Sliding Discrete Fourier Transform

The most popular algorithms for generating discrete Fourier Transform are undoubtedly fast Fourier Transforms (e.g. radix-2). In this section we would like to recall the Sliding DFT (SDFT) which is an online algorithm that calculates DFT of a sliding window.

Let us consider a signal $\mathbf{X}_{0,L} = (x_0, \ldots, x_{L-1})$ of length L. The classical DFT of N-sample

long signal segment $\mathbf{X}_{k,N} = (x_k, \ldots, x_{k+N-1})$ for f-th harmonic bin is given by the formula:

$$\mathcal{F}(\mathbf{X}_{k,N})(f) = \sum_{n=0}^{N-1} x_{n+k} e^{-2\pi i n f/N}, \tag{6.4}$$

where $k \geq 0$ is a window index and n is a time index. In order to calculate the DFT of the one-sample shifted window $\mathbf{X}_{k+1,N}$ we use equation (Jacobsen and Lyons 2003):

$$\begin{aligned} \mathcal{F}(\mathbf{X}_{k+1,N})(f) &= \sum_{n=0}^{N-1} x_{n+k+1} e^{-2\pi i n f/N} \\ &\overset{[l=n+1]}{=} \sum_{l=1}^{N} x_{l+k} e^{-2\pi i (l-1) f/N}, \end{aligned} \tag{6.5}$$

with substitution $l = n + 1$. Now one can add the last term separately, add the 0-th term and subtract it outside the sum operator:

$$\begin{aligned} \mathcal{F}(\mathbf{X}_{k+1,N})(f) = x_{N+k} e^{-2\pi i f(N-1)/N} - x_k e^{2\pi i f/N} + \\ + \sum_{l=0}^{N-1} x_{l+k} e^{-2\pi i (l-1) f/N}. \end{aligned} \tag{6.6}$$

Finally one can factor out the common term $e^{2\pi i f/N}$ and obtain formula for SDFT for f-th harmonic bin:

$$\mathcal{F}(\mathbf{X}_{k+1,N}, f) = e^{2\pi i f/N} \left(\mathcal{F}(\mathbf{X}_{k,N}, f) + x_{N+k} - x_k \right), \tag{6.7}$$

since f is integer and thus, $e^{-2\pi f} = 1$.

SDFT algorithm is especially beneficial in case of DFT calculation from a one-sample sliding window. The algorithm is really simple and its computational complexity is $O(N)$ for a single update, which is much lower than $O(N \log_2(N))$ for FFT. Moreover, SDFT outperforms FFT even when the spectrum is being updated at every S samples, for certain S, since SDFT for N such updates takes $O(N^2)$ and FFT - $O(N^2 \log_2(N)/S)$.

6.3.4 Online algorithm for CMS calculation

As we presented in Section 6.3.3 SDFT can impressively speed up online DFT computation in specific cases. The idea underlying fast CMS online update is based on incorporation of SDFT algorithm. In this section we present two novel approaches to update the CMS. Both of them can give a possibility for online calculation of CMS.

Let us recall that SDFT computes DFT at a fixed number of points, i.e. size of the basis signal cannot increase. This is a crucial feature, which point out the need of analysis two separate cases. Let us consider signal $\mathbf{X}_{0,L}$ and corresponding spectrogram $\mathbf{Spec}(n, f)$ for a given spectral frequency f and time indexes $n = 0, \ldots, K-1$. Then a new measurement x_L is recorded and spectrogram $\mathbf{Spec}(n, f)$ can be updated. There are two possible ways to update the CMS. The first one is to calculate $(K+1)$-sample long DFT for each frequency bin at every new spectrum arrival. Therefore the range of the signal for which CMS is calculated increases

with respect to time. Namely, for a given spectral and cyclic frequencies increasing-size CMS_{IS} is given by formula:

$$CMS_{IS}(\alpha, f, \mathbf{X}_{0,L+1}) = \sum_{n=0}^{K} \mathbf{Spec}(n, f) e^{-2\pi i \alpha n/(K+1)}, \tag{6.8}$$

since the time axis of the updated spectrogram consist of $K+1$ points. In the second case K-sample long DFT is calculated for each frequency bin. Thus, the oldest spectrum of spectrogram is left out in CMS calculation when the new spectrum arrives. Indeed, for a given spectral and cyclic frequencies moving-window $CMS_{MW}$is defined as:

$$CMS_{MW}(\alpha, f, \mathbf{X}_{0,L+1}) = \sum_{n=1}^{K} \mathbf{Spec}(n, f) e^{-2\pi i \alpha n/K}, \tag{6.9}$$

since the time axis of the updated spectrogram consists of K points. Each of the case will be analyzed separately and slightly different algorithms are going to be presented for each approach.

Increasing-size CMS algorithm

Recall that CMS procedure consists of two steps. The first one is simply computation of the spectrogram. Let us consider STFT with rectangular window. Let us denote $\mathbf{Spec}_{K-1}$ as the spectrogram with $K-1$ time points for each of N frequency bins. Due to (6.1), the updated spectrogram $\mathbf{Spec}_K$ is given by the formula:

$$\begin{aligned} \mathbf{Spec}(K, f) = \Big| e^{2i\pi f/N} [STFT(K-1, f) + \\ + x_L - x_{L-N-1}] \Big|^2. \end{aligned} \tag{6.10}$$

The second step of the CMS_{IS} algorithm is calculation of the DFT for each of N frequency bins. In this approach SDFT cannot be used in this step, since length of each time series corresponding to a frequency bin f is increasing in time. Thus, FFT might be used instead.

Table 6.1: Computational cost for CMS_{IS}

novel algorithm	
step	**computational cost**
STFT update	$O(N)$
K-long FFT for each f	$O(NK \log_2 K)$
final complexity	$\boldsymbol{O(N \log_2(2K^K))}$
standard algorithm	
step	**computational cost**
STFT update	$O(N \log_2 N)$
K-long FFT for each f	$O(NK \log_2 K)$
final complexity	$\boldsymbol{O(N \log_2(NK^K))}$

The computational complexity of each step of CMS_{IS} update is given in Table 6.1. Moreover

the novel algorithm is compared with the standard one based on double FFT usage. Clearly, the final computational complexity is lower for the CMS_{IS} with SDFT comparing to CMS_{IS} based on double FFT. The computational complexity for novel algorithm is $O(N\log_2(2K^K))$ and $O(N\log_2(NK^K))$ for the standard one. This proves the benefits of the proposed method.

Moving-window CMS algorithm

The proposed algorithm for CMS_{IS} is efficient, although one can look for even quicker method. The main drawback is obviously the second step, where the FFT has to be applied. In order to overcome this issue, the special case of CMS is analyzed, where the SDFT can be used for both stages. Clearly, the first phase in CMS_MW procedure is exactly the same like in CMS_{IS}, i.e. $\mathbf{Spec}_{K-1}$ is updated to $\mathbf{Spec}_K$ using SDFT. Once the $\mathbf{Spec}_K$ is computed, the K-sample long DFT of the spectrogram (6.10) is calculated for each of N frequency bins. Obviously, in this approach the length of time points do not increase with respect to time. Thus, there is a possibility to apply a SDFT algorithm and CMS_{MW} is expressed by formula:

$$\begin{aligned} CMS_{MW}(\alpha, f, \mathbf{X}_{0,L+1}) = e^{2\pi i\alpha/N}[\, CMS(\alpha, \mathbf{X}_{0,L}, f) \\ -\mathbf{Spec}(0, f) + \mathbf{Spec}(K-1, f)] \end{aligned} \tag{6.11}$$

In Table 6.2 computational cost for CMS_{MW} is presented. The novel and standard algorithms

Table 6.2: Computational cost for CMS_{MW}

novel algorithm	
step	**computational cost**
STFT update	$O(N)$
single f CMS updatevia SDFT	$O(K)$
final complexity	$\boldsymbol{O(N(K+1))}$
standard algorithm	
step	**computational cost**
STFT update	$O(N\log_2 N)$
single f CMS updatevia FFT	$O(K\log_2 K)$
final complexity	$\boldsymbol{O(N(\log_2 N + K\log_2 K))}$

are compared. In this approach the usage of SDFT is even more beneficial. The computation complexity for proposed method is just $O(N(K+1))$, since STFT update takes $O(N)$ and N updates of K-sample long spectra via SDFT takes $O(NK)$. Naive algorithm which involves double FFT takes finally $O(N(\log_2 N + K\log_2 K))$, i.e. $O(N\log_2 N)$ for STFT update and N K-sample long FFT's ($O(K\log_2 K)$ each). The assumption for fixed length of DFT in calculation of CMS gave a possibility for double usage of SDFT and speed up the algorithm significantly. Furthermore, it is more reasonable to assume fixed number of time points, otherwise the sample size will increase rapidly and it would be impossible to storage such amount of data. Moreover, it also affects the computational time.

6.3.5 Conclusions

The cyclic modulation spectrum is effective tool for visualization of cyclostationary properties of the signal, although the well known algorithms are not efficient enough for online computation. In order to overcome this issue two novel algorithms that involve SDFT for CMS update calculation have been proposed. Two different cases have been diagnosed and described. They differ in the way of CMS updating. In one case, length of DFT calculated in second step of CMS is fixed (CMS_{MW}), while in the second one it can increase in time (CMS_{IS}). For each case the novel algorithm was introduced and compared with the standard one based of double FFT. It was presented that proposed methods can significantly speed up the CMS calculation. The smallest computational complexity was obtained for the CMS_{MW}. It can reduce complexity of update from $O\left(N\left(\log_2 N + K\log_2 K\right)\right)$ in standard method to $O\left(N(K+1)\right)$. The novel update algorithm is more efficient and give a possibility for online calculation for each new recorded measurement.

References

[1] Jerome Antoni. “Fast computation of the kurtogram for the detection of transient faults”. In: *Mechanical Systems and Signal Processing* 21.1 (2007), pp. 108–124.

[2] Jérôme Antoni. “Cyclostationarity by examples”. In: *Mechanical Systems and Signal Processing* 23.4 (2009), pp. 987–1036.

[3] Jérôme Antoni et al. “Cyclostationary modelling of rotating machine vibration signals”. In: *Mechanical systems and signal processing* 18.6 (2004), pp. 1285–1314.

[4] Julia Antoni and David Hanson. “Detection of surface ships from interception of cyclostationary signature with the cyclic modulation coherence”. In: *Oceanic Engineering, IEEE Journal of* 37.3 (2012), pp. 478–493.

[5] Davide Astolfi, Francesco Castellani, and Ludovico Terzi. “Fault prevention and diagnosis through SCADA temperature data analysis of an onshore wind farm”. In: *Diagnostyka* 15 (2014).

[6] Tomasz Barszcz and Adam JabŁoński. “A novel method for the optimal band selection for vibration signal demodulation and comparison with the Kurtogram”. In: *Mechanical Systems and Signal Processing* 25.1 (2011), pp. 431–451.

[7] W Bartelmus and R Zimroz. “A new feature for monitoring the condition of gearboxes in non-stationary operating conditions”. In: *Mechanical Systems and Signal Processing* 23.5 (2009), pp. 1528–1534.

[8] A Bartkowiak and R Zimroz. “Dimensionality reduction via variables selection–Linear and nonlinear approaches with application to vibration-based condition monitoring of planetary gearbox”. In: *Applied Acoustics* 77 (2014), pp. 169–177.

[9] Ryszard Błażej, B Kirjanów, and Tomasz Kozłowski. “A high resolution system for automatic diagnosing the condition of the core of conveyor belts with steel cords”. In: *Diagnostyka* 15.4 (2014), pp. 41–45.

[10] P Borghesani. “The envelope-based cyclic periodogram”. In: *Mechanical Systems and Signal Processing* 58 (2015), pp. 245–270.

[11] P Borghesani et al. “Testing second order cyclostationarity in the squared envelope spectrum of non-white vibration signals”. In: *Mechanical Systems and Signal Processing* 40.1 (2013), pp. 38–55.

[12] Andrzej Cichocki, Rafal Zdunek, and Shun-ichi Amari. “New algorithms for non-negative matrix factorization in applications to blind source separation”. In: *2006 IEEE International Conference on Acoustics Speech and Signal Processing Proceedings*. Vol. 5. IEEE. 2006, pp. V–V.

[13] Jacob A Crossman et al. “Automotive signal fault diagnostics-part I: signal fault analysis, signal segmentation, feature extraction and quasi-optimal feature selection”. In: *IEEE Transactions on Vehicular Technology* 52.4 (2003), pp. 1063–1075.

[14] JH Fourie et al. “Condition monitoring of fabric-reinforced conveyor belting using digital x-ray imaging”. In: *Bulk Solids Handling* 25.5 (2005), p. 290.

[15] Harry L Hurd and Abolghassem Miamee. *Periodically correlated random sequences: Spectral theory and practice*. Vol. 355. John Wiley & Sons, 2007.

[16] Aapo Hyvärinen and Erkki Oja. “A fast fixed-point algorithm for independent component analysis”. In: *Neural computation* 9.7 (1997), pp. 1483–1492.

[17] Aapo Hyvärinen and Erkki Oja. “Independent component analysis: algorithms and applications”. In: *Neural networks* 13.4 (2000), pp. 411–430.

[18] Eric Jacobsen and Richard Lyons. “The sliding DFT”. In: *Signal Processing Magazine, IEEE* 20.2 (2003), pp. 74–80.

[19] Andrew KS Jardine, Daming Lin, and Dragan Banjevic. “A review on machinery diagnostics and prognostics implementing condition-based maintenance”. In: *Mechanical systems and signal processing* 20.7 (2006), pp. 1483–1510.

[20] Li Li and Liangsheng Qu. “Machine diagnosis with independent component analysis and envelope analysis”. In: *Industrial Technology, 2002. IEEE ICIT’02. 2002 IEEE International Conference on*. Vol. 2. IEEE. 2002, pp. 1360–1364.

[21] Yang Liu, Tianshuang Qiu, and Hu Sheng. “Time-difference-of-arrival estimation algorithms for cyclostationary signals in impulsive noise”. In: *Signal Processing* 92.9 (2012), pp. 2238–2247.

[22] Qinghua Mao et al. “Research on Magnetic Signal Extracting and Filtering of Coal Mine Wire Rope Belt Conveyer Defects”. In: *2011 Third International Conference on Measuring Technology and Mechatronics Automation*. Vol. 3. IEEE. 2011, pp. 18–22.

[23] PD McFadden and JD Smith. “Model for the vibration produced by a single point defect in a rolling element bearing”. In: *Journal of sound and vibration* 96.1 (1984), pp. 69–82.

[24] AD Nembhard et al. “Fault diagnosis of rotating machines using vibration and bearing temperature measurements”. In: *Diagnostyka* 14.3 (2013), pp. 45–51.

[25] Jakub Obuchowski, Agnieszka Wylomańska, and Radosław Zimroz. “Recent developments in vibration based diagnostics of gear and bearings used in belt conveyors”. In: *Applied Mechanics and Materials*. Vol. 683. Trans Tech Publ. 2014, pp. 171–176.

[26] Amani Raad, Jerome Antoni, and Ménad Sidahmed. “Indicators of cyclostationarity: Theory and application to gear fault monitoring”. In: *Mechanical Systems and Signal Processing* 22.3 (2008), pp. 574–587.

[27] Robert Bond Randall. *Vibration-based condition monitoring: industrial, aerospace and automotive applications*. John Wiley & Sons, 2011.

[28] MJ Roan, JG Erling, and LH Sibul. “A new, non-linear, adaptive, blind source separation approach to gear tooth failure detection and analysis”. In: *Mechanical Systems and Signal Processing* 16.5 (2002), pp. 719–740.

[29] Randy S Roberts, William A Brown, and Herschel H Loomis Jr. “Computationally efficient algorithms for cyclic spectral analysis”. In: *Signal Processing Magazine, IEEE* 8.2 (1991), pp. 38–49.

[30] Mateusz Sawicki et al. “An Automatic Procedure for Multidimensional Temperature Signal Analysis of a SCADA System with Application to Belt Conveyor Components”. In: *Procedia Earth and Planetary Science* 15 (2015), pp. 781–790.

[31] Paweł K Stefaniak et al. “Diagnostic Features Modeling for Decision Boundaries Calculation for Maintenance of Gearboxes Used in Belt Conveyor System”. In: *Advances in Condition Monitoring of Machinery in Non-Stationary Operations*. Springer, 2016, pp. 251–263.

[32] Jacek Urbanek, Tomasz Barszcz, and Jerome Antoni. “Time–frequency approach to extraction of selected second-order cyclostationary vibration components for varying operational conditions”. In: *Measurement* 46.4 (2013), pp. 1454–1463.

[33] Huaqing Wang et al. “A Compound fault diagnosis for rolling bearings method based on blind source separation and ensemble empirical mode decomposition”. In: *PloS one* 9.10 (2014), e109166.

[34] Michael Wilkinson et al. “Comparison of methods for wind turbine condition monitoring with SCADA data”. In: *IET Renewable Power Generation* 8.4 (2014), pp. 390–397.

[35] Agnieszka Wyłomańska et al. “Periodic autoregressive modeling of vibration time series from planetary gearbox used in bucket wheel excavator”. In: *Cyclostationarity: Theory and Methods*. Springer, 2014, pp. 171–186.

[36] Li Xian-Guo et al. “Research on Fault Detection Algorithm of Steel Cord Conveyor Belt Based on Gabor Filtering and Image Fusion.” In: *Journal of Convergence Information Technology* 6.11 (2011).

[37] Shen Yin et al. “Data-based techniques focused on modern industry: an overview”. In: *IEEE Transactions on Industrial Electronics* 62.1 (2015), pp. 657–667.

[38] Radoslaw Zimroz and Walter Bartelmus. “Gearbox condition estimation using cyclo-stationary properties of vibration signal”. In: *Key Engineering Materials*. Vol. 413. Trans Tech Publ. 2009, pp. 471–478.

[39] Radoslaw Zimroz, Walter Bartelmus, et al. “Diagnostics of bearings in presence of strong operating conditions non-stationaritya procedure of load-dependent features processing with application to wind turbine bearings”. In: *Mechanical Systems and Signal Processing* 46.1 (2014), pp. 16–27.

[40] Radoslaw Zimroz, Monika Hardygóra, and Ryszard Blazej. “Maintenance of belt conveyor systems in Poland–an overview”. In: *Proceedings of the 12th International Symposium Continuous Surface Mining-Aachen 2014*. Springer. 2015, pp. 21–30.

[41] Radoslaw Zimroz, Jakub Obuchowski, and Agnieszka Wylomanska. “Vibration Analysis of Copper Ore Crushers Used in Mineral Processing PlantProblem of Bearings Damage Detection in Presence of Heavy Impulsive Noise”. In: *Advances in Condition Monitoring of Machinery in Non-Stationary Operations*. Springer, 2016, pp. 57–70.

[42] Radoslaw Zimroz, Jacek Wodecki, et al. “Self-propelled mining machine monitoring system–data validation, processing and analysis”. In: *Mine planning and equipment selection*. Springer, 2014, pp. 1285–1294.